THE EFFECTS OF SITE-SPECIFIC IRRIGATION MANAGEMENT ON SOIL MOISTURE AND POTATO PRODUCTION IN SOUTHERN ALBERTA

by

Danielle Crawford

Submitted in partial fulfilment of the requirements
for the degree of Master of Science

at

Dalhousie University
Halifax, Nova Scotia
August 2020

TABLE OF CONTENTS

LIST OF FIGURES

LIST OF TABLES

ABSTRACT

Site-specific water management can increase water use efficiency by up to 30% but determining whether adopting the technology for site-specific irrigation will be beneficial enough to consider the additional cost is still an open question. The objectives of this study are to determine the effect of site-specific water management has on soil moisture at a field scale and to determine whether site-specific water management can reduce yield variability. Additionally, the heterogeneity of soil apparent electrical conductivity and elevation was explored as driving factors in soil moisture differences between management zones delineated using these variables. Russet Burbank potatoes were grown in Southern Alberta in a field divided into three management zones. In a two-year study conducted in the growing seasons of 2018 and 2019, plots were delineated from each of the management zones and treated with site-specific irrigation prescriptions, while uniform irrigation was used for the rest of the study area. The effect of site-specific irrigation was monitored using soil moisture sensors installed in each of the plots. The effect of uniform irrigation was also monitored using soil moisture sensors installed in the management zones in areas under uniform irrigation prescriptions. The site-specific irrigation schedule was based on an 80% maximum allowable depletion of available soil moisture. Soil moisture depletion was calculated from soil moisture sensor data for each plot. Soil moisture sensors were also used to assess soil water movement in the rootzone. Soil moisture surveys were conducted at 15 cm and 30 cm depths and were used to spatially assess soil moisture by co-kriging soil moisture surveys with soil apparent electrical conductivity and elevation. Yield variability was not improved under site-specific irrigation, but in some areas, a 10-30% reduction in total irrigation did not negatively impact yield. Hydrological differences were determined between the management zones, but relationships between soil moisture and the management zones could not be confirmed due to a lack of soil moisture sensor data. The reliance on soil moisture sensors to inform the irrigation prescriptions may have led to a moisture deficit which resulted in lower potato yields. This effect could be mitigated by installing additional soil moisture sensors in each of the management zones to provide a method to corroborate soil moisture observations. Assessing field properties for variability is a prudent step before determining whether a management zone derived site-specific irrigation management strategy informed by soil moisture sensor data as some fields may show more benefits using observational experience.

LIST OF ABBRIVATIONS USED

AITC – Alberta Irrigation Technology Centre

ANOVA – analysis of variance

ASL – above sea level

BD – bulk density

ECa – soil apparent electrical conductivity

FAO – Food and Agriculture Organization

FC – field capacity

FPI – fuzziness performance index

GPS – global positioning system

GWC – gravimetric water content

ILP – integer limiting programming

ISODATA – Iterative Self-Organizing Data Organizing Technique

LOOCV – leave-one-out cross-validation

MAD – maximum allowable depletion

MPE – modified partition entropy

MSE – mean square error

MZ – management zone

RMSE – root mean square error

SMRID – St. Mary's River Irrigation District

SSIM – site-specific irrigation management

UIM – uniform irrigation management

VRI – variable rate irrigation

VWC – volumetric water content

ACKNOWLEDGEMENTS

I would like to thank my committee members, Dr Haibo Niu, Dr Kenny Corscadden and Dr Peter Harvard for their assistance in the completion of this thesis. I would especially like to thank Dr Willemijn Appels for her continued assistance and support and for pushing me to apply for a Master of Science degree. I would also like to thank Nathan Linder for his work during field seasons and Dr Brandon Heung for his assistance with geostatistics. Finally, I would like to thank my partner, Benjamin Nicholas. Without his support and encouragement, this document would have never been completed. This study was conducted in the treaty 7 territory and the traditional territory of the Niitsitpi (Blackfoot), Nakoda (Stoney) and Tsuut'ina.

CHAPTER 1. INTRODUCTION

For millennia, humans have recognized the benefits of irrigation practices. Jordan and Egypt have archeological evidence of irrigation practises dating back to 6000 BCE; meanwhile, the Incans, Mayans and Aztecs constructed irrigation systems in Meso and South America (Sojka, Bjorneberg, & Entry, 2002). Irrigation practices enable agriculture in areas where the evapotranspiration rate is high, and the precipitation rate is low, thus growing the land base that can be used for food production (Taylor, 2014). When comparing yields of corn, cotton, soybeans, and wheat grown under dryland conditions to their irrigated counterparts, irrigated fields show less variability and significantly higher yields (Assefa et al., 2012; Payero & Khalilian, 2017). It has been estimated that 40 % of the world's food and fibre are grown on irrigated lands, which consist of 17 % of the total land cultivated for agriculture (Evans et al., 2013).

Although Canada is ranked fourth in the world for freshwater resources (Gleick, 2014), these water resources are not evenly distributed throughout the country. The areas that are associated with large-scale agriculture are also some of the country's driest, with nearly 70 % of farmland in Canada in the prairie provinces of Alberta and Saskatchewan (Statistics Canada, 2016). Both provinces have moisture deficits when comparing the yearly cumulative precipitation to yearly cumulative evapotranspiration which vary from 100 mm in the northern parts of both provinces to 400mm in the south (Agriculture and Agri-Food Canada & Government of Canada, 2013). As agricultural food production is most efficient when the difference between evapotranspiration and available water

within a field is minimal, irrigation is necessary in these areas to maintain production values.

In Southern Alberta, irrigation and agriculture are intrinsically linked. Precipitation is low in Southern Alberta's prairie region, with average precipitation ranging between 350 and 500 mm per year (Downing & Pettapiece, 2006) while potential evapotranspiration which ranges from 1050 mm to 1200 mm (Alberta Environment and Sustainable Resource Development, 2013). This results in a 500 mm deficit in moisture. However, the high number of growing degree days makes the area ideal for crop growth, if sufficient additional water resources can be brought to agricultural land (Downing & Pettapiece, 2006). Because of this and good-quality surface water sources, irrigation is prevalent in Alberta, more than in any other province, accounting for 67 % of the total irrigated land in Canada (Statistics Canada, 2010). Irrigated agriculture accounts for 63 % of the total freshwater usage in Alberta (Alberta Environment, 2007). Irrigation water used in Southern Alberta is obtained from surface waters, most prevalently from the tributaries of the South Saskatchewan River (Alberta Agricultural and Rural Development, 2010). Climate change is expected to impact Southern Alberta by increasing temperatures and the increasing number of growing degree days (Barrow & Yu, 2005). These climatic changes are expected to increase the average moisture index 20-30% by 2050, indicating drier conditions as the climate continues to warm. These drier conditions are not likely to be offset by the expected increase in precipitation, leading to an increased reliance on irrigation for agriculture, especially during drought periods (Barrow & Yu, 2005). Furthermore, irrigated production is roughly seven times as valuable as dryland

production; the average production on irrigated farmland is approximately $2400/ha, compared to dryland production, which averages $329/ha (Kulshreshtha et al., 2016). Expanding irrigation in Southern Alberta would be economically beneficial for agricultural production, but limits on water allocation established in 2006 make expansion difficult (Alberta Environment and Parks, 2006). Studies have shown using site-specific irrigation management (SSIM) can improve water use efficiency by up to 30 % (Evans et al., 2013; Sadler et al., 2005). However, implementing SSIM is expensive and implementation may not be practical in all areas. Determining how SSIM can change soil moisture dynamics and crop production in a field is still an open question. Significant impacts will have to be achieved for SSIM to benefit individual producers.

1.1 Research Objectives

The study presented in this thesis addresses the knowledge gap regarding the effects site-specific irrigation management on potato production and soil moisture distribution, I have designed a study to compare the yield of areas with SSIM to those with uniform irrigation. The following questions will be answered:

1. Are the three management zones delineated in the study area hydrologically different?
2. Is heterogeneity of ECa and elevation the driving factor for soil moisture differences under uniform irrigation prescriptions?
3. Can site-specific irrigation management be used to reduce potato yield variability?

CHAPTER 2. LITERATURE REVIEW

2.1 IRRIGATION SYSTEMS OF ALBERTA

Irrigation management technology and philosophy have undergone many changes over the past half-century. Up to the mid-1960's, flood or gravity irrigation was the predominate form of irrigation used in Southern Alberta (Wang et al., 2015). This irrigation strategy used the simplest form of irrigation technology, whereby a waterway was dammed, and water would saturate a field beyond field capacity to ensure that water was available for crops during dry periods. Flood irrigation is an ineffective strategy for several reasons: it can increase the salinity of the soil as the water evaporates, increases leaching of essential nutrients, is an inefficient use of water resources because of water evaporation, and has a low application efficiency when compared to other irrigation methods (Cox et al., 2018; Howell, 2003).

Starting in the 1970's, farm operators began utilizing center pivot and wheel-move irrigation systems. Wheel-move systems were developed prior to center pivot systems and allow sprinkler systems to be moved in a field but apply irrigation when the system is stationary (Hill, 2000). Center pivot irrigation systems are self propelled overhead sprinkler systems which move in a circle from a central point (Daugherty & Eaton, 1975). They were first patented by Frank Zybach in 1952 (Hokcell, 2000; Splinter, 1976), but were used less often than wheel-move systems until the 1990's (Alberta Agriculture and Rural Development, 2014). Center pivot irrigation systems have since become the most used irrigation system in Canada (Alberta Agriculture and Forestry, 2016).; by 2015, high-

and low-pressure pivot systems accounted for 80% of all irrigation systems in the province, with low-pressure systems being used in approximately 72% of farms with irrigation systems (Alberta Agriculture and Forestry, 2016).The most significant benefit for producers of a center pivot irrigation system is that it can be automated, and thus, have less intensive labor requirements than flood and wheel-move irrigation (Splinter, 1976). Because it applies water in small increments, crops must be watered throughout the growing season, so there is a reduction in the erosion of topsoil and leaching of nutrients through the soil profile. It can also significantly improve yields on coarse-textured soils, which have a limited water holding capacity and therefore need more frequent irrigation to produce crops (Splinter, 1976). Center pivot irrigation systems treat fields as uniform environments onto which uniform volumes of water are applied and thus are optimal for homogeneous field conditions. As most commercial fields have heterogeneous properties like soil texture, soil depth, and topography, which affect optimal crop growth, the management of center pivot irrigation systems is often based on the combination of properties that cover the largest area in the field.

2.2 Precision Irrigation

Precision irrigation systems use differences in soil properties to subdivide a field into smaller sectors, or management zones, which share physical properties. The irrigation rate for the management zone is customized to the shared physical properties (Alaba, Chandra, & Aghil, 2016; Haghverdi et al., 2015; Villalobos & Fereres, 2016). This differs from conventional irrigation systems that apply a uniform volume of water over large sections of land, ignoring the inherent heterogeneity of soil and topography that can

occur in a single field (Evans et al., 2013). Precision irrigation is a relatively new irrigation system that requires large amounts of data and the use of novel technologies (Evans et al., 2013).

Loyoza et al. (2016) identified five levels for the automation of irrigation systems (Table 1).

Table 1: Categories of automation within irrigation systems (Lozoya et al., 2016)

Level 0	Empirical open loop irrigation	No automation, irrigation systems are controlled manually; irrigation rate is determined using farmers observation and experience.
Level 1	Time-based open-loop irrigation	Simple automation of irrigation systems using a timer with no sensor inputs and is based on farmers observation and experience
Level 2	Feed-forward open-loop irrigation	Automated irrigation which replaces water at the rate of evapotranspiration and crop use; the system uses sensors or weather station data to determine the irrigation rate and timing.
Level 3	Closed-loop irrigation	An automated irrigation system which applies irrigation based on in-field sensor data which detect predetermined low thresholds and stops irrigation when sensors detect a predetermined high threshold; it is often based on soil water content.
Level 4	Model-based closed-loop irrigation	All irrigation systems are automated with a mathematical model which optimizes the irrigation rate based on predictive algorithms.

Precision irrigation is currently at Level 1 to 2, with attempts being made to increase automation to Level 3 (Lozoya et al., 2016) and Level 4 (Seidel et al., 2015). As the level of automation within an irrigation system increases, more data collection is necessary to create an accurate representation of conditions within a field. Soil moisture sensor data can help with this process, but sensors must be installed using a design that captures the spatial heterogeneity within the field. This may mean that many sensor stations are required throughout the field. Weather station data may also be used to provide information for evapotranspiration rates, such data should be collected as closely to the field as practically possible. This level of data acquisition can be expensive and time-consuming, and the interpretation of the data acquired requires more expertise than current assessments of soil conditions and water availability for irrigation scheduling (Sadler et al., 2005).

Precision irrigation systems, which can be adjusted to site-specific differences within a field and are automated by prescription maps, are also known as variable rate irrigation systems (Evans et al., 2013). VRI systems utilize in-field measurements and mathematical modelling to create irrigation management strategies that may vary within a field depending on environmental factors and differences in crop water requirements (Lozoya et al., 2016; Vukobratovic et al., 2014). Currently, VRI systems are commercially available, but have not been widely adopted by producers due to the expense of installing the systems. Those promoting precision irrigation technology have made claims about how the technology can benefit individual farm operators (Evans et al., 2013). The potential benefits of precision irrigation are the positive effect that the technology may have on

crop production by improving resource use efficiency. VRI has been shown to use approximately 30% less water compared to conventional irrigation systems (Haghverdi et al., 2015), which is becoming a more important aspect to farming as climate change impacts typical water cycles. Precision irrigation technology can be used to reduce over- and under-irrigation in specific parts of fields, thereby having the potential for increased yields in heterogeneous fields (Evans et al., 2013; Lozoya et al., 2016). Incidentally, by using different irrigation rates throughout a single field, nitrogen leaching (Fridgen et al., 2000) and the topsoil erosion are also reduced. Site-specific salinity problems may also be addressed by mapping the highly saline areas and delineating them into separate management zones that can have different irrigation rates from the rest of the field (Alaba et al., 2016). Topographic differences can be separated into management zones using slope and elevation as variables (Fridgen et al., 2000). There is also a promise of improved products from VRI systems; improving the quality of products has been suggested as another benefit of using VRI systems (Evans et al., 2013). However, there are very few studies on how VRI can improve yields; most studies to date have focused on either water management (Lozoya et al., 2016; Rowshon & Amin, 2010) or the development of tools to improve the delineation process (Evans et al., 2013; Haghverdi et al., 2015).

VRI systems are controlled in two ways. The first is through varying the travel speed of the center pivot during its rotation; these are described as sector-controlled systems (Fig. 1a). In sector-controlled systems, the travel speed of the system is increased or decreased to change the irrigation application rate.

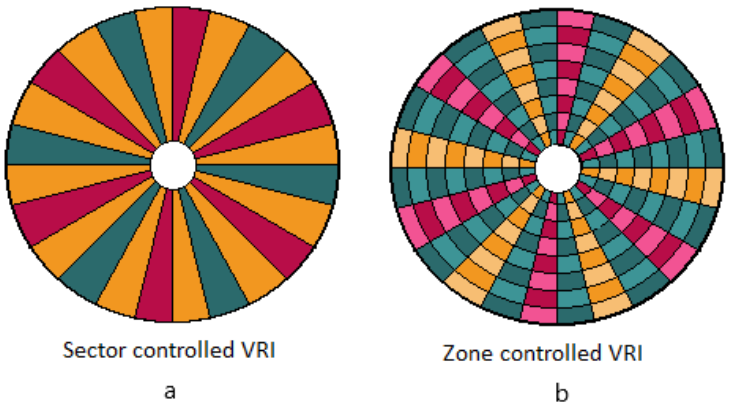

Figure 1: Examples of management zones for sector controlled (a) and zone controlled (b) variable rate irrigation systems

A GPS tracker system mounted onto the pivot arm helps control the speed as the pivot system moves around the field. Management zones for sector-controlled systems are shaped like wedges (Figure 1a). The second is through control of the sprinklers: these are described as zone-controlled systems (Figure 1b). Variable flow rate sprinklers can vary the effective irrigation rate by opening and closing the sprinkler head (King et al., 2005; Sadler et al., 2005). Management zones are shaped like concentric circles overlaid on top of the wedges (Fig 1b). Because of the level of automation necessary for implementation, zone controlled VRI requires the highest amount of data collection of all the precision irrigation techniques. The adoption of VRI in agriculture has been slow, because of high costs which is explained by the increased cost of VRI systems and the costs associated with the collection of data for the field, which include, the intensive monitoring required, and the expertise necessary for the technology to be successfully implemented (Sadler et al., 2005).

2.3 Management Zone Delineation

Delineation of management zones is a critical step in precision irrigation water management. Because precision irrigation techniques incorporate the spatial variability of plant available water, drainage conditions, infiltration rates, and soil water holding capacity rather than the average of these variables as is done with conventional irrigation techniques (Lozoya et al., 2016), mapping these attributes the first step in delineation. Direct determination of these variables is time-consuming and often requires significant disturbance, therefore indirect, proxy variables are preferred (Haghverdi et al., 2015). Topography and soil apparent electrical conductivity (ECa) are useful and popular for two reasons; first, they can be measured with an automated tool at a high spatial density throughout an entire field, and second, they require less invasive sampling or laboratory testing. ECa features well-established correlations with soil texture, bulk density, organic matter content, and cation exchange capacity (Alaba et al., 2016; Brady, 2008; de Lara, Khosla, & Longchamps, 2017; Haghverdi et al., 2015). Using ECa to directly predict soil texture has been explored, but due to the confounding factors of soil moisture, salinity, and organic matter, ECa can only be partially correlated with soil texture (McCutcheon et al., 2006). Fridgen (2000) explored the use of topography and ECa to create management maps in a field. The topographic details that were assessed were slope and elevation. There are clear correlations between topography, slope, soil texture and ECa, and the effect these characteristics have on hydraulic conductivity (Alaba et al., 2016; de Lara et al., 2017; Fridgen et al., 2000; Haghverdi et al., 2015). Alternatively, it has been suggested that an analysis of historical yield maps would provide a better indication of plant water

use (Haghverdi et al., 2015). Yield measurements in single field studies show that depressions outperform those on hills, unless ponding occurs, because of the higher moisture content found in toe-slopes (Fridgen et al., 2000). However, this may not provide the most appropriate information for the creation of management zones, because temporal differences of yield are difficult to determine, and yield is affected by other factors including pests and disease which differ from year to year.

Delineation of management zones uses decision-making computer software by necessity. Soil properties which affect infiltration, water holding ability and drainage are never discrete and rely on a continuum of data points for assessment. As delineation is defined by creating clear boundaries surrounding areas with similar properties, it is necessary to determine where a data point lies along a spectrum. Various soil properties may have different spatial distributions; management zone delineation based on multiple properties can be achieved using statistical clustering methods (Alaba et al., 2016; de Lara et al., 2017; Haghverdi et al., 2015; Haghverdi et al., 2016). Principle component analysis is used to determine an individual parameter's importance within a dataset by decoupling dependant variables and assessing them as independent variables (Haghverdi et al., 2015). Haghverdi, et al (2015) explored different modelling techniques which are used in the determination of management zones. The methods examined the use of fuzzy k-means, Gaussian mixture, integer limiting programming (ILP), and Iterative Self-Organizing Data Organizing Technique (ISODATA). These modelling methods are all unsupervised clustering tools; unsupervised clustering uses algorithms to identify clusters within a data set while supervised clustering utilizes the experience of the software user

and requires controlled sites to train the algorithm. The benefit of using unsupervised clustering is that a user does not have to be trained to use the software or be familiar with the site, as unsupervised clustering use iterative processes that analyze the data into best-fit clusters (Fridgen et al., 2004). All four methods performed similarly in the determination of management zones; the methods were assessed using the overall variance of available water capacity (Haghverdi et al., 2015). All methods also identified the same number of optimal management zones (Haghverdi et al., 2015). Fuzzy k-means analysis benefits from being widely used, simple and efficient at determining clusters (Haghverdi et al., 2015). It is the method used by the Management Zone Analyst software (Fridgen et al., 2004), a popular operational package to determine management zones (Alaba et al., 2016; Al-Gaadi et al., 2015; de Lara et al., 2017). The Management Zone Analyst software features built-in evaluating tools which can assess the optimal number of management zones that need to be employed within a field. This is an important step in management zone delineation as the number of management zones should limit the variability of the measured field characteristics while not creating more management zones than necessary. Evaluating the optimal number of management zones in the statistical clustering process involves two measures: the fuzziness performance index (FPI) and the modified partition entropy (MPE). The goal of management zone delineation is to minimize the value of both FPI and MPE to assure the delineated zones have minimal overlap (FPI) and the smallest amount of disorganization (MPE) (Boydell & McBratney, 2002).

2.4 CONCLUSION

The effects of VRI on decreasing water use in irrigated agriculture has been demonstrated in some environments (Sadler et al., 2005). Delineation methods for management zones based on proxy variables for soil properties & drainage characteristics have been established. However, firm evidence of the effects of VRI on yield improvement is limited. An important factor here is that methods for irrigation scheduling in management zones based on multiple field properties is poorly understood.

CHAPTER 3. METHODS

3.1 FIELD DESCRIPTION

The study site for the 2018 and 2019 field seasons is located at Alberta Irrigation Technology Centre (49.6903 N, -112.7341 W), 8 km east of Lethbridge, Alberta (Figure 2 A&B). The mean elevation for the field site is 907.2 m with a minimum elevation of 903.6 m and a maximum elevation of 911.9 m. The 30-year mean annual precipitation (1981 – 2010) at the Lethbridge airport weather station, located approximately 7 km from the field site, is 360 mm of precipitation throughout the year, with 250 mm falling in the growing season (Government of Canada, 2019). The average growing season begins May 14 and ends October 27, consisting of 166 days. The average number of frost-free days in Lethbridge is 124 days; the average date for last spring frost is May 17 and the average date for the first fall frost is September 18 (Government of Canada, 2019). The climate for the study area is characterized as Dfb 19 (Ackerman, 1941) with warm, dry summers and cold winters which are broken up by strong orographic winds from the west. The mean annual temperature is 5.9˚C with average minimum and maximum growing season temperatures of 3.9˚C and 26.1˚C (Government of Canada, 2019). The average annual wind speed is 18 km/h.

The field is approximately 2.3×10^5 m^2 and is divided into quarters which are managed using a four-year crop rotation of spring and winter wheat, potatoes, and sugar beets. Irrigation water is withdrawn from St. Mary River and is supplied by the St. Mary River Irrigation District (SMRID), one of 13 irrigation districts in Southern Alberta. The field site

is located on Orthic Dark Brown Chernozemic soil (Agriculture and Agri-Food Canada, Research Branch & Alberta Agriculture, Food and Rural Development, Conservation and Development Branch, 2005) with a sandy clay loam texture (Yari et al., 2017). Russet Burbank potatoes were chosen as the experimental crop and were seeded in the northwest quarter in 2018 and southwest quarter in 2019 (Figure 2C).

The field is equipped with a Valley model 8000 center pivot irrigation system with 5 spans, a length of 294 m and 129 sprinklers. The sprinkler system is a low elevation spray application package where sprinklers are installed on drop tubes approximately 2 m above ground level. Each sprinkler consists of a Nelson rotator sprinkler nozzle (R3000, D6-Red) and 1.2 bar pressure regulator (Nelson Irrigation Inc., Walla Walla, Washington, USA). The center pivot irrigation system was retrofitted with a Valmont VRI zone control system in 2012, which divided the lateral span into 12 sprinkler banks. Each sprinkler bank consists of 10-12 individual sprinklers.

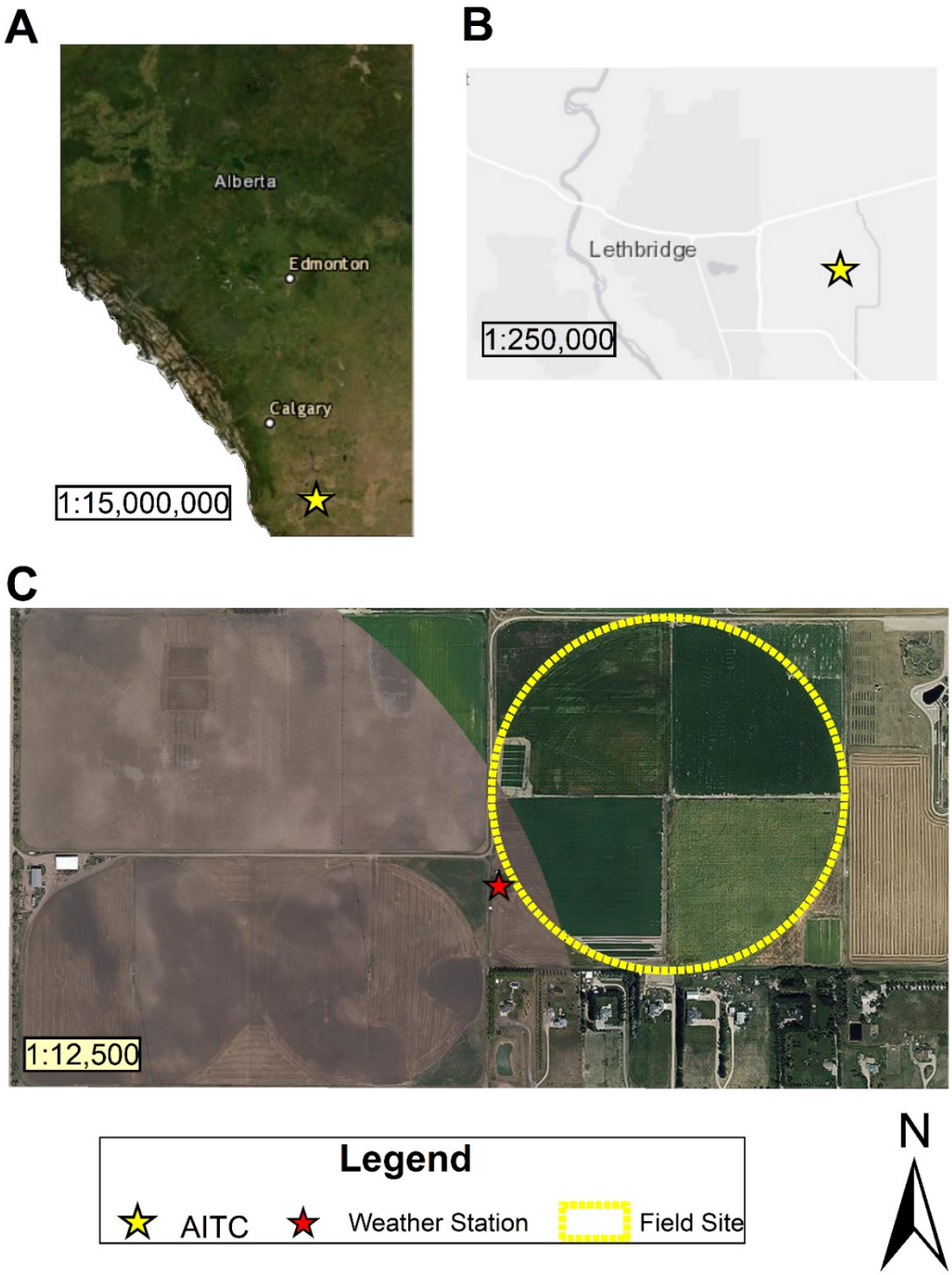

Figure 2: General site map for study areas in 2018 and 2019.

3.2 Management Zone Delineation

The delineation of management zones was not a topic of study and a pre-existing management zone map was used to select the experimental plots. The management zones were delineated in 2013 by Yari et al (2017) with the Management Zone Analyst software (Fridgen et al., 2004) using ECa and elevation. ECa data was collected using an EM38 instrument (Geonics Limited, Mississauga, Ontario, Canada) and Veris 3100 (Veris Technologies, Inc., Salina, Kansas, USA), leaving out the northeast section due to on-going farm operations. The point data was used to predict ECa for three quarter sections using the ordinary kriging interpolation method in ArcGIS (version 10.2.2, ESRI, Redlands, California, USA) (Figure 3A). The elevation point data was obtained using a real time kinematic global navigation satellite system receiver (Figure 3B) which was kriged the same way as ECa to produce an elevation map. Yari et al (2017) used the Management Zone Analyst software to partition data into clusters. The clusters were evaluated by the software which attempted to reduce the weighted within-group sum of squares errors by evaluating clustering characteristics using FPI and MPE to identify the optimal number of clusters. The minimum FPI and MPE were calculated for three clusters, indicating that three management zones were optimal. Three management zones were delineated from the results, producing Figure 4. After the management zones were delineated, soil textural properties, pH and organic matter were evaluated (Table 2).

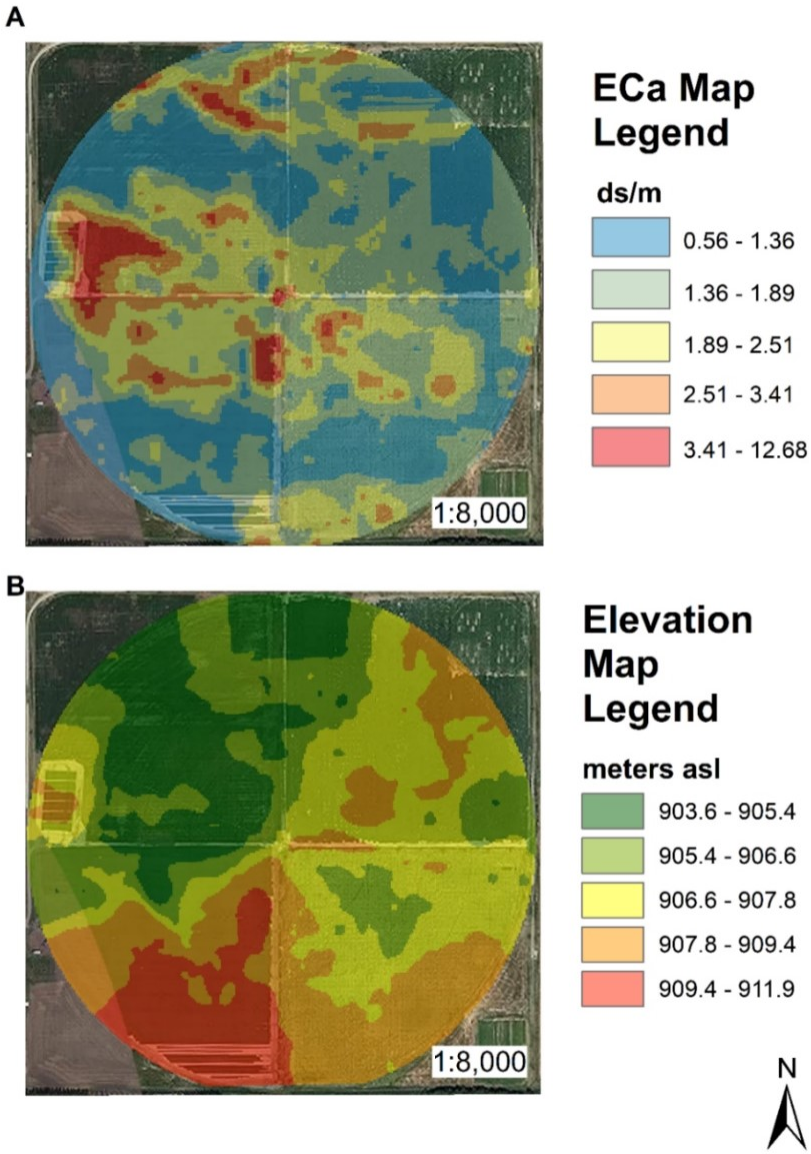

Figure 3: Apparent soil electrical conductivity (EC_a) and elevation raster maps

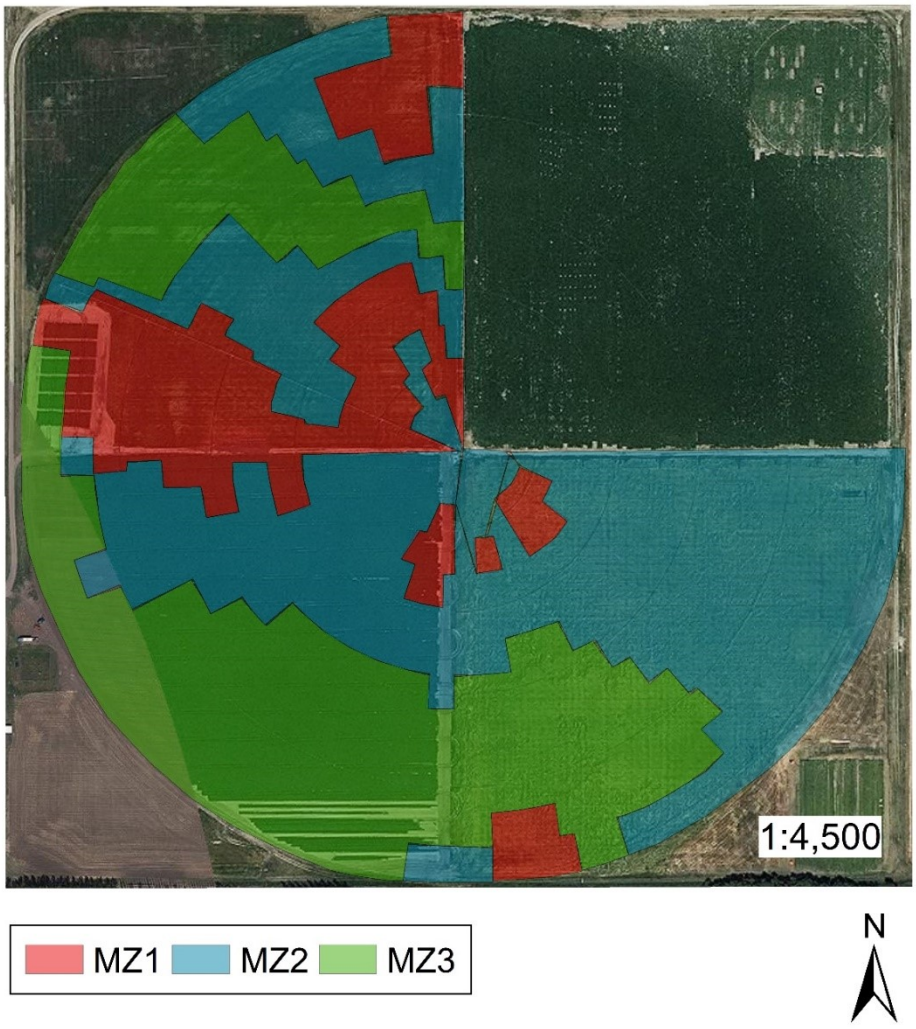

Figure 4: Management zone map developed by Yari et al (2017).

Table 2: Summary of soil properties from Yari (2017). Percent of sand, silt, clay, and organic matter (OM), and pH are summarized.

Zone	Sand (%)	Silt (%)	Clay (%)	pH	OM (%)
1	50.2	24.4	25.4	7.74	2.57
2	52.9	23.8	23.3	7.80	2.61
3	53.3	23.3	23.4	7.76	2.59

3.3 Plot Selection

Using the management map in Figure 4, management zones 1, 2 and 3 accounted for 36%, 38% and 26% of the total area in the 2018 study area, respectively, and 8%, 38%

and 54% in the 2019 study area. The irrigation applications under the normal operating procedure used level 0 automation (Lozoya et al., 2016) where the operator made irrigation decisions with observations and experience rather than using sensors. The field was irrigated using uniform irrigation management (UIM) except where ponding was observed. Plots were delineated from three management zones to examine the effects of site-specific irrigation management (SSIM) on soil moisture and potato yield. Yield and soil moisture comparisons between uniform irrigation management (UIM) and SSIM could be examined by applying SSIM treatments to the plots and using the normal operating procedure for the rest of the field. The plots were selected using the management zone map created by Yari et al (2017). The plots were selected under the 7^{th} and 8^{th} sprinkler banks in 2018 and 6^{th} and 7^{th} sprinkler banks in 2019. Each management zone had a single plot approximately 4000 m^2, except the plot in MZ1-2019, where a lack of space required the plot to be 1760 m^2.

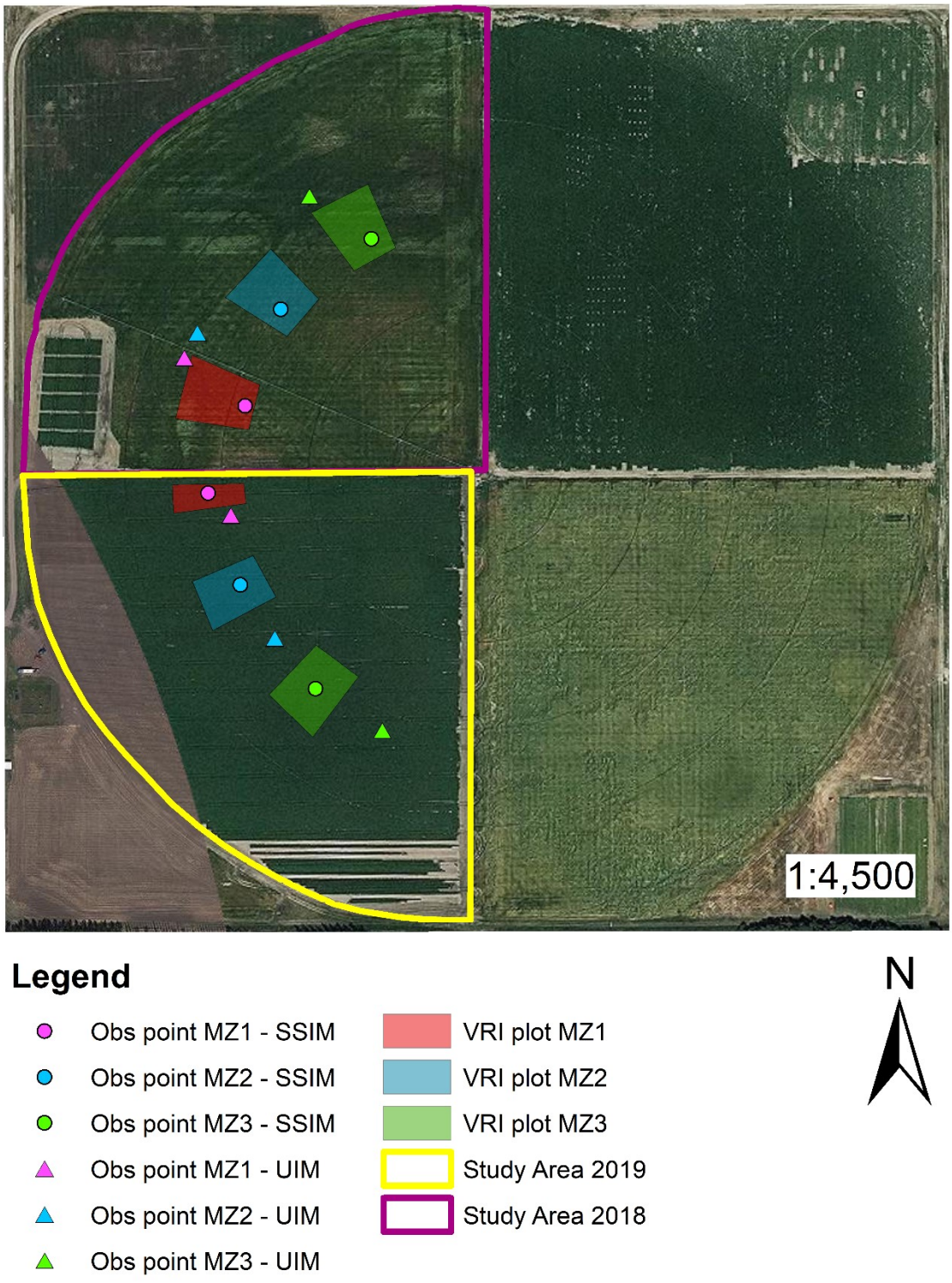

Figure 5: Detailed site map for AITC study site in 2018 and 2019

3.4 Volumetric Water Content Observations

The height of the effective root zone for potatoes has been shown to be 60 cm from the top of the ridge (Stalham & Allen, 2004). This depth was chosen as the maximum sensor installation depth. The SSIM plots were installed with four soil moisture sensors in 2018 and five soil moisture sensors in 2019. In the SSIM 2018 plots, four HOBO 10HS soil moisture smart sensors (model S-SMD-M005) were installed horizontally in the soil at 15, 30, 45 and 60 cm from the top of the potato hill. At UIM observation stations, soil moisture sensors were installed at the same depths as SSIM; however, Acclima TDR-315 soil moisture sensors were used instead of HOBO 10HS soil moisture smart sensors. In 2019, after laboratory experiments described in Appendix 1 were conducted, it was determined that vertical installation was more accurate when sensors are placed 15 cm apart. The installation was changed to accommodate these findings. In SSIM plots, four HOBO 10HS soil moisture smart sensors were installed, whereby two were installed horizontally at 15 cm and 25 cm and two were installed vertically in boreholes at 30 cm and 50 cm, extending 10 cm into the soil profile. Additionally, a HOBO EC5 soil moisture smart sensor (model S-SMC-M005) was installed horizontally at 5 cm. In the UIM monitoring stations, the sensors were installed vertically in boreholes at 5, 20, 35 and 50, extending 15 cm into the soil profile. Soil moisture data was downloaded no later than 24 hours before a scheduled irrigation event. Once the soils moisture data was downloaded, the observations were corrected using the soil specific calibration.

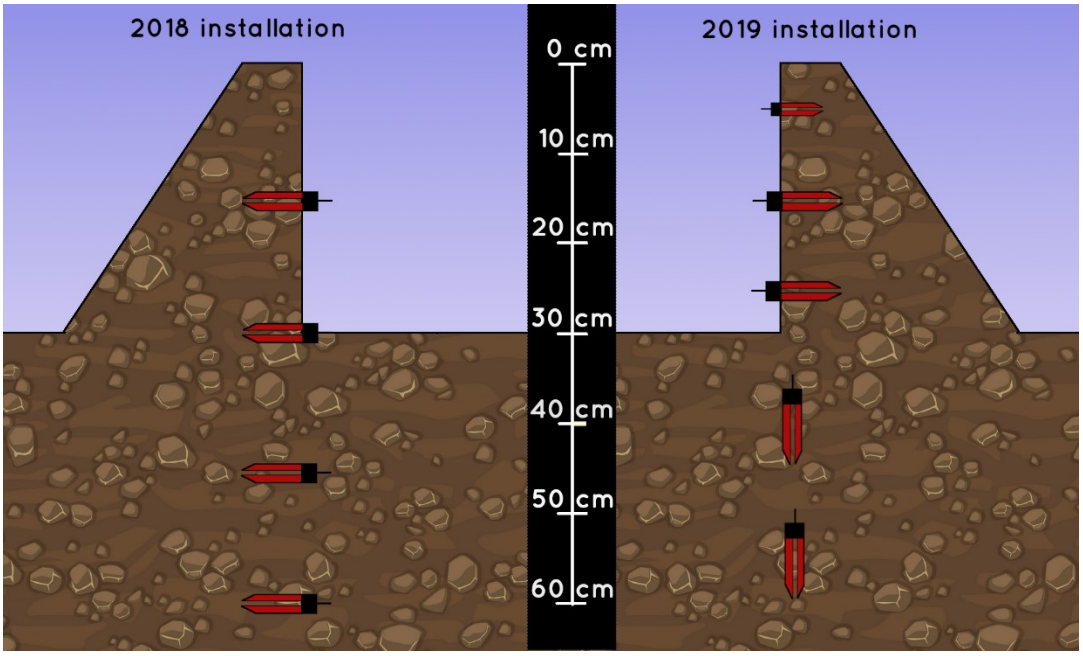

Figure 6: Sensor installation in 2018 & 2019

3.5 Soil Calibration Procedure

A 2334 mL container was used for calculating a calibration line for HOBO 10HS soil moisture smart sensors, Acclima TDR-315 soil moisture sensors and the Stevens HydroGo portable moisture probe. Soil was collected from three sites randomly selected in the study area. The soil was oven-dried and mechanically ground to remove aggregates and homogenize samples. Gravimetric water content was used to adjust the water content of six-1kg soil samples in 0.05 kg/kg increments. The rewetted soil was packed into the container and weighed. One sensor was placed vertically through the center of the sample. Soil moisture observations were taken every 10 secs for 5 mins and averaged at the end of the run. The soil was oven dried to determine bulk density and volumetric water content of the sample. This was repeated with 4 different HOBO 10HS soil moisture smart sensor for a total of 4 runs per GWC increment. The procedure was

repeated with Acclima TDR-315 soil moisture sensors. To calibrate the Stevens HydroGo portable moisture probe, it was inserted into each of the samples at the end of each run and read out three times and averaged. The average of each of the runs was compared to the calculated VWC to create a calibration line for each sensor type. The 10HS calibration line was also used for the EC5 sensor.

3.6 Soil Moisture Survey

Soil moisture surveys were conducted using a Stevens HydroGo portable moisture probe on various dates throughout the 2018 and 2019 growing season (Figure 7). Soil moisture survey data was collected on July 19, Aug 2, Aug 16, and Aug 23 in 2018 and on July 10, July 22, Aug 9, Aug 28, Sept 2, and Sept 17 in 2019. The data was used to produce soil moisture maps for the study area. In 2019, points were added to the soil moisture survey to improve prediction accuracy.

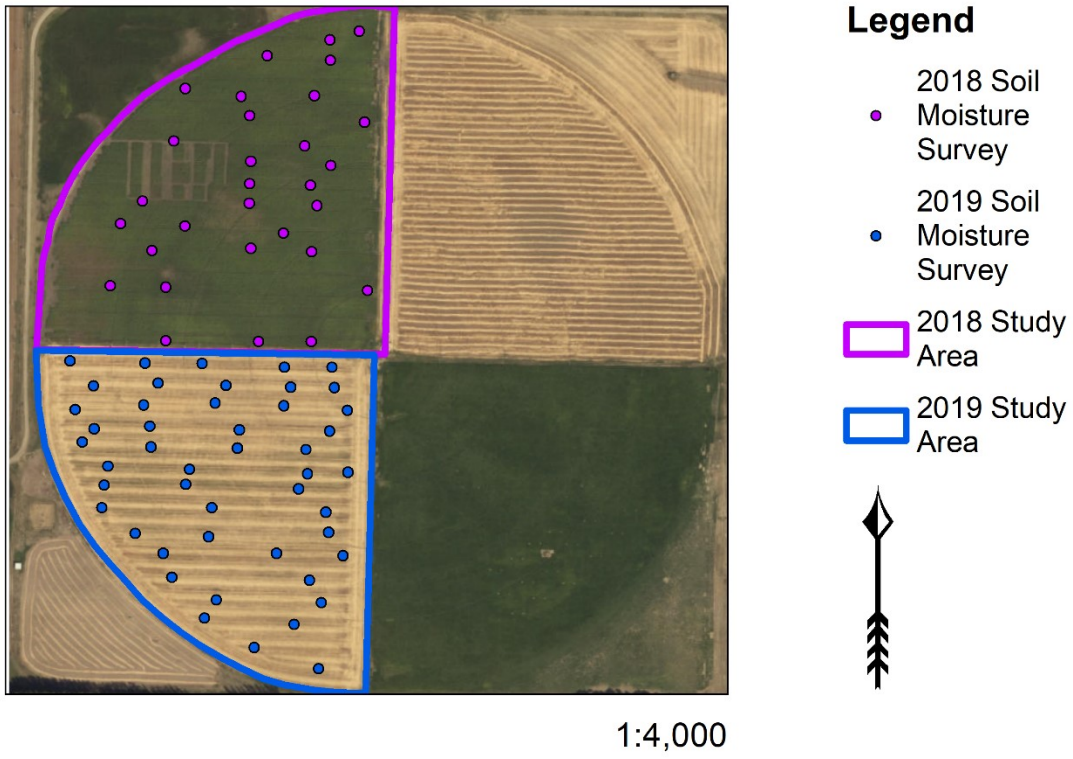

Figure 7: Soil moisture survey points in study areas for 2018 and 2019.

3.7 Weather Observation

Weather observations were used to calculate the reference evapotranspiration. Daily observations were downloaded from the weather station located at AITC (49.6867 N, -112.7449 W, elev. 906.87m ASL) with the current and historical Alberta weather station viewer (Alberta Agriculture and Forestry, 2019). The daily reference evapotranspiration was calculated using the Penman-Monteith procedure in the FAO-56 guideline (Allen et al., 1998, Eq. 1):

$$ET_0 = \frac{0.408\Delta(R_n - G) + \gamma \frac{900}{T + 273} u_2 (e_s - e_a)}{\Delta + \gamma(1 + 0.34u_2)} \quad \text{Eq. 1}$$

Where ET_0 is the reference evapotranspiration (mm/day), R_n is the net radiation at the crop surface (MJ/m^2/day), G is the soil heat flux density (MJ/m^2/day), T is the air temperature at 2 m height (°C), u_2 is the wind speed at 2 m height (m/s), e_s is the saturation vapour pressure (kPa), e_a is the actual vapour pressure (kPa), Δ is the slope vapour pressure curve (kPa/°C), and γ is the psychrometric constant (kPa/°C). The weather station also recorded a reference evapotranspiration which was averaged with the reference evapotranspiration calculated using Eq 1.

$$ET = k_c ET_0 \quad \text{Eq. 2}$$

A linear interpolation of the FAO potato crop coefficients from a semi-arid environment at four growth stages (k_c) was applied to the daily reference evapotranspiration rate (ET_0) using Eq 2. The weather data was also used to calculate growing degree days (McMaster & Wilhelm, 1997, Eq. 3):

$$GDD = \max\left(\frac{T_{max} + T_{min}}{2} - T_{base}, 0\right) \quad \text{Eq. 3}$$

Where GDD is the growing degree days, T_{max} is the daily maximum temperature (°C), T_{min} is the daily minimum temperature (°C), and T_{base} is the base temperature (°C), which was set at 5°C.

3.8 Irrigation Procedure

The AITC irrigation schedule was set by the operator with irrigation applications occurring on Tuesdays and Thursdays, which limited the study to varying the irrigation rate on pre-defined dates. The soil moisture observation equipment did not directly activate the

irrigation system or automatically create an irrigation application via a feedback loop. Instead, the observation data was downloaded 24 hrs prior to a scheduled irrigation event and used to determine the amount of irrigation necessary for each plot. The management strategy for the site-specific irrigation plots used a maximum allowable depletion trigger where the total soil water content was not allowed to fall below MAD. MAD was defined as when soil water falls below 80% of the total available water which corresponded with a VWC of 22.5% or 169 mm/60 cm. Total available water was determined using recommendations from Alberta Agriculture and Forestry using the sandy clay loam parameters for field capacity and permanent wilting point. The MAD and total available water was assumed to be the same throughout all three management zones. Soil moisture data was downloaded the day before a scheduled irrigation event, and it was used to calculate the total water content for the effective root zone. The average daily water loss was calculated using the change in effective root zone water content in the preceding 48-72 hrs without precipitation or irrigation events. The average daily water loss was used to forecast the daily water loss until the next irrigation event. If the water content in the effective root is forecasted to drop below MAD before the next irrigation event (Point B on Figure 8), an irrigation event would be scheduled for the preceding irrigation event (Point A on Figure 8). If the water content in the effective root zone was above the maximum allowable depletion level and not forecast to fall below MAD before the next irrigation event , no irrigation was scheduled for the current event (Point D on Figure 8). The procedure for downloading and forecasting the data would be repeated before the next scheduled irrigation event to account for changing conditions

during the interim period (Point E on Figure 8). The water quantity for an individual irrigation application was calculated by subtracting the VWC calculated in the soil profile from the field capacity VWC (Point C on Figure 8), unless the water requirement exceeded 25 mm, which was the estimated maximum infiltration rate of the soil. When this occurred, the total requirement was divided into two successive applications.

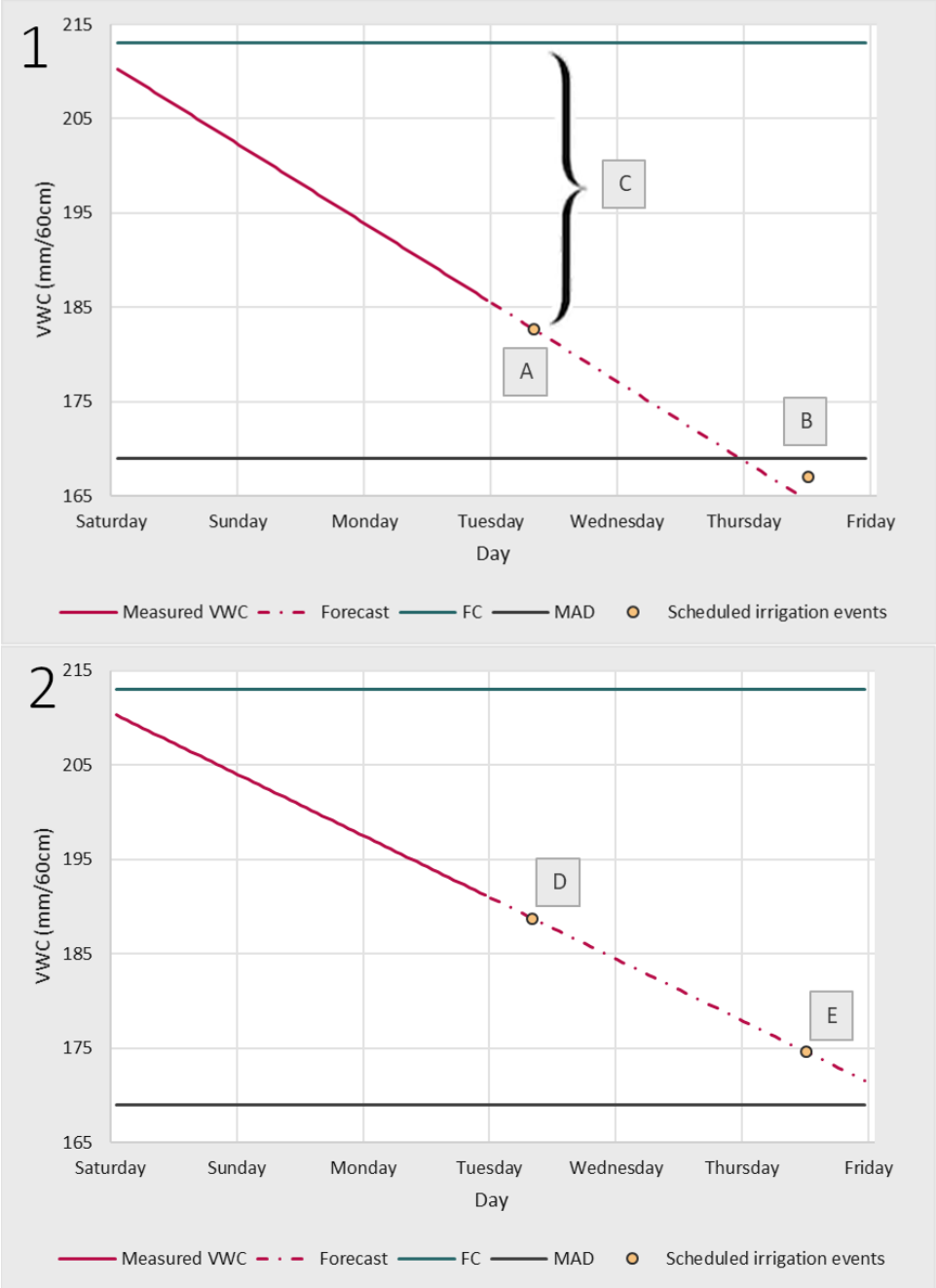

Figure 8: Two example of volumetric water content data used to determine irrigation applications.

3.9 Crop Characteristics

Russet Burbank potatoes were used as the crop for this study in 2018 and 2019. Potato planting occurred on May 17 in 2018 and May 9 in 2019. During the growing period, observations of the potato plants were made to help determine growth stages which were used to determine crop coefficient for ET_c calculation. Harvesting occurred on September 17 in 2018 and September 16 in 2019. Potatoes were harvested from the three SSIM plots and from three management zones under uniform irrigation. Samples consisted of potatoes harvested from a single 3 m row and were replicated three times in each SSIM plot and UIM zone for a total of 18 samples. Harvested potatoes were counted and graded by weight. Five graded categories were used: less than 113 g, 113-170 g, 170-284 g, 284-396 g and greater than 396 g, with marketable potatoes consisting of potatoes between 113 g and 396 g without deformities. The number of potatoes in each category was recorded and each category was weighed to calculate total weight, marketable weight, total numbers, and marketable numbers. A weighted average for the field using the area of each management zone will be used to estimate the average yield for each study area

Statistical analysis of total weight, marketable weight, total numbers, and marketable numbers was conducted using ANOVA multiple means comparison (p=0.05). Differences were evaluated within the set of SSIM samples, within the set of UIM samples and between the SSIM and the UIM samples in each management zone. If significant differences in the means were found, the Fisher pairwise comparison was used to identify groupings.

3.10 GEOSTATISTICAL ANALYSIS

The soil moisture survey data was used to interpolate a continuous surface map using three kriging methods with RStudio (2016) and the following R packages: plyr (Wickham, 2011), dplyr (Wickham et al., 2019), raster (Hijmans, 2019), rgdal (Bivand, Keitt, & Rowlingson, 2019), sp (Bivand, Pebesma, & Gomez-Rubio, 2013), gstat (Gräler, Pebesma, & Heuvelink, 2016), EnvStats (Millard, 2013), rgeos (Bivand. & Rundel, 2019), ithir (Malone, 2016) and MASS (Venables & Ripley, 2002). The Shapiro-Wilk test determined whether the VWC, digital elevation data and ECa were normally distributed. The data collected on July 22, 2019 was interpolated using three kriging methods: ordinary kriging, universal kriging, and co-kriging with elevation and ECa to determine which method resulted in a continuous map with the highest accuracy. Ordinary kriging dissects the variation of a georeferenced dataset into two sources: variation which is random and spatially uncorrelated, and variation that is spatially correlated or autocorrelated. Ordinary kriging uses the model:

$$Z(s) = \mu + \varepsilon'(s) \quad \text{Eq. 4}$$

Where $Z(s)$ is the targeted variable, μ is an unknown constant, and $\varepsilon'(s)$ is a spatially correlated stochastic part of the variation.

Universal kriging adds a deterministic trend component to the spatial correlation and uses the model:

$$Z(s) = \mu(s) + \varepsilon'(s) \quad \text{Eq. 5}$$

Where $Z(s)$ is the estimation of the targeted variable, $\mu(s)$ is a deterministic function, and $\varepsilon'(s)$ is the spatially correlated stochastic part of the variation. Co-kriging uses other georeferenced variables to predict the targeted variable and uses the model:

$$z_0^* = \sum_{i=1}^{n} \lambda_i z_i + \sum_{j=1}^{m} \beta_j t_j + \sum_{k=1}^{p} \gamma_k u_k \quad \text{Eq. 6}$$

Where z_0^* is the estimation of the targeted variable, λ_1, λ_2, … λ_i are the primary variable at n locations, β_1, β_2, … β_j, and γ_k, γ_k … γ_k are the secondary variables at m and p locations, z_1, z_2 … z_i, t_1, t_2 … t_j, and u_1, u_2 … u_k are the weights given to each variable.

Semivariograms were calculated for each method using:

$$\gamma(h) = \frac{1}{2N(h)} \sum_{i=i}^{N(h)} [z(x_i + h) - z(x_i)]^2 \quad \text{Eq. 7}$$

where $\gamma(h)$ is the experimental semivariogram value at distance h, $N(h)$ is the number of sample pairs at distance h, and $z(x_i + h)$ and $z(x_i)$ are two sample points separated by distance h. The semivariograms were used to determine if VWC was spatially correlated and to summarize the spatial variability if spatial correlation were found. If there was evidence of spatial correlation, the data was modelled using each of the kriging methods. The strength of the spatial correlation was determined using the nugget-to-sill ratio (Eq 8).

$$NTS = \frac{C_0}{C + C_0} \quad \text{Eq. 8}$$

The nugget variance (C_0) and the total sill ($C+C_0$) were used to determine the nugget-to-sill ratio (NTS). A ratio of <0.25 was considered strongly spatially dependent, 0.25-0.75 was considered moderately spatially dependent, and >0.75 was considered weakly spatially dependent (Cambardella et al., 1994). Several theoretical semivariogram models were tested for each kriging method: Gaussian, circular, spherical, and exponential. The theoretical models were assessed with model validation using leave-one-out cross validation (LOOCV) procedure. LOOCV is used when an additional independently sampled data set is unavailable and the data which was collected is sparse. LOOCV uses leaves a data point out of a sample *n*, fits the model to the data subset *n-1* and uses this model to predict the left-out data point. The process is repeated for all of *n* to calculate *n* predicted values. The predicted and observed values from *n* repetitions were used to calculate goodness-of-fit statistics using the R package ithir (Malone, 2016) which computed the coefficient of determination, concordance, MSE, RMSE and bias. The coefficient of determination was calculated using:

$$r^2 = \left(\frac{n(\sum xy) - (\sum x)(\sum y)}{\sqrt{(n\sum x^2 - (\sum x)^2)(n\sum y^2 - (\sum y)^2)}} \right)^2 \quad \text{Eq. 9}$$

Where r^2 is the coefficient of determination, n is the number of observations, and x and y is a set of paired observations to be correlated. The concordance was calculated using:

$$\rho_c = \frac{2\rho\sigma_x\sigma_y}{\sigma_x^2 + \sigma_y^2 + (\mu_x - \mu_y)^2} \quad \text{Eq. 10}$$

Where ρ_c is the concordance correlation coefficient, ρ is the correlation coefficient between two variables , σ_x and σ_y is the standard deviation of two variables, σ_x^2 and σ_y^2

are the variances of two variables, and μ_x and μ_y are the means of the two variables. The MSE was calculated using:

$$MSE = \frac{1}{n}\sum_{i=1}^{n}(Y_i - \hat{Y}_i)^2 \quad \text{Eq. 11}$$

Where the MSE is the mean square error, n is the number of observations, Y_i is the observations of a variable, and the $\hat{Y}_i$ are the paired predictions of the variable. The RSME was calculated using:

$$RMSE = \sqrt{MSE} \quad \text{Eq. 12}$$

Where the root mean square error (RMSE) is the square root of the calculated value of Eq. 11. The bias was calculated using:

$$Bias = \frac{y - \hat{y}}{n} \quad \text{Eq. 13}$$

Where $Bias$ is the bias of the predicted values relative to the observed values, y is the observed value, $\hat{y}$ is the predicted value, and n is the number of paired values.

Once these calculations were completed, the most accurate semivariogram model from each kriging method was then compared to each other using LOOCV results to determine which kriging method showed the most accurate predictions.

After the kriging method was determined, the remainder of the soil moisture survey data sets were also processed to create continuous soil moisture prediction maps for 15 cm and 30 cm depths at each date, adjusting the semivariograms to determine if spatial correlations exist in the rest of the data sets. The mean VWC was calculated for each map

and subtracted from the raster values to create a normalized VWC map for each date. The normalized VWC maps were grouped by year and stacked using the R package raster (Hijmans, 2019). A seasonal average and standard deviation were calculated from the stacked normalized VWC maps to visualize seasonal trends. The normalized seasonal average VWC value was calculated for each management zone in both years using ArcMap to determine if there were generalized differences between the management zones soil water content. These comparisons cannot be confirmed with statistical methods due to the lack of independence when using the co-kriging method to create prediction maps.

CHAPTER 4. RESULTS

4.1 WEATHER

4.1.1 2018

Daily average temperature from the planting date to the harvest date in 2018 was 16.5˚C during the growing period, with a cumulative 1448 growing degree days. Evapotranspiration ranged from 0 to 8.8 mm/day with 98 out of 123 days after planting exceeding 0 (Figure 9). There was 115 mm of rainfall during this period. Uniform prescriptions were 12 or 15 mm per irrigation event in 29 events, totaling 440 mm of irrigation throughout the growing season (Figure 10A). Each SSIM plot received different irrigation amounts: SSIM1-2018 received 217 mm in 15 irrigation events, SSIM2-2018 received 250 mm in 17 irrigation events, and SSIM3-2018 received 393 mm in 25 irrigation events (Figure 10B).

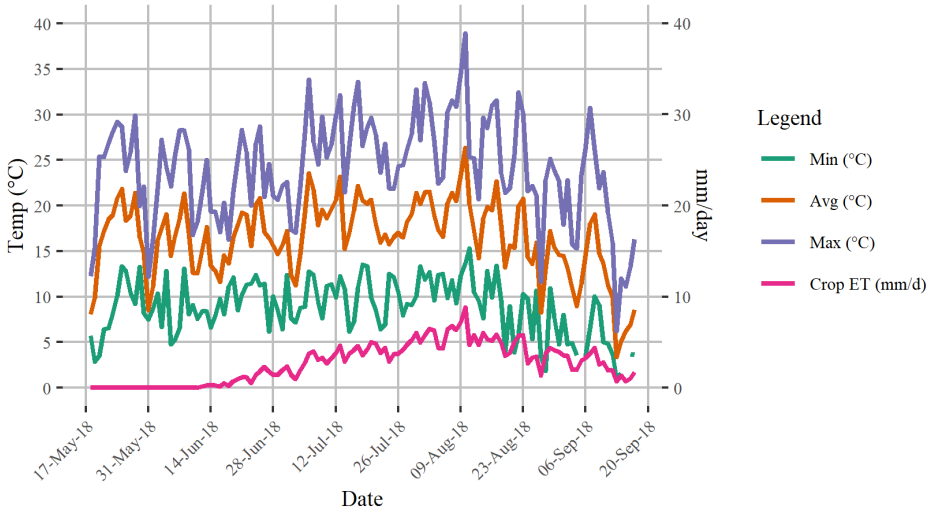

Figure 9: Temperature and evapotranspiration data from May 17, 2018 to Sept 17, 2018.

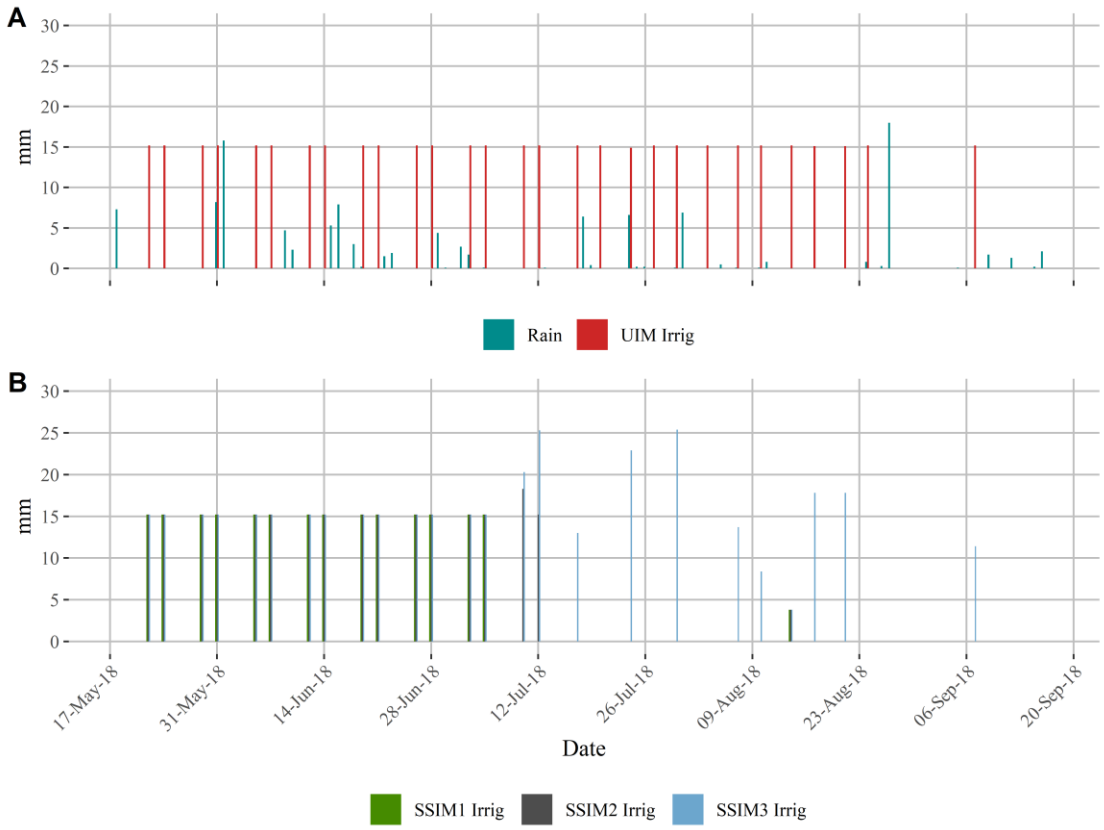

Figure 10: Rainfall and irrigation data collected from May 15, 2018 to Sept 17, 2018

4.1.2 2019

Daily average temperature from the planting date to the harvest date in 2019 was 15.4˚C with a cumulative 1434 growing degree days in 2019. Evapotranspiration ranged from 0 to 7.2 mm/day with 98 out of 131 days after seeding exceeding 0 (Figure 11). There was 154 mm of rainfall. Uniform prescriptions ranged from 6 mm to 18 mm per irrigation event in 24 events, totaling 354 mm of irrigation throughout the growing season (Figure 12A). SSIM1-2019 received 278 mm in 19 irrigation events, SSIM2-2019 received 207 mm in 14 irrigation events, and SSIM3-2019 received 213 mm in 14 irrigation events (Figure 12B).

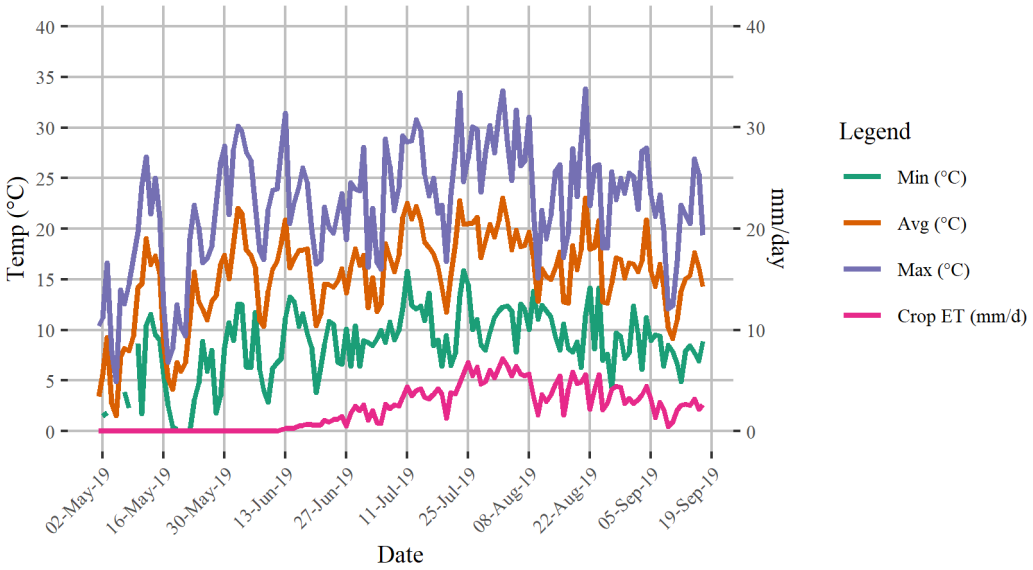

Figure 11: Temperature and evapotranspiration data from May 1, 2019 to Sept 17, 2019

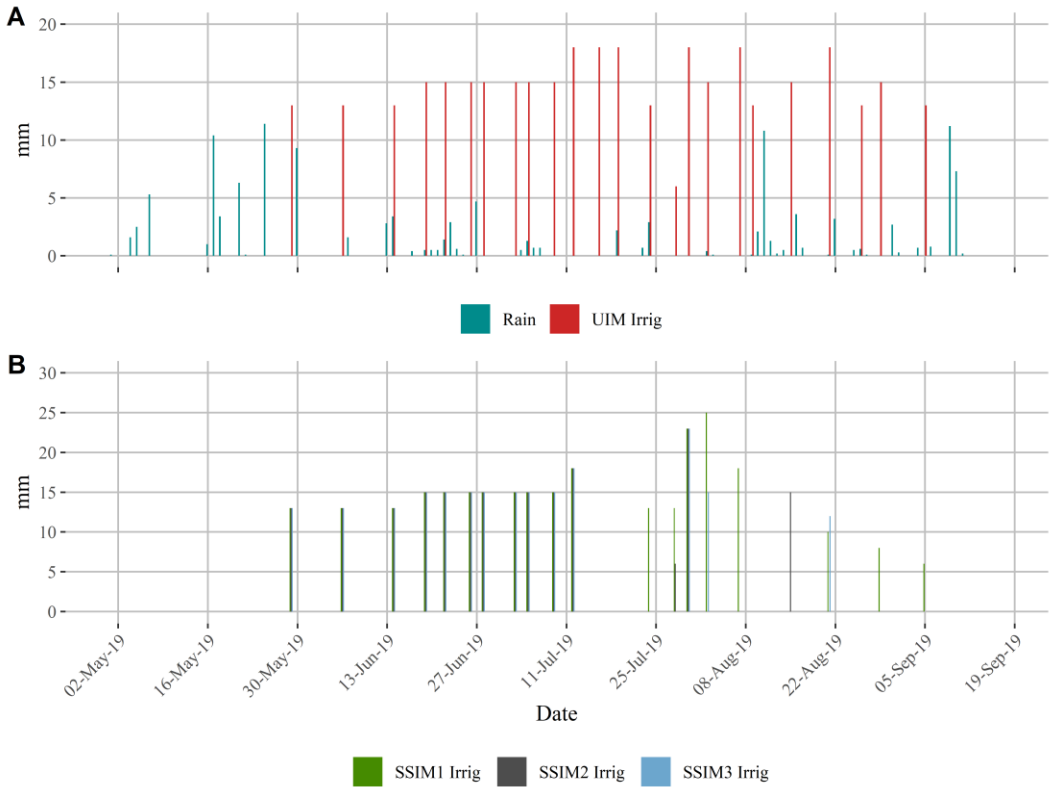

Figure 12: Rainfall and irrigation data collected from May 1, 2019 to Sept 17, 2019

4.2 Soil Moisture

4.2.1 Calibration of Soil Moisture Sensors

Calibration lines were calculated for to calibrate soil moisture sensor data to the soil in the study area. The Stevens calibration was used on Stevens HydroGo portable moisture probe survey data, the Acclima calibration line was used on Acclima TDR-315 soil moisture sensors, and HOBO calibration line was used on HOBO EC5 and 10HS soil moisture sensors (Figure 13). The best Acclima and HOBOware soil calibration functions were a polynomial trendline with coefficient of determination (R^2) of 0.9901 and 0.9894 respectively (Table 3). The best Hydra Probe soil moisture calibration was a linear trendline with a coefficient of determination (R^2) of 0.9857 (Table 3).

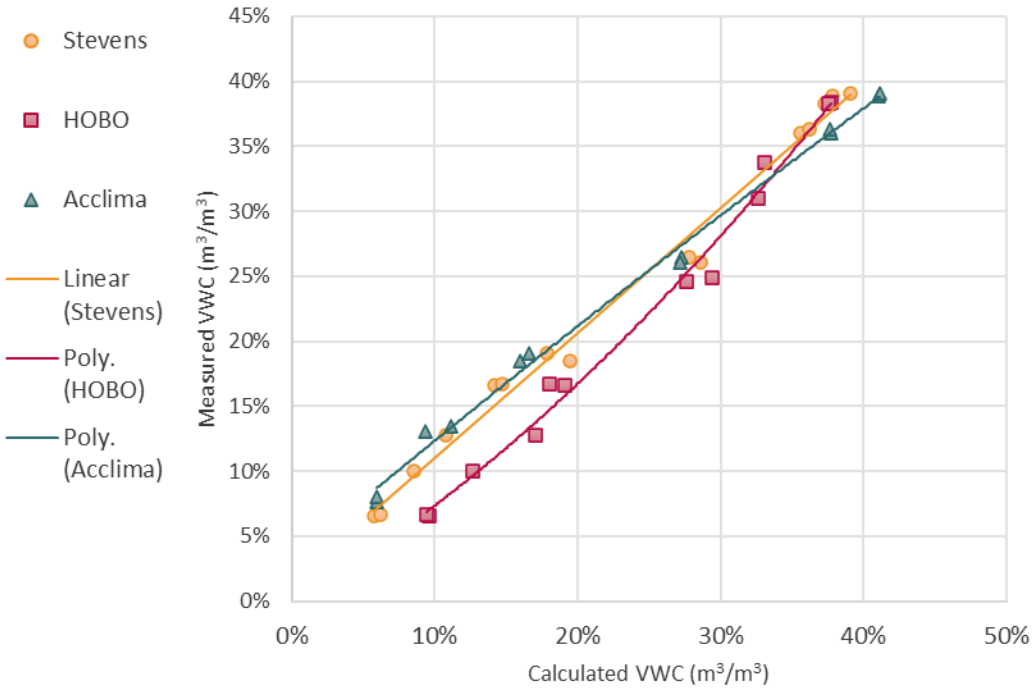

Figure 13: Calibration data used for correcting moisture sensor data and the corresponding trend lines

Table 3: Calibration equations used to correct moisture sensor data

SENSOR	EQUATION	R^2
HOBOWARE	$y = 1.0106x^2 + 0.634x$	0.9894
STEVENS	$y = 1.0095x$	0.9857
ACCLIMA	$y = -8 \times 10^{-5}x^2 + 0.0125x$	0.9901

4.2.2 2018

Uniform irrigation

VWC data obtained from UIM monitoring stations is presented in Figure 14. Soil moisture sensors for management zone 1 and 2 were connected to the same data logger and stopped reading from August 7 to September 7. The data logger used for management zone 3 was broken before installation and was not replaced until August 23.

The soil profile in UIM1 and UIM2 displayed a high VWC in the 60 cm sensor and a noticeably lower VWC in each subsequent sensor. The soil profile in UIM3 differed where the daily differences between sensors was small and varied throughout the dataset. Data collected from UIM3 falls between 0.204 and 0.271 for all sensors while management zone 1 and 2 show distinct differences between each of the sensors with no overlap between sensors at different depths. The precipitation events observed in UIM 1 and 2 did not generate an observable response in individual sensors at all depths (Figure 14), but precipitation did generate a well-defined response in UIM3.

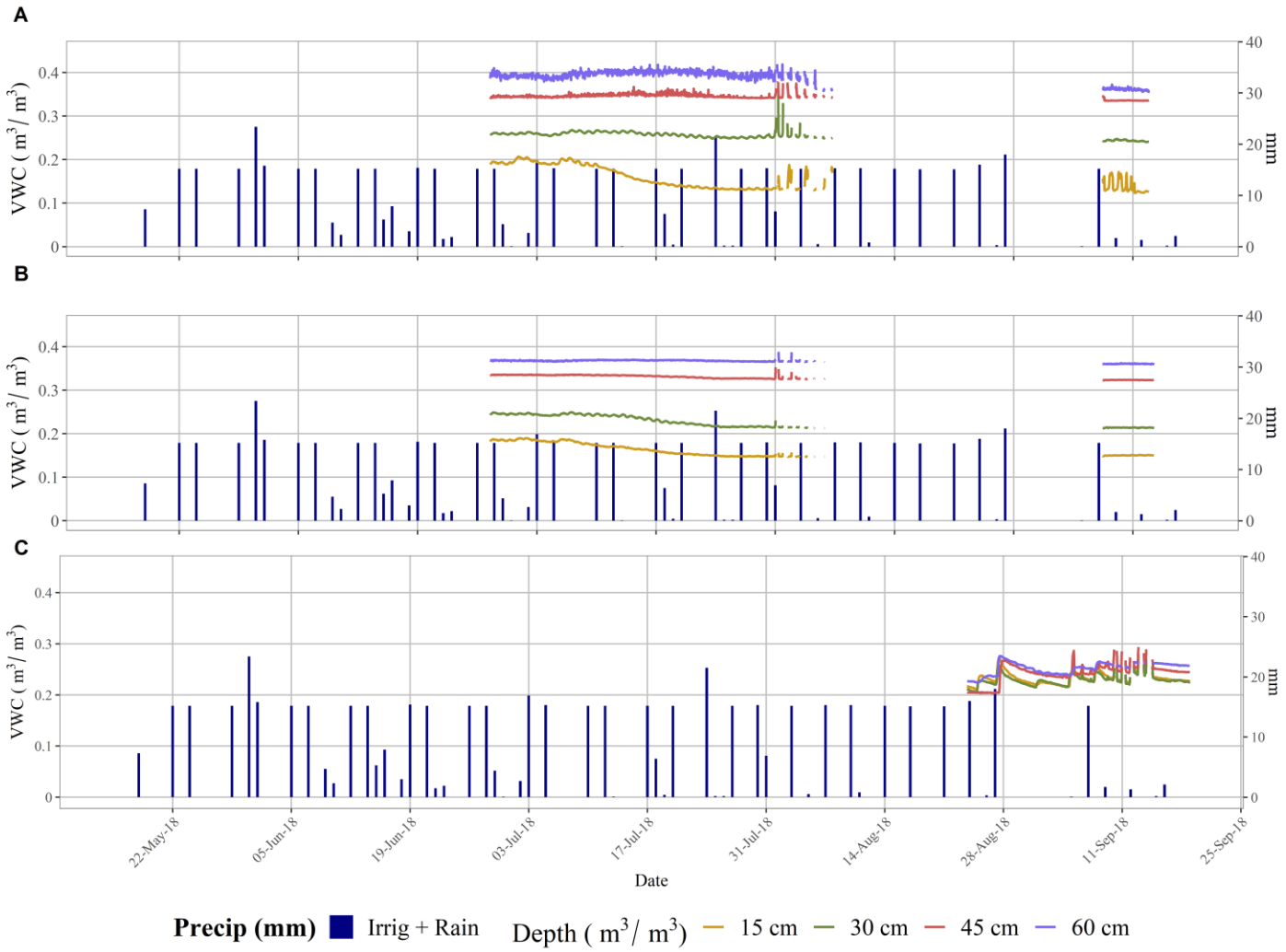

Figure 14: Volumetric water content (m^3/m^3) from soil moisture sensors installed at 15, 30, 45, and 60 cm depth for UIM1 (A), UIM2 (B), and UIM3 (C) under uniform irrigation applications, 2018

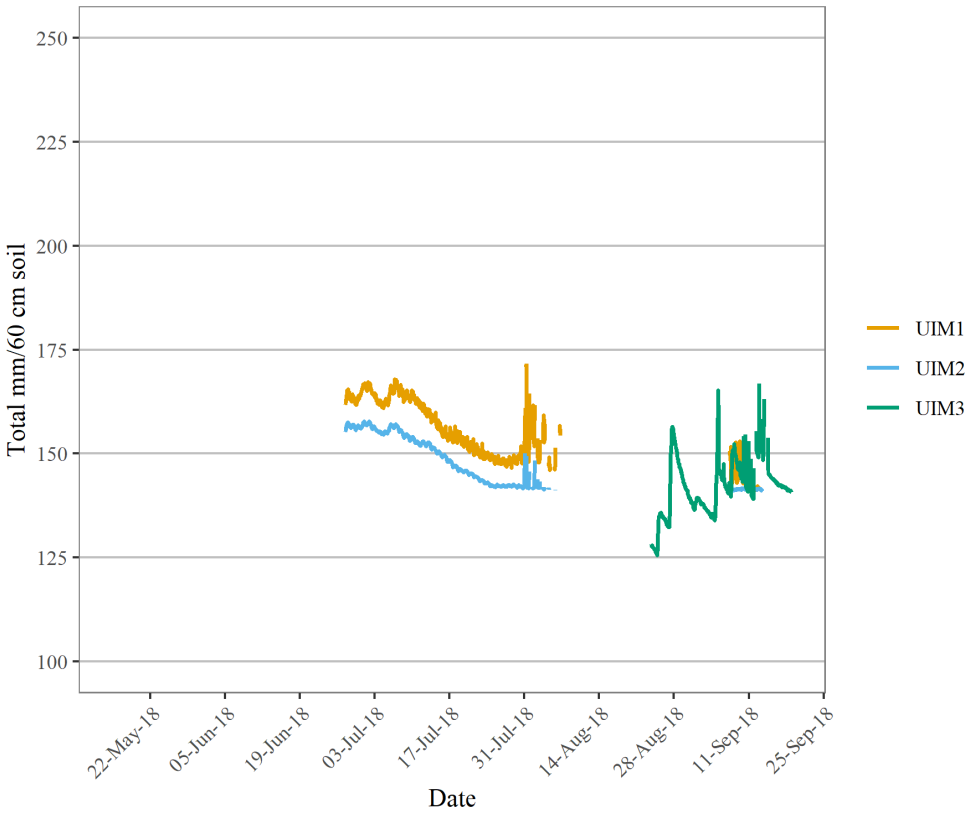

Figure 15: Total volumetric water content (mm/60 cm soil) in three management zones (UIM1, UIM2, UIM3) receiving uniform irrigation applications, 2018

Soil moisture sensor readings were analyzed for precipitation responses occurring within the 48 hours after a precipitation event (Table 4). In UIM1, between 48% and 65% of the total average VWC response to precipitation events occurred in the first 24 hours, and in UIM2, between 51% and 53% of the response was occurred in the first 24 hrs. Although the response was higher in the lower depths (Table 4), the response was not observable in most precipitation events and occurred when the response was high in all sensors. In the shorter monitoring period for UIM3, the first 24 hours contained between 64% and

95% of the precipitation responses in the 48 hours following an event. Some of these responses fall below the margin of error of the Acclima sensors. The peak of the VWC response to precipitation lagged by between 1 and 24 hours after the recorded event, with the quickest response occurring in the shallow sensors and longer lags observed in each depth. This was a result of the attenuation of the infiltration front in the soil profile and the revolution time of the irrigation pivot. Despite the low signal response in the sensors after precipitation, a response was observable when the data was integrated, and soil moisture calculated for the 60 cm profile (Figure 15).

The VWC levels in the 30 cm profile began a gradual decrease after July 12 in UIM2, while in UIM1, a decrease was observed in the period immediately before the sensor malfunction. A decrease in UIM3 could not be confirmed. The VWC levels in the 45 and 60 cm depths exhibited a gradual, constant decrease over the monitoring period in both UIM1 and UIM2. Over the monitoring period, the 60 cm soil moisture profile became drier in UIM1, with losses of 8%, 4%, 2%, and 4% in the 15, 30, 45, and, 60 cm sensors respectively, for a total of -22mm/60cm in the entire profile. The soil moisture profile in UIM2 also became drier over the monitoring period, with losses of 4%, 3%, 1%, and 1% in the 15, 30, 45 and 60 cm sensors respectively, for a total of -15mm/60cm in the entire profile. The soil moisture profile in UIM3 displayed an increase in soil moisture over the monitoring period, with a gain of 4%, 4%, 7%, and 5% in the 15, 30, 45, and 60 cm sensors respectively, for a total of +28 mm/60cm in the entire profile.

Table 4: Average precipitation response with standard deviation (st dev) to uniform irrigation in the UIM1, UIM2, and UIM3 monitoring stations.

	UIM1		UIM2		UIM3	
SENSOR	Average	St dev	Average	St dev	Average	St dev
15 CM	0.026	0.037	0.006	0.003	0.034	0.018
30 CM	0.010	0.002	0.007	0.003	0.029	0.026
45 CM	0.000	0.002	0.005	0.001	0.036	0.030
60 CM	0.005	0.009	0.012	0.004	0.020	0.012

Site-specific irrigation

The soil profiles in SSIM 1 and 2 featured a high VWC in the 45 cm and 60 cm sensor which frequently were undiscernible from one another. The sensors installed in 15 cm and 30 cm in SSIM 1 diverged from each other with the 15 cm sensor showing much lower VWC readings for the entire time series, while the 30 cm sensor readings were consistently between those from the 15 cm and the 45/60 cm sensors. The soil moisture levels in the top 30 cm of the soil profile in SSIM 2 overlapped, with the 15 cm sensor readings diverging from the 30 cm readings after a precipitation event and converging back to the 30 cm VWC in the subsequent days. The SSIM3 soil moisture levels in the top 30 cm of the soil profile also exhibited this divergence/convergence trend, and the 45 cm and 60 cm sensors displayed a small difference between the VWC readings throughout the time series.

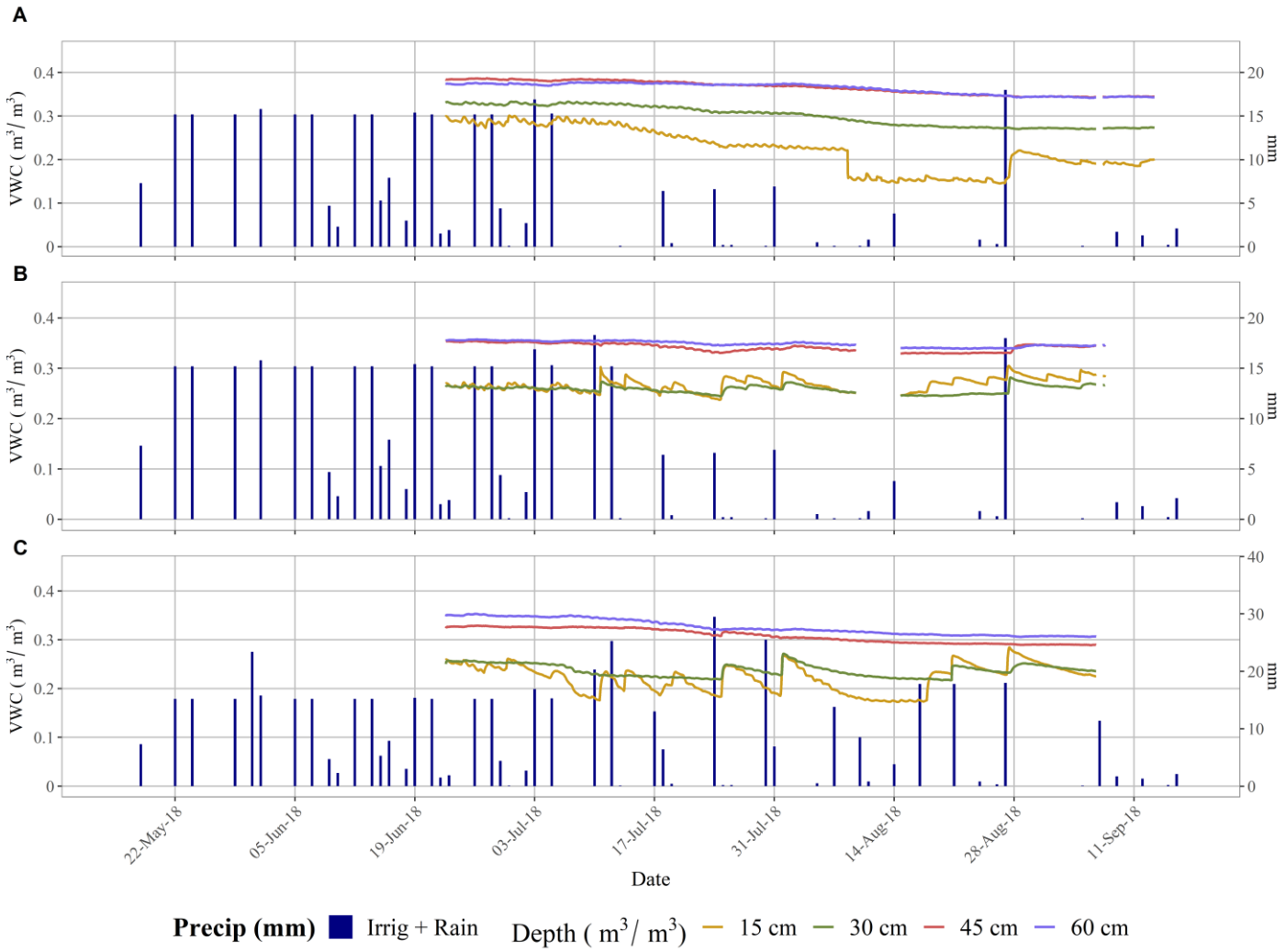

Figure 16: Volumetric water content (m^3/m^3) from soil moisture sensors installed at 15, 30, 45, and 60 cm depth for SSIM1 (A), SSIM2 (B), and SSIM3 (C) under variable rate irrigation applications, 2018

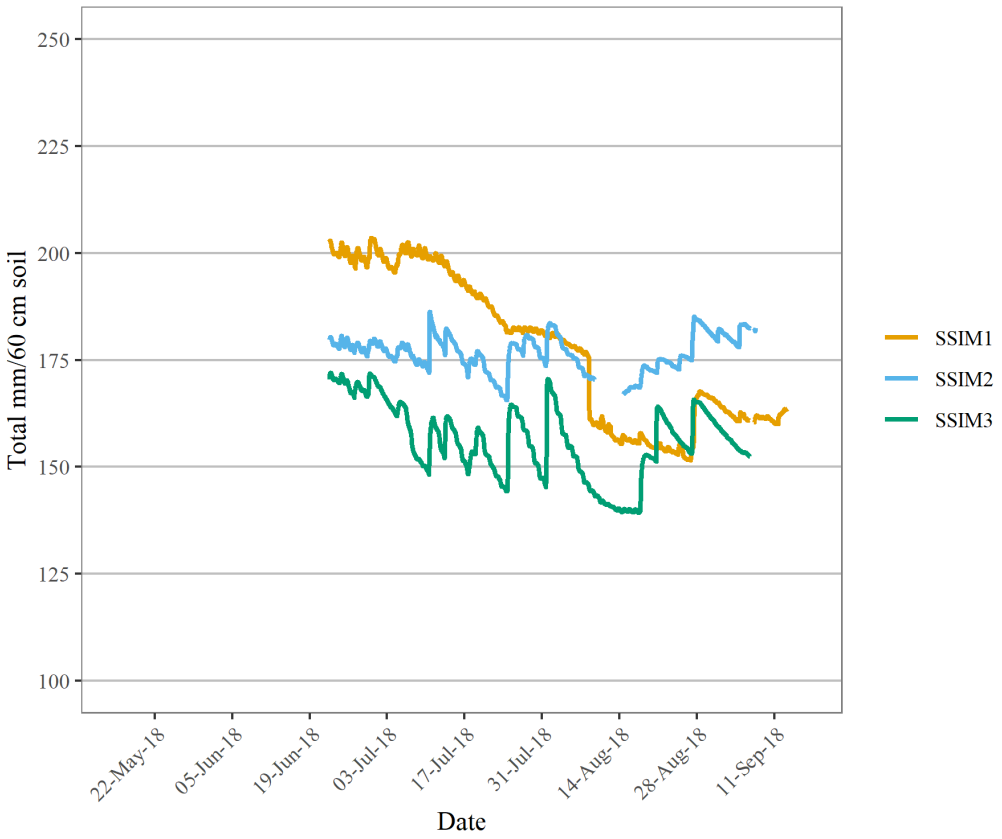

Figure 17: Total volumetric water content (mm/60 cm soil) in three management zones receiving variable rate irrigation applications, 2018

The precipitation events observed in SSIM 1 generated an observable response in the 15 and 30 cm sensors early in the season (Figure 16). However, a malfunction was discovered when a response was not observed after several rainfall events and a new sensor was installed on Aug 8, leading to a decline in VWC readings. A good response to the Aug 27 precipitation event was observed, which was also the last precipitation event greater than 2mm. Precipitation events in SSIM 2 and 3 did generate good responses in the individual sensors except in SSIM 3 after Aug 1, where precipitation events became unobservable and after Aug 17 in SSIM 2, where responses unassociated with

precipitation are observed. Soil moisture sensor readings were analyzed for precipitation responses occurring within the 48 hours after a precipitation event (Table 5). In SSIM1, between 73% and 98% of the total average VWC response to precipitation events occurred in the first 24 hours, and in SSIM2, between 71% and 100% of the response was occurred in the first 24 hrs. In SSIM 3, between 61% and 99% of the total average VWC response was observed in the first 24 hours. Some of these responses fall below the margin of error of the HOBO sensors. The 60 cm sensor in all plots, there was often no direct link to an increase in VWC and precipitation. The peak of the VWC response to precipitation lagged by between 1 and 24 hours after the recorded event, with the quickest response occurring in the shallow sensors and longer lags observed in each depth. This was a result of the attenuation of the infiltration front in the soil profile and the revolution time of the irrigation pivot. The responses to precipitation were also observable when the data was integrated, and soil moisture calculated for the 60 cm profile (Figure 17).

In SSIM1, the VWC levels in all sensors displayed a gradual decrease beginning shortly after installation. This continued for the entire monitoring period for the 30, 45 and 60 cm sensors. The 15 cm sensor displayed a distinct drop when a malfunctioning sensor was replaced and a steep incline after the Aug 27 precipitation event. The VWC levels in SSIM2 were generally maintained in the 15 and 30 cm sensors with increases after precipitation, while the 45 and 60 cm sensors displayed a small gradual decrease during the monitoring period. In SSIM3, a small gradual decrease was observed in all sensors over the monitoring period with increases observed after precipitation in the 15 and 30

cm sensors. Over the monitoring period, the 60 cm soil moisture profile became drier in SSIM1, with losses of 10%, 6%, 4%, and 3% in the 15, 30, 45, and, 60 cm sensors respectively, for a total of -39mm/60cm in the entire profile. A small increase in soil moisture within the 60 cm profile in UIM2 over the monitoring period was observed, with a change of +1%, 0%, -1%, and -1% in the 15, 30, 45 and 60 cm sensors respectively, for a total of +2mm/60cm in the entire profile. The soil moisture profile in SSIM3 displayed a decrease in soil moisture over the monitoring period, with losses of 3%, 2%, 4%, and 4% in the 15, 30, 45, and 60 cm sensors respectively, for a total of -19 mm/60cm in the entire profile.

Table 5: Average precipitation response with standard deviation (st dev) to uniform irrigation in the SSIM1, SSIM2, and SSIM3 monitoring stations.

	SSIM1		SSIM2		SSIM3	
SENSOR	Average	St dev	Average	St dev	Average	St dev
15 CM	0.029	0.022	0.028	0.016	0.045	0.023
30 CM	0.003	0.002	0.016	0.011	0.023	0.015
45 CM	0.001	0.000	0.004	0.005	0.003	0.003
60 CM	0.002	0.001	0.000	0.000	0.000	0.000

4.2.3 2019

Uniform irrigation

The soil profile in UIM1 displayed a high, frequently overlapping VWC in the 30, 45, and 60 cm sensor and a noticeably lower VWC in the 15 cm sensor. The soil profile in UIM2 displayed high VWC levels in the 30 cm sensor throughout the monitoring period, an intermediate VWC level which frequently overlaps in the 45 and 60 cm sensors, and a drier VWC level in the 15 cm sensor. In the beginning of the season, the soil profile in

UIM3 showed distinct differences in the daily data between the 15 and 30, and 45 and 60 cm sensors, followed by a period where sensor data at the different depths converge and diverge rapidly, with a stabilization of VWC and less difference between any of the monitored soil layers than what was observed at the beginning of the monitoring period.

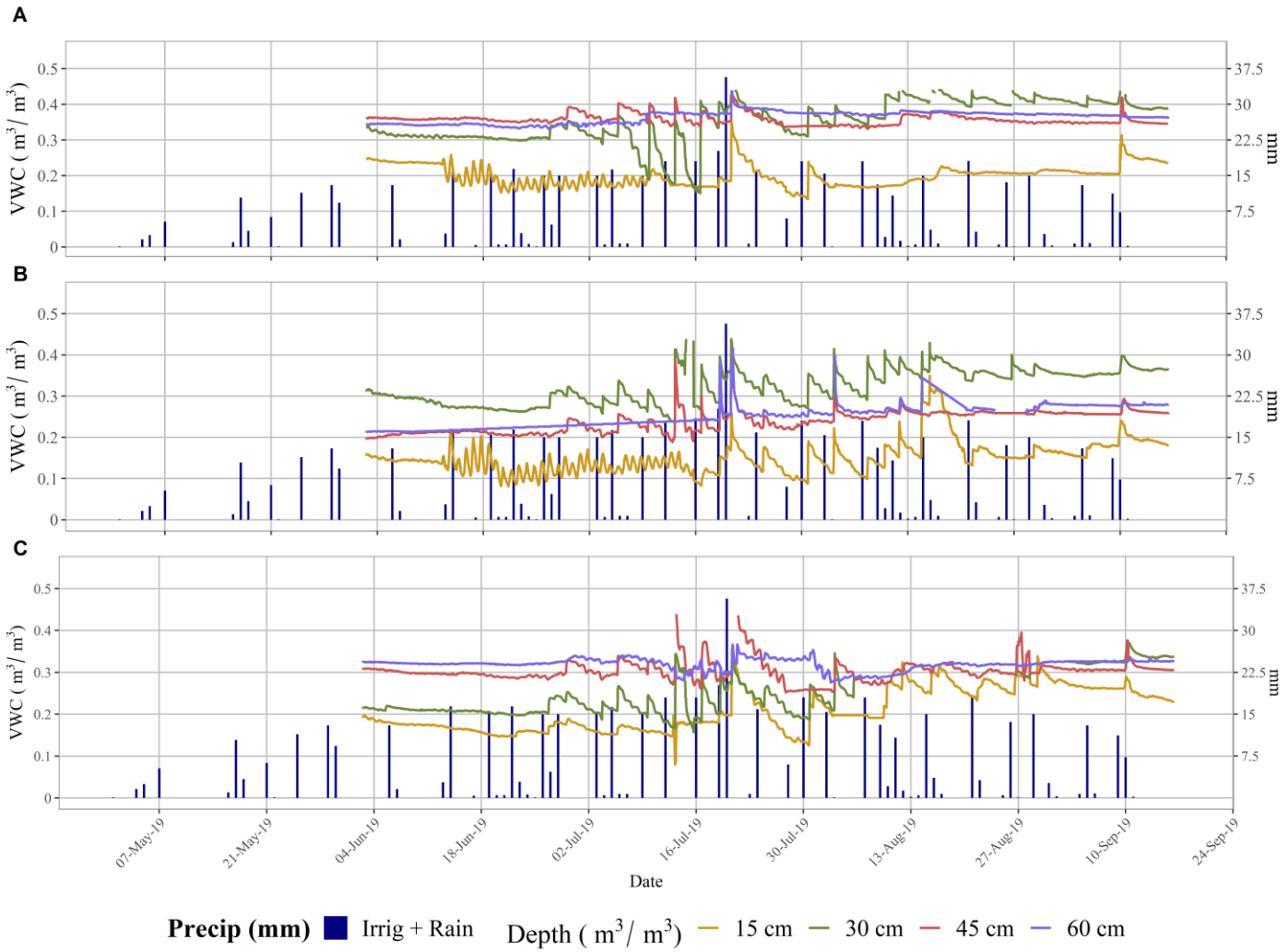

Figure 18: Volumetric water content (m^3/m^3) from soil moisture sensors installed at 5-15 cm (15 cm), 20-30 cm (30 cm), 35-45 cm (45 cm) and 50-60 cm (60 cm) depths for UIM1 (A), UIM2 (B), and UIM3 (C) under uniform

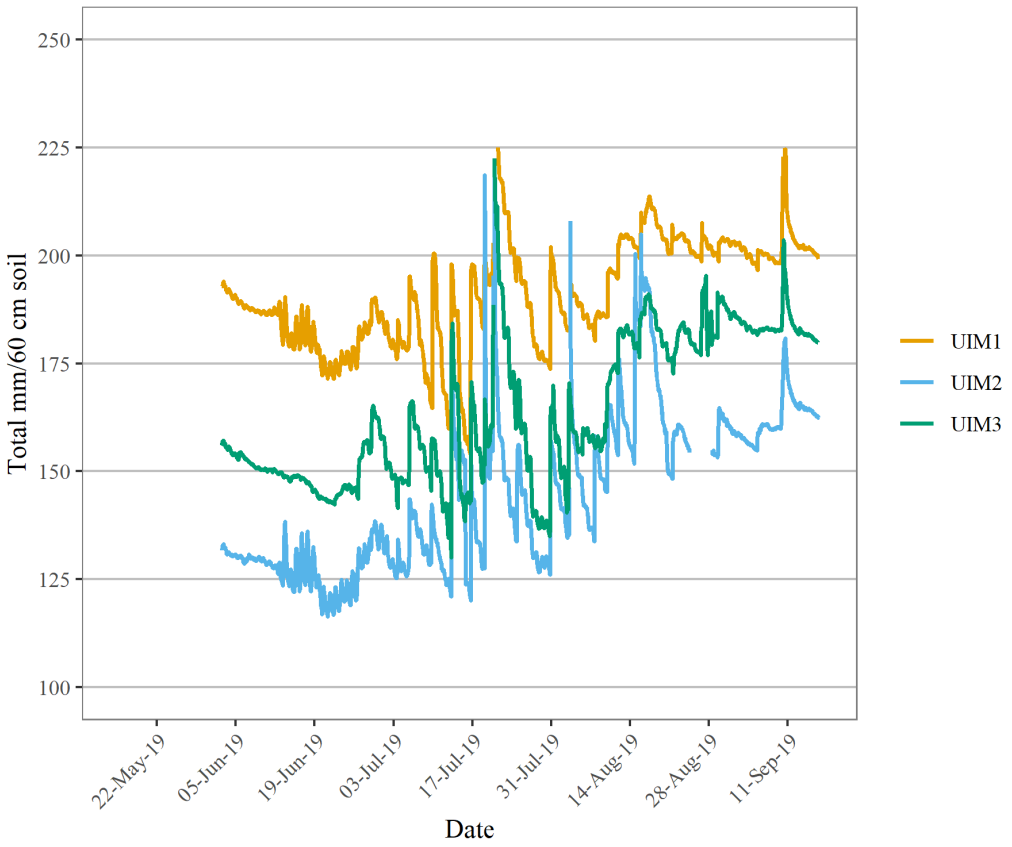

Figure 19: Total volumetric water content (mm/60 cm soil) in three management zones receiving uniform irrigation applications, 2019

The precipitation events observed in UIM 1, 2, and 3 did not always generate an observable response in individual sensors at all depths at the beginning of the monitoring period but responses improved as the season progressed (Figure 18). Soil moisture sensor readings were analyzed for precipitation responses occurring within the 48 hours after a precipitation event (Table 6). Between 76% and 85% of the total average VWC response to precipitation events occurred in the first 24 hours in UIM1, between 61% and 77% in UIM2, and between 53% and 75% in UIM3. The peak of the VWC response to precipitation lagged by between 1 and 24 hours after the recorded event, with the

quickest response occurring in the shallow sensors and longer lags observed in each depth. This was a result of the attenuation of the infiltration front in the soil profile and the revolution time of the irrigation pivot. Responses to precipitation were more easily observable when the data was amalgamated and the total soil moisture for the 60 cm profile was calculated (Figure 19).

Over the monitoring period, the 60 cm soil moisture profile showed a slight increase in VWC throughout the monitoring period in UIM1, with losses of 1% in both the 15 cm and 45 cm sensor, and gains of 6% and 2% in the 30 and 60 cm sensors respectively, for a total of +7mm/60cm. The soil moisture profile in UIM2 also showed an increase of VWC over the monitoring period, with gains of 2%, 5%, 6%, and 7% in the 15, 30, 45 and 60 cm sensors respectively, for a total of +30mm/60cm. The soil moisture profile in UIM3 displayed an increase in soil moisture over the growing period contained to the top 30 cm, with gains of 4% and, 12% in the 15 and 30 cm sensors respectively and no change in the 45 and 60 cm sensor, for a total of +23 mm/60cm.

Table 6: Average precipitation response with standard deviation (st dev) to uniform irrigation in the UIM1, UIM2, and UIM3 monitoring stations in 2019.

	UIM1		UIM2		UIM3	
SENSOR	Average	St dev	Average	St dev	Average	St dev
15 CM	0.042	0.048	0.082	0.034	0.040	0.042
30 CM	0.078	0.056	0.076	0.054	0.061	0.059
45 CM	0.028	0.028	0.064	0.100	0.061	0.075
60 CM	0.012	0.015	0.061	0.134	0.026	0.033

Site-specific irrigation

Irrigation scheduled before July 20 was undifferentiated between SSIM and the UIM due to a technical problem with uploading the prescriptions. This resulted in the SSIM plots receiving the uniform irrigation prescription rather than the site-specific prescription until July 20.

The soil profile in SSIM1 and 3 displayed four distinct VWC layers during the uniform irrigation period (May 15 – July 20), where the 5 cm, 15 cm, and the 60 cm sensors remain within a consistently separated VWC range which is drier in the 5 cm sensor and wettest in the 60 cm sensor. The 15 cm, 25 cm, and 40 cm sensors showed intermediary VWC levels, where the VWC observations in 25 cm and 40 cm sensors were often overlapping and consistently higher than the 15 cm sensor.

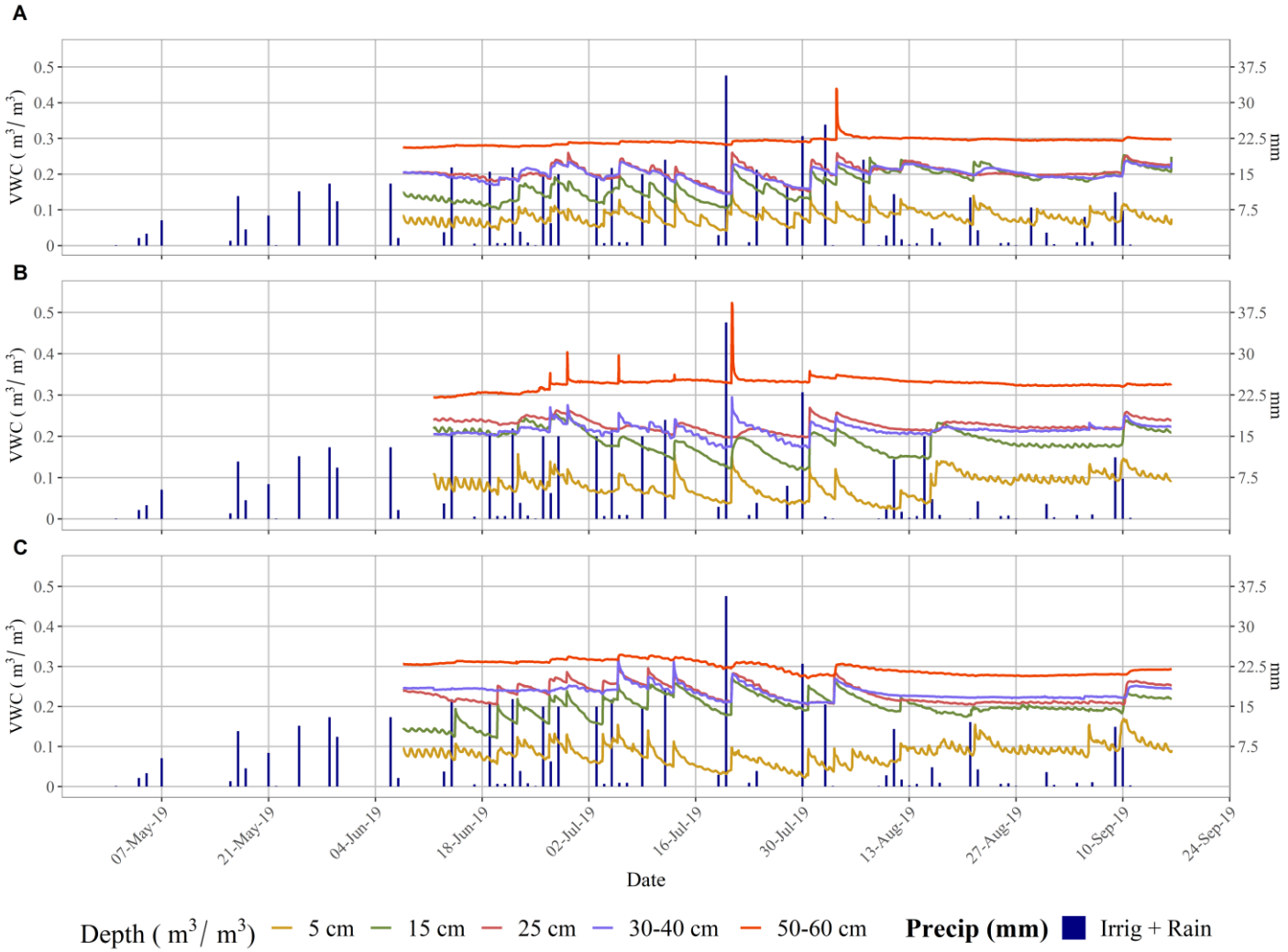

Figure 20: Volumetric water content (m^3/m^3) from soil moisture sensors installed at 5, 15, 25, 30-40, and 50-60 cm depth for SSIM1 (A), SSIM2 (B), and SSIM3 (C) under variable rate irrigation applications, 2019

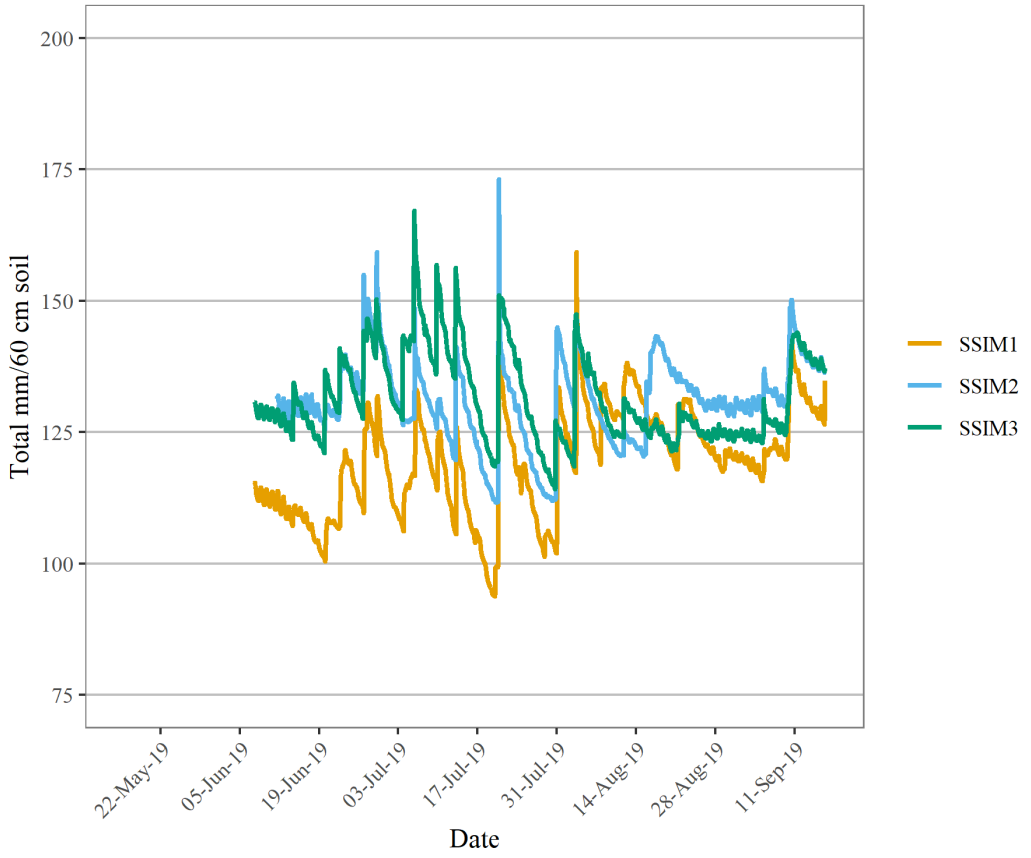

Figure 21: Total volumetric water content (mm/60 cm soil) in three management zones receiving variable rate irrigation applications, 2019.

After site-specific irrigation prescriptions were applied on July 20, the VWC readings in the 15 cm sensor joined the range of VWC in the 25 and 40 cm sensors and began overlapping, with the 5 cm VWC remaining consistently drier and the 60 cm VWC consistently wetter. In SSIM2, VWC in the 15, 25, and 40 cm sensor frequently overlapped with a noticeably lower VWC in the 5 cm sensor and higher VWC in the 60 cm sensor. This trend persisted throughout the monitoring period, with a slight divergence occurring in the middle of the series from the 15 cm sensor where VWC was drier than the VWC in the 25 cm and 40 cm sensor. The precipitation events observed in SSIM 1, 2,

and 3 generated an observable response in individual sensors at depths greater than 40 cm during most of the events and an occasional response in 60 cm sensor (Figure 20). Soil moisture sensor readings were analyzed for precipitation responses occurring within the 48 hours after a precipitation event (Table 7). In SSIM1, between 88% and 97% of the total average VWC response to precipitation events occurred in the first 24 hours. In SSIM2, between 84% and 98% of the total average VWC response to precipitation events occurred in the first 24 hours. In SSIM3, between 85% and 95% of the total average VWC response to precipitation events occurred in the first 24 hours. The peak of the VWC response to precipitation lagged by between 1 and 24 hours after the recorded event, with the quickest response occurring in the shallow sensors and longer lags observed in each depth. This was a result of the attenuation of the infiltration front in the soil profile and the revolution time of the irrigation pivot. Responses to precipitation were more easily observable when the data was amalgamated and the total soil moisture for the 60 cm profile was calculated (Figure 21).

Over the monitoring period, the 60 cm soil moisture profile showed a slight increase in VWC throughout the monitoring period in SSIM1, with increases of 2% in both the 25 cm and 50-60 cm sensor, and 7% and 1% in the 15 and, 30-40 cm sensors respectively, with no change in VWC observed in the 5 cm sensor, for a total of +14mm/60cm in the entire profile. The soil moisture profile in SSIM2 also showed an increase of VWC over the monitoring period, with gains of 2% in both the 5 cm and 30-40 cm sensors, 3% in the 50-60 cm sensor and no change in the 15 cm and 25 cm sensors, for a total of +9mm/60cm in the entire profile. The soil moisture profile in SSIM3 displayed an increase in soil

moisture over the growing period contained to the top 30 cm, with gains of 1%, 8% and, 2% in the 5, 15 and, 25 cm sensors respectively, no change in the 30-40 and a 1% decrease in the 50-60 cm sensor, for a total of +9mm/60cm in the entire profile.

Table 7: Average precipitation response with standard deviation (st dev) to uniform irrigation in the SSIM1, SSIM2, and SSIM3 monitoring stations in 2019.

	UIM1		UIM2		UIM3	
SENSOR	Average	St dev	Average	St dev	Average	St dev
5 CM	0.067	0.027	0.070	0.039	0.071	0.026
15 CM	0.055	0.031	0.039	0.031	0.061	0.031
30 CM	0.037	0.033	0.018	0.021	0.039	0.024
45 CM	0.027	0.023	0.042	0.033	0.031	0.031
60 CM	0.013	0.036	0.040	0.059	0.007	0.007

4.3 POTATO YIELD

4.3.1 2018

The average total weight and marketable weight of potato samples collected in SSIM 3 was significantly higher than those collected from SSIM 1 and 2 (Table 8, Table 9). The total number of potatoes collected from SSIM 1, 2 and 3 were all significantly different from each other and the highest number of potatoes per m^2 was found in SSIM 2, followed by SSIM 1 and SSIM 3. The number of marketable potatoes per m^2 were not significantly different in any SSIM plot. UIM 1 samples were significantly higher than UIM 2 and 3 in total weight, marketable weight, total number, and marketable number. Samples collected from SSIM 1 had statistically fewer marketable potatoes and had significantly lower total and marketable weights when compared to UIM 1. SSIM 2

samples had significantly lower marketable weight and marketable numbers, and significantly higher total number of potatoes per m^2 when compared to UIM 2. Samples collected from SSIM 3 had significantly higher total weight and marketable weight, with significantly higher total numbers and marketable numbers when compared with UIM 3. The average yield for the study area using SSIM yields was determined to be 6.2 kg/m^2 using weighted total yield and 3.9 kg/m^2 using weighted marketable yield, while UIM yields calculated 6.9 kg/m^2 using weighted UIM total yields and 5.0 kg/m^2 using weighted marketable yield.

Table 8: Statistical analysis of the total weight and total numbers of potato yields in 2018 using ANOVA (p = 0.05). Within treatment indicates comparisons between UIM1, UIM2 and UIM3 potato yields or between SSIM1, SSIM2, and SSIM3 potato yields. Between treatment indicates comparisons between the paired SSIM and UIM treatment within each management zone. Means with different letters are significantly different.

	Total weight (kg/m^2)			Total number (#/m^2)		
	Mean	Within treatment	Between treatment	Mean	Within treatment	Between treatment
SSIM1	5.4	a	a	61.1	a	A
SSIM2	6.2^{ae}	a	b	67.6^{b}	b	B
SSIM3	7.2^{b}	b	c	55.2^{c}	c	C
UIM1	8.0^{c}	c	d	60.3^{a}	d	A
UIM2	6.1^{de}	d	b	49.4^{d}	e	D
UIM3	6.4^{d}	d	e	47.0^{d}	e	E

Table 9: Statistical analysis of the marketable weight and marketable numbers of potato yields in 2018 using ANOVA (p = 0.05). Within treatment indicates comparisons between UIM1, UIM2 and UIM3 potato yields or between SSIM1, SSIM2, and SSIM3 potato yields. Between treatment indicates comparisons between the paired SSIM and UIM treatment within each management zone. Means with different letters are significantly different.

	Marketable weight (kg/m^2)			Marketable number (#/m^2)		
	Mean	Within treatment	Between treatment	Mean	Within treatment	Between treatment
SSIM1	3.0[a]	a	a	17.7[a]	a	A
SSIM2	3.4[a]	a	b	21.5[a]	a	B
SSIM3	5.7[b]	b	c	30.8[a]	a	C
UIM1	6.0[c]	c	d	31.7[b]	b	D
UIM2	4.4[d]	d	e	25.0[c]	c	E
UIM3	4.3[d]	d	f	22.1[c]	c	F

4.3.2 2019

Samples collected from SSIM 1 and 2 were statistically similar in total yield, marketable yield, total number, and marketable number (Table 10, Table 11). Total weight of samples collected from SSIM 3 were significantly lower from SSIM 1 and 2. SSIM 1 samples were significantly lower from samples from UIM 1 in all variables used to assess potato samples, SSIM 2 samples were significantly higher than samples collected from UIM 2 in all variables, and SSIM 3 samples were significantly lower than samples collected from UIM3 in all variables.

Table 10: Statistical analysis of the total weight and total numbers of potato yields in 2019 using ANOVA (p = 0.05). Within treatment indicates comparisons between UIM1, UIM2 and UIM3 potato yields or between SSIM1, SSIM2, and SSIM3 potato yields. Between treatment indicates comparisons between the paired SSIM and UIM treatment within each management zone. Means with different letters are significantly different.

	Total weight (kg/m^2)			Total number (#/m^2)		
	Mean	Within treatment	Between treatment	Mean	Within treatment	Between treatment
SSIM1	7.5^{a}	a	a	74.3^{a}	a	a
SSIM2	7.3^{a}	a	b	72.0^{a}	a	b
SSIM3	5.3^{b}	b	c	50.1^{b}	b	c
UIM1	9.2^{c}	c	d	75.6^{c}	c	d
UIM2	6.0^{d}	d	e	69.8^{c}	c	e
UIM3	7.0^{e}	e	f	69.6^{c}	c	f

Table 11: Statistical analysis of the marketable weight and marketable numbers of potato yields in 2019 using ANOVA (p = 0.05). Within treatment indicates comparisons between UIM1, UIM2 and UIM3 potato yields or between SSIM1, SSIM2, and SSIM3 potato yields. Between treatment indicates comparisons between the paired SSIM and UIM treatment within each management zone. Means with different letters are significantly different.

	Marketable weight (kg/m^2)			Marketable number (#/m^2)		
	Mean	Between treatment	Within treatment	Mean	Between treatment	Within treatment
SSIM1	4.9^{a}	a	a	28.3^{a}	a	a
SSIM2	4.6^{a}	a	b	27.5^{a}	a	b
SSIM3	3.3^{b}	b	c	18.8^{b}	b	c
UIM1	6.5^{c}	c	d	35.9^{c}	c	d
UIM2	3.2^{d}	d	e	19.0^{d}	d	e
UIM3	4.2^{d}	d	f	25.5^{cd}	cd	f

Samples collected from UIM 1, 2 and 3 had significantly different total weights. UIM 1 samples had significantly different marketable weights when compared to UIM 2 and 3.

UIM 1 marketable numbers were significantly different from UIM 2. Total numbers between UIM 1, 2 and 3 showed no significant difference. The average yield for the study area using SSIM yields was determined to be 6.2 kg/m^2 using weighted total yield and 3.9 kg/m^2 using weighted marketable yield, while UIM yields calculated 6.8 kg/m^2 using weighted UIM total yields and 4.0 kg/m^2 using weighted marketable yield.

4.4 GEOSTATISTICS

4.4.1 Field statistics

Elevation and ECa is summarized in Table 12. ECa and elevation 2018 uses data confined by the boundary of the 2018 quarter section and ECa and elevation 2019 uses the boundary of the 2019 quarter section (Figure 4).

Table 12: Statistical summary for soil apparent electrical conductivity (ECa) and elevation for data within the 2018 and 2019 quarter sections. Minimum, mean, and maximum values, standard deviation, count, skewness (skew), kurtosis (kurt), and the Anderson-Darling (A-D) normality p-value are summarized.

	MIN	MEAN	MAX	ST.DEV	COUNT	SKEW	KURT	A-D
ECA 2018 (DS/M)	0.618	1.983	4.689	0.850	6900	0.675	0.218	>0.001
ECA 2019 (DS/M)	0.314	1.676	6.011	0.738	53628	0.977	1.370	>0.001
ELEVATION 2018 (M)	903.6	905.2	907.3	0.6	6900	0.181	0.173	>0.001
ELEVATION 2019 (M)	904.3	908.8	911.9	1.9	51012	-0.526	-0.727	>0.001

Elevation and ECa data in 2018 and 2019 fit normal distribution with p-values of >0.001. The correlation between ECa and elevation at shared points was calculated for each quarter section and was determined to be 0.14 in 2018 and -0.49 in 2019.

4.4.2 Comparison of kriging methods

The volumetric water content, ECa, and elevation point data used for a comparison of ordinary and universal kriging and co-kriging methods were determined to be normal (Table 13).

Table 13: Statistical summary of volumetric water content obtained on July 22, 2019 (VWC), apparent electrical conductivity (ECa), and elevation. Minimum, mean, and maximum values with standard deviation, skewness (SKEW), kurtosis (KURT) and the p-value of the Shapiro-Wilk normality test (SHAPIRO) are summarized.

	MIN	MEAN	MAX	ST.DEV	SKEW	KURT	SHAPIRO
VWC	28.3	37.4	46.4	4.6	-0.1324	-0.9068	0.2213
ECa	0.922	1.873	3.327	0.658	0.3901	-0.8537	0.0588
Elevation	904.6	907.9	911.2	1.8	-0.1874	-1.1794	0.0513

Volumetric water content shows a moderate negative correlation to elevation and a very weak positive correlation with ECa. ECa shows a moderate negative correlation to elevation (Table 14)

Table 14: Correlation between volumetric water content (VWC) obtained from the soil moisture survey conducted on July 22, 2019, apparent electrical conductivity (ECa) and elevation, n = 40.

	VWC	ECa	Elevation
VWC	1	0.086	-0.408
ECa	0.086	1	-0.288
Elevation	-0.40	-0.288	1

Two co-kriging methods were compared due to the low correlation of ECa. One method would use both elevation and ECa, and the other would use elevation alone.

Ordinary and universal kriging and co-kriging methods were used to create a prediction map from the soil water content observations obtained during the soil moisture survey on July 22, 2019. Four semivariogram models were used to fit the data for each method: spherical, exponential, Gaussian, and circular (Appendix 2, page 113). It was determined that the exponential model provided the best fit for the data in all four methods.

Comparing the leave-on-out cross-validation results for all kriging methods, the co-kriging method had the highest combined precision and accuracy when predicting soil water content, but the differences between the kriging methods were small (Table 15).

Table 15: Leave-one-out cross-validation results for ordinary (ORD) and universal kriging (UNI) and co-kriging methods using elevation and ECa (CO 2var) and elevation alone (CO 1var) as secondary variables. Semivariogram models were constructed using soil moisture as the primary variable and the exponential model as the theoretical semivariogram. The co-efficient of determination (R^2), concordance, mean square error (MSE), root mean square error (RMSE) and bias were used as assessment parameters

	R^2	CONCORDANCE	MSE	RMSE	BIAS
ORD	0.38	0.58	12.76	3.57	0.10
UNI	0.32	0.54	14.63	3.82	-0.10
CO 2VAR	0.38	0.59	12.77	3.57	0.01
CO 1VAR	0.38	0.58	12.93	3.60	0.03

The co-kriging method shared a coefficient of determination of 0.38 with the ordinary kriging method, but the ordinary kriging method had a higher bias, 0.10 compared to 0.01 indicating a higher tendency to overestimate predictions compared to co-kriging.

The universal kriging method was the least accurate, with a coefficient of determination of 0.32 and underestimated soil water predictions with a bias of -0.10. This method had the highest RMSE, displaying the lowest precision of the three models. All three kriging methods had a weak correlation between the predicted and observed soil water content, indicating that approximately 60% of the soil moisture variation is unexplained. Additional data points in the soil moisture survey may have helped capture more of the spatial variation, but it may also be explained by additional factors which were unmeasured in this study. Heil and Schmidhalter (2012) found that bulk density is a key factor in predicting soil water content at a larger scale, with organic matter also improving predictions. All predicted values of soil water content fell within the range of the original observations in all three methods.

4.4.3 Geostatistical evaluation of soil moisture surveys

Volumetric water content data was surveyed at 15 and 30 cm depths on four dates in 2018 and six dates in 2019 (Table 16). Sampling was increased in the 2019 surveys which is reflected in the higher sampling numbers in 2019. The soil moisture survey on Sept 2, 2019 was interrupted due to equipment failure, resulting in a partial survey covering approximately half of the extent of previous surveys.

The data obtained from 15 cm displayed lower minimum, mean and maximum values than the data obtained from 30 cm from the same location in both years. The VWC data generated from the July 19, 2018 soil moisture survey at 15 cm depth could not be determined to be sampled from a normal population, as were the soil moisture surveys conducted on July 22 and Aug 9, 2019 at the 15 cm depth, and on September 2 and 17,

2019 at 30 cm depth. All other soil moisture surveys collected data that was determined to be sampled from a normal population (Table 16).

*Table 16: Statistical summary for soil volumetric water content surveys collected during the 2018 and 2019 growing seasons. Minimum (MIN), mean, and maximum (MAX) values, standard deviation, count, skewness (SKEW), kurtosis (KURT), and the Shapiro-Wilk normality p-value are summarized. * indicates data that is not from a normally distributed population*

DATE	DEPTH	MIN	MEAN	MAX	ST.DEV	COUNT	SKEW	KURT	SHAPIRO
19-JUL-18	15 cm	16.5	28.7	34.3	4.3	27	-1.09	1.09	0.027*
	30 cm	30.4	38.6	45.1	4.0	27	-0.62	-0.62	0.062
02-AUG-18	15 cm	15.3	23.3	31.6	4.1	32	-0.24	-0.23	0.397
	30 cm	21.8	31.4	39.3	4.6	32	-0.35	-0.76	0.271
16-AUG-18	15 cm	11.2	20.3	30	5.0	29	0.14	-0.58	0.608
	30 cm	16.7	27.6	39.7	5.7	29	0.24	-0.02	0.842
23-AUG-18	15 cm	13.5	21.9	27.8	3.1	30	-0.48	0.62	0.757
	30 cm	22.1	28.8	35.3	3.4	30	0.26	-0.52	0.611
10-JUL-19	15 cm	16.0	23.5	32.1	3.2	44	0.47	0.68	0.487
	30 cm	26.8	37.9	46.6	4.6	44	-0.13	-0.78	0.210
22-JUL-19	15 cm	21.9	26.6	42.5	4.3	40	1.94	4.48	<0.001*
	30 cm	28.3	37.4	46.4	4.6	40	-0.13	-0.91	0.221
09-AUG-19	15 cm	11.2	19.0	41.7	5.7	68	1.49	3.53	<0.001*
	30 cm	22.8	32.4	43.3	5.0	68	0.24	-0.56	0.367
28-AUG-19	15 cm	16.2	24.7	36.4	4.4	47	0.63	0.55	0.225
	30 cm	22.2	36.8	45.7	5.4	47	-0.75	0.40	0.083
02-SEP-19	15 cm	19.0	26.3	34.6	4.2	30	0.17	-0.91	0.578
	30 cm	20.0	37.9	45.9	5.7	30	-1.08	1.94	0.044*
17-SEP-19	15 cm	6.0	14.5	21.1	3.8	49	-0.06	-0.82	0.386
	30 cm	12.3	21.6	33.2	5.0	49	0.63	0.15	0.047*

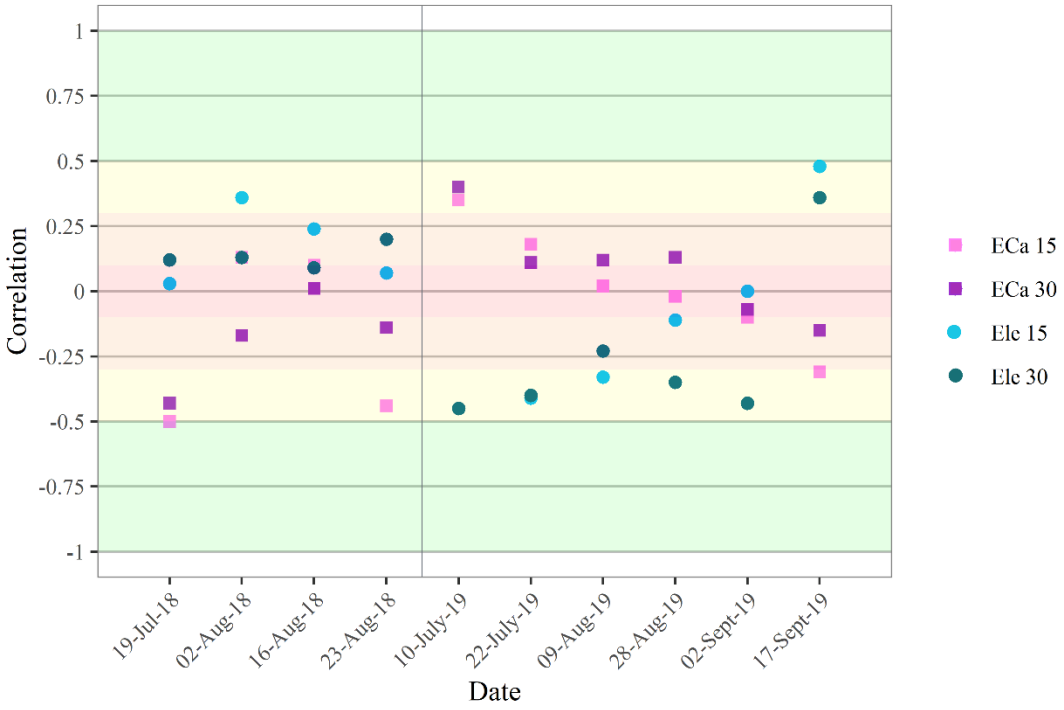

Figure 22: Correlation between volumetric water content, and elevation and soil apparent electrical conductivity (ECa) using survey data collected on various dates in 2018 and 2019. Elevation and ECa was correlated to VWC data collected at 15 cm depth (ECa 15, Ele 15) and 30 cm depth (ECa 30, Ele 30). Background colours indicate four levels used to assess correlations: high (green), moderate (yellow), low (orange), and negligible (red).

In 2018, correlations between VWC and ECa, and VWC and elevation show no consistent pattern at either the 15 or 30 cm depth (Figure 22). ECa had a generally negative correlation with VWC which ranged from a negligible to moderate relationship and elevation had a positive relationship which ranged between negligible and moderate. In 2019, the change in correlational relationships between ECa and VWC and elevation and VWC showed an observable trend (Figure 22). A trend was observed in the relationship between VWC and elevation in 2019 at 15 cm which began as a moderate, negative correlation and ended with a moderate, positive correlation with a generally linear relationship. The 30 cm VWC and elevation also displays this trend, but Aug 28 and Sept 2

had correlations which fall outside the trend. A similar, albeit reversed, trend in the relationship between VWC and ECa was observed. The trend between the 30 cm VWC and ECa was less pronounced and less linear than the 15 cm trend.

*Table 17: Model parameters for semivariograms fitted to volumetric water content (VWC) (%) and used in co-kriging. VWC data collected in 2018 and 2019 and is the primary variable. The theoretical model used, partial sill (C), nugget (C_0), total sill ($C+C_0$), nugget-to-sill ratio and range are summarized. * indicates semivariograms created from data that could not be confirmed as normal.*

VWC SEMIVARIOGRAM MODELS							
DATE	DEPTH	MODEL	C	C_0	$C + C_0$	NUGGET-TO-SILL RATIO	RANGE (M)
7/19/18	15 cm*	Exp	16.1	5.5	21.6	0.256	81.3
	30 cm	Exp	11.0	6.9	17.9	0.387	74.5
8/02/18	15 cm	Sph	16.5	1.9	18.4	0.103	81.3
	30 cm	Exp	12.7	12.9	25.6	0.505	82.5
8/16/18	15 cm	Exp	31.4	8.7	40.1	0.216	81.7
	30 cm	Exp	14.1	14.6	28.8	0.509	81.7
8/23/18	15 cm	Sph	7.9	2.6	10.5	0.247	81.5
	30 cm	Cir	6.3	6.9	13.2	0.524	72.5
7/10/19	15 cm	Exp	12.8	1.7	14.5	0.115	82.2
	30 cm	Sph	13.7	8.7	22.4	0.390	82.2
7/22/19	15 cm*	Sph	17.4	1.3	18.7	0.071	78.1
	30 cm	Exp	30.5	1.4	31.9	0.043	81.9
8/09/19	15 cm*	Exp	31.4	8.7	40.1	0.216	81.7
	30 cm	Exp	14.1	14.6	28.8	0.509	81.7
8/28/19	15 cm	Exp	19.6	6.0	25.6	0.234	78.4
	30 cm	Exp	29.0	10.6	39.6	0.267	81.4
9/02/19	15 cm	Sph	18.4	1.0	19.5	0.054	73.9
	30 cm*	Sph	31.8	6.4	38.3	0.168	73.9
9/17/19	15 cm	Exp	17.3	1.3	18.6	0.070	62.9
	30 cm*	Exp	18.6	7.9	26.4	0.298	81.2

Several theoretical semivariogram models were used for the spatial interpretation of the empirical semivariograms and cross-variograms created using collocated VWC, ECa and elevation: exponential, spherical, and circular (Table 17). The semivariogram models

were applied to each dataset and the model displaying the highest spatial autocorrelation was chosen to predict VWC. Thirteen datasets used the exponential model to describe the semivariogram, six which used the spherical model, and one which used the circular model. The fitted semivariograms had ranges between 62.9 m and 82.5 m, which were shared with the ECa and elevation semivariograms and the related cross-variograms.

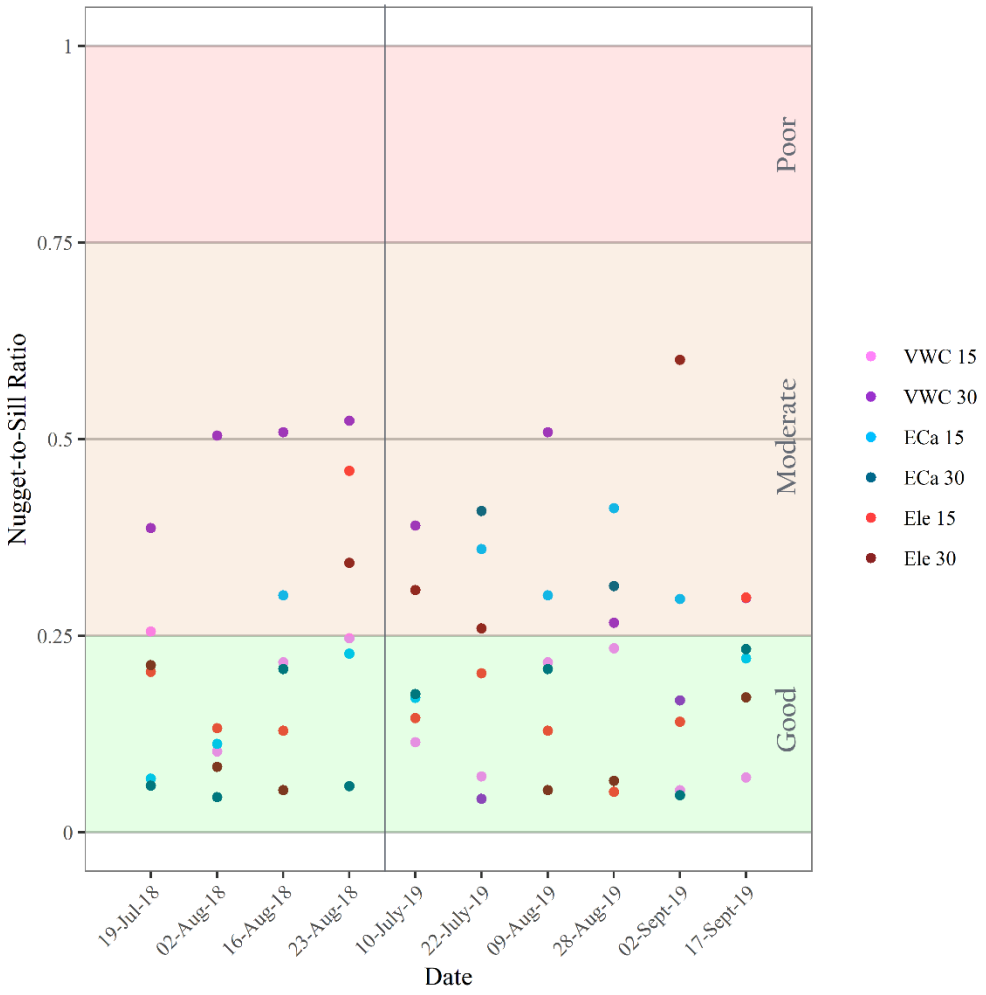

Figure 23: Nugget-to-sill ratios for theoretical semivariograms modelled using co-kriging methods. VWC was used as the primary variable and ECa and elevation as secondary variables. Background colours indicate three levels used to assess nugget-to-sill ratios: good (green), moderate (orange), and poor (red).

Spatial autocorrelation of VWC data was variable in both years but exhibited good to moderate spatial autocorrelation. In 2018, the 15 cm VWC observations had an average nugget-to-sill ratio of 0.206 while 30 cm VWC observations had an average of 0.481. In 2019, VWC data collected at 15 cm had an average nugget-to-sill ratio of 0.109, while VWC at 30 cm had an average of 0.239. These values indicate that VWC data collected in 2018 exhibited less spatial autocorrelation than the data collected in 2019 and also that higher spatial autocorrelation was obtained from VWC collected at 15 cm. Data obtained from 15 cm displayed high spatial dependence except on July 19, 2018, while VWC data from 30 cm ranged from high to moderate. The collocated ECa and elevation display similar spatial dependence trends where good to moderate spatial autocorrelation was found in both secondary variables. In 2018, ECa collocated with VWC data had an average nugget-to-sill ratio of 0.177 using 15 cm VWC and 0.093 using 30 cm VWC, while in 2019, the average nugget-to-sill ratio was 0.252 using the 15 cm VWC and 0.198 using the 30 cm VWC. Elevation data collocated with the 2018 VWC surveys had an average nugget-to-sill ratio of 0.232 using the 15 cm VWC and 0.173 using the 30 cm VWC. In 2019, elevation collocated with VWC data had an average nugget-to-sill ratio of 0.138 using 15 cm VWC and 0.209 when using 30 cm VWC.

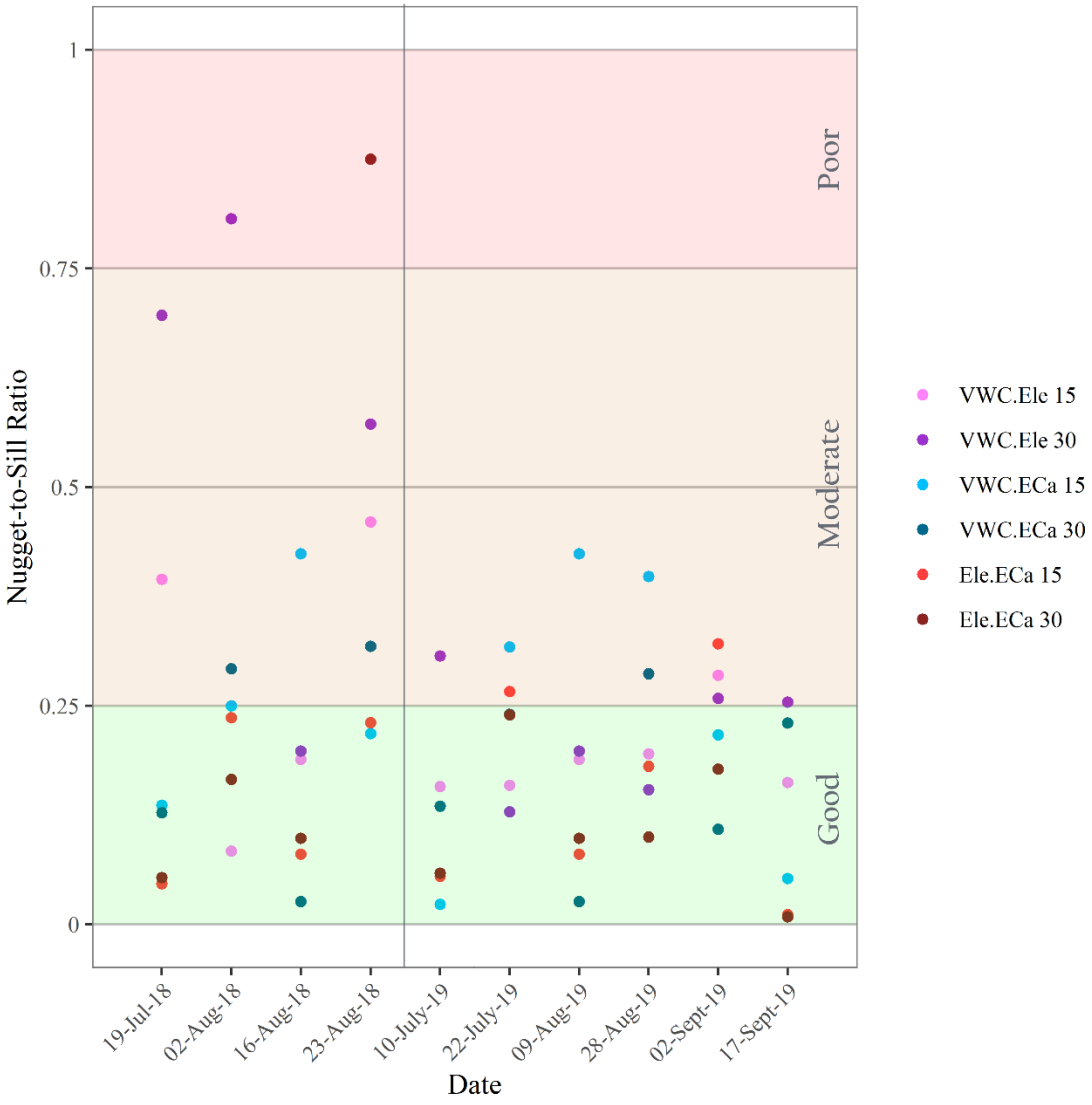

Figure 24: Nugget-to-sill ratios for theoretical cross-variograms modelled using co-kriging methods. VWC was used as the primary variable and ECa and elevation as secondary variables. Background colours indicate three levels used to assess nugget-to-sill ratios: good (green), moderate (orange), and poor (red).

The cross-variograms constructed from the covariance of VWC survey data and collocated elevation and ECa have good-to-moderate spatial autocorrelation with two exceptions, which were poor. The elevation data collocated with 15 cm VWC data from 2018 and 2019 had an average nugget-to-sill ratios of 0.282 and 0.164, respectively. The elevation collocated with the 30 cm VWC had an average nugget-to-sill ratio of 0.569 in

2018 and 0.0.186 in 2019. Elevation data collocated with 2019 VWC surveys had a better spatial autocorrelation than the elevation data collocated with 2018 VWC, with nugget-to-sill ratios indicating that eight out of twelve datasets have good spatial autocorrelation ranging from 0.129 to 0.198 and a total range of 0.129 and 0.307. In 2018, the ECa data collocated with 15 cm and 30 cm VWC surveys have average nugget-to-sill ratios of 0.257 and 0.191, respectively, indicating good to moderate spatial autocorrelation at both depths. In 2019, the ECa collocated with 15 cm and 30 cm VWC in 2018 had average nugget-to-sill ratios of 0.204 and 0.147, respectively. This indicated that better spatial autocorrelations were found in ECa data collocated to the 30 cm VWC in both years and that 2019 displayed a higher spatial autocorrelation than 2018. The cross-variograms constructed from ECa and elevation semivariograms in 2018 had an average nugget-to-sill ratios of 0.148 using data collocated to 15 cm VWC and 0.298 using data collocated to 30 cm VWC. In 2019, collocated elevation and ECa had average nugget-to-sill ratios of 0.131 using 15 cm VWC collocated data and 0.098 using 30 cm VWC collocated data, with similar spatial autocorrelations found at both depths.

Table 18: Leave-one-out cross-validation results for VWC predictions calculated using semivariogram models constructed using co-kriging methods. Semivariogram models were constructed using soil moisture as the primary variable and soil electrical conductivity and elevation as secondary variables. The co-efficient of determination (R^2), concordance, mean square error (MSE), root mean square error (RMSE), normalized root mean square error (NORM RMSE), and bias were used as assessment parameters.

	GOODNESS-OF-FIT SUMMARY						
DATE	DEPTH	R^2	CONCORDANCE	MSE	RMSE	NORM RMSE	BIAS
7/19/18	15 cm	0.282	0.498	12.36	3.52	0.198	-0.048
	30 cm	0.419	0.597	8.81	2.97	0.202	-0.005
8/02/18	15 cm	-0.024	0.081	19.80	4.45	0.273	-0.055
	30 cm	0.060	0.239	19.33	4.40	0.251	0.044
8/16/18	15 cm	0.444	0.635	12.87	3.59	0.191	0.024
	30 cm	0.177	0.347	24.64	4.96	0.216	0.052
8/23/18	15 cm	0.321	0.506	6.27	2.50	0.175	-0.019
	30 cm	0.107	0.291	9.83	3.14	0.238	-0.114
7/10/19	15 cm	0.406	0.572	5.98	2.45	0.152	0.002
	30 cm	0.335	0.532	13.54	3.68	0.186	-0.068
7/22/19	15 cm	0.377	0.573	11.04	3.32	0.161	-0.005
	30 cm	0.384	0.587	12.77	3.57	0.197	0.011
8/09/19	15 cm	0.231	0.459	25.99	5.10	0.167	-0.110
	30 cm	0.222	0.383	18.58	4.31	0.210	-0.031
8/28/19	15 cm	0.223	0.389	14.26	3.78	0.187	0.031
	30 cm	0.301	0.488	19.27	4.39	0.187	0.004
9/02/19	15 cm	0.278	0.466	11.92	3.45	0.221	-0.042
	30 cm	0.354	0.540	19.88	4.46	0.172	-0.120
9/17/19	15 cm	0.423	0.610	7.88	2.81	0.186	0.051
	30 cm	0.423	0.597	13.86	3.72	0.178	-0.010

Goodness-of-fit tests conducted on predicted VWC compared to the VWC survey observations are summarized in. In 2018, goodness-of-fit tests conducted on predicted VWC compared to the VWC survey observations calculated an average R^2 value of 0.205 using the 15 cm VWC and 0.153 using the 30 cm VWC, while in 2019, the average R^2 was 0.323 for 15 cm VWC and 0.336 for 30 cm VWC. The average concordance in 2018 was 0.344 for 15 cm VWC and 0.295 in 30 cm VWC, and in 2019, was 0.512 and 0.521,

respectively. These values indicated that predicted VWC using 2019 survey data was more accurate than VWC predicted using 2018 survey data. However, normalized RMSE values calculated from the ratio of residual variances to the total range of VWC survey data indicated a higher variance in 2019 predictions. The normalized RSME in 2019 averaged 0.163 in the 15 cm VWC and 0.122 in the 30 cm VWC, while in 2018, the average RMSE for the 15 cm was 0.121 and 30 cm VWC was 0.101. Bias was determined and displayed a range of -0.120 and 0.051 with seven out of twelve models displaying a negative bias, indicating an underestimation of predicted values.

4.4.4 Seasonal patterns of shallow soil moisture

2018

The normalized average and standard deviation VWC maps in 2018 using 15 cm soil moisture survey data display normalized VWC which ranged from 4.4% above average to 2.9% below average, a total difference of 7.3% or 16 mm in the calculated top layer (0 – 22.5 cm) (Figure 25).

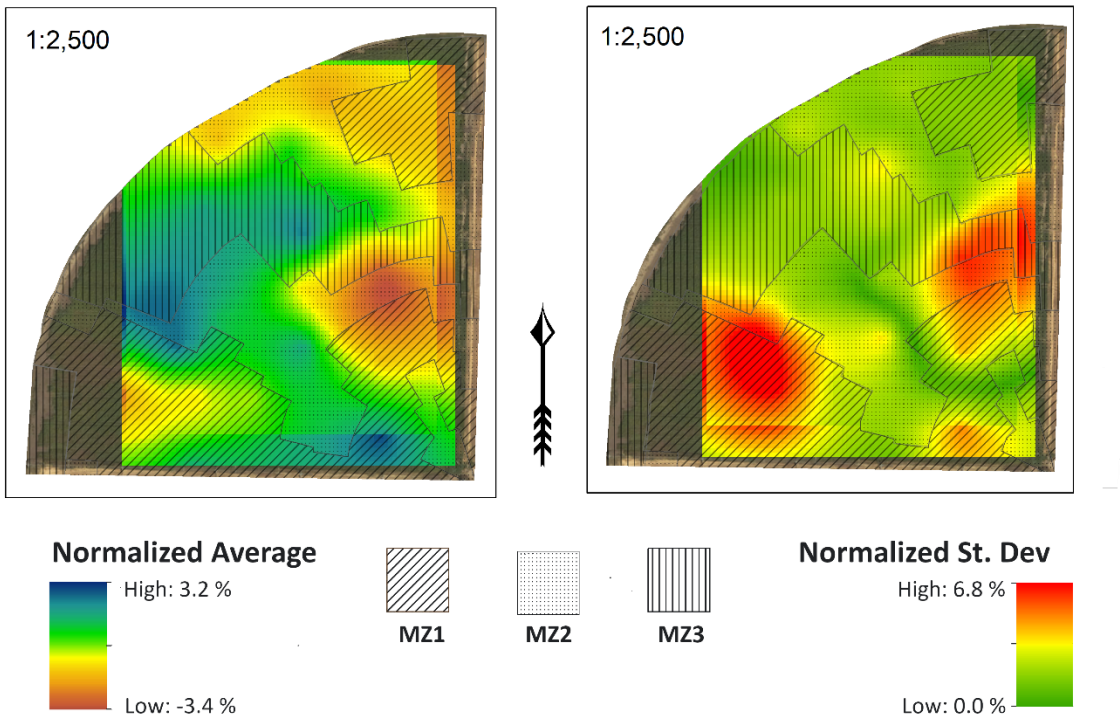

Figure 25: The normalized average and normalized standard deviation of co-kriged VWC maps with an overlay of three management zones. VWC data was collected at 15 cm depth during July - September 2018. Data collected from Aug 2, 2018 was excluded.

The standard deviation ranged from 0 to 5.8% and the highest standard deviation occurred in some areas with the highest and lowest average soil water content, but also do not adhere to the management zone map. No patterns that adhered to the management zone map were observable, and all management zones display wet and dry conditions (Figure 25). Areas with high standard deviation are found in some of the drier areas. The observable straight lines in each of the maps occur due to small changes in surveys and how the limits of each raster image were calculated.

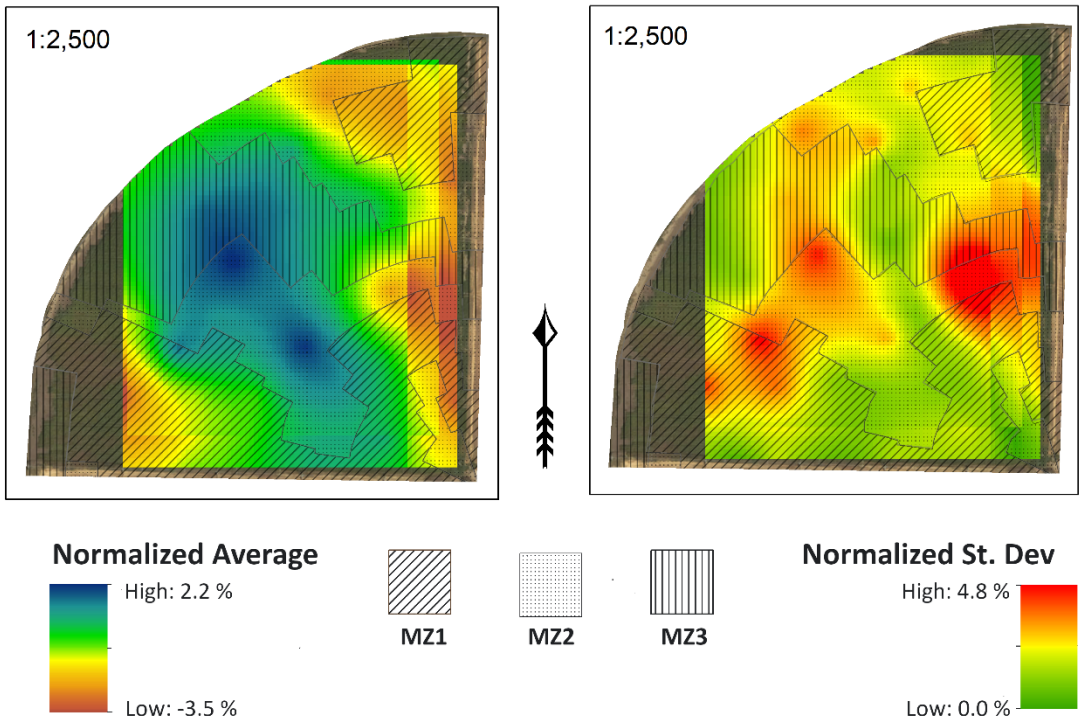

Figure 26: The normalized average and normalized standard deviation of co-kriged VWC maps with an overlay of three management zones. VWC data was collected was collected at 30 cm depth during July - September 2018.

The normalized average and standard deviation VWC maps in 2018 using 30 cm soil moisture survey data display normalized VWC (Figure 26) which ranged from 2.2% above average to 3.5% below average, a total difference of 5.7% or 9 mm in the calculated top layer (22.5 – 37.5 cm) A large area of above average VWC occurred in the middle of the field with decreasing values along the field margins. The normalized average soil moisture did not display patterns that adhere to the management zone map, although wet areas of the field were contained within MZ1 and MZ2. All the management zones displayed areas which had both low and high standard deviations from normal soil moisture. The

standard deviation ranged from 0 to 4.8% and is distributed similarly to the standard deviation of the 15 cm stack.

Table 19: Normalized average soil water content from three management zones in 2018. Normalized soil water content derived from predicted VWC. The mean, standard deviation, skewness, kurtosis, and number of prediction points used is summarized.

	MZ1	MZ2	MZ3	MZ1	MZ2	MZ3	MZ1	MZ2	MZ3
DEPTH	15 cm			15 cm no Aug 2			30 cm		
MEAN	-0.11	-0.07	0.28	-0.29	-0.05	0.71	-0.73	0.07	0.60
ST.DEV	1.29	1.18	1.06	1.28	1.32	1.19	1.05	1.31	0.92
KURT	-0.07	0.19	0.58	-0.75	-0.65	-0.04	-0.86	-0.76	3.06
SKEW	0.57	0.14	-0.01	0.21	-0.29	-0.76	-0.11	-0.51	-1.52
N	2213	2328	1594	2213	2328	1594	2213	2328	1594

Table 20: Standard deviation of normalized soil water content from three management zones in 2018. Normalized soil water content derived from predicted VWC. The mean, standard deviation, skewness, kurtosis, and number of prediction points used is summarized.

	MZ1	MZ2	MZ3	MZ1	MZ2	MZ3	MZ1	MZ2	MZ3
DEPTH	15 cm			15 cm no Aug 2			30 cm		
MEAN	2.76	2.07	2.09	2.80	2.00	1.97	1.47	1.72	1.61
ST.DEV	1.18	1.03	1.05	1.53	1.14	1.13	0.68	0.73	0.63
SKEW	-0.58	0.35	0.88	-0.59	0.99	1.18	0.44	1.63	0.55
KURT	0.28	0.95	0.93	0.50	1.25	1.29	0.59	0.91	-0.14
N	2208	2275	1594	2208	2308	1594	2208	2308	1594

The VWC survey from 15 cm taken on Aug 2, 2018 displayed a low concordance and correlation and was removed from the stack to compare to the stack which included all datasets. The exclusion resulted in a wider spread of normalized values between the management zones and the standard distribution and skewness increased in management zones 2 and 3. However, the average normalized VWC trend in the zones remained the same, with management zone 3 displaying higher total average VWC and

management zone 1 displaying lower total average VWC. The normalized average VWC calculated with all 2018 datasets from each management zone determined that management zone 3 had the highest overall average VWC from the three zones at both depths in 2018 and management zone 1 had the lowest (Table 19, Table 20) with a difference of 1% in the 15 cm VWC maps when excluding the Aug 2 and 1.3% in the 30 cm VWC map. Given that the average seasonal soil moisture had a total difference of 7.3% and 5.7% in the 15 and 30 cm depths, respectively, the differences between management zones was small in comparison. Management zone 2 had an intermediary VWC average which was close to the mean at both depths. The overall averages in the normalized 30 cm VWC had a larger distribution of predicted values than the overall averages found in the 15 cm normalized VWC. The standard deviation for the normalized average at 15 cm was highest in management zone 1, followed by management zone 2 and 3, respectively (Table 20). In the 30 cm depth, management zone 2 displayed the highest standard deviation, followed by management zone 1 and2.

2019

The normalized average and standard deviation VWC maps in 2019 using 15 cm soil moisture survey data display normalized VWC (Figure 27) which ranged from 7.6% above average to 3.1% below average, a total difference of 10.7% or 24 mm in the calculated top layer (0 – 22.5 cm).

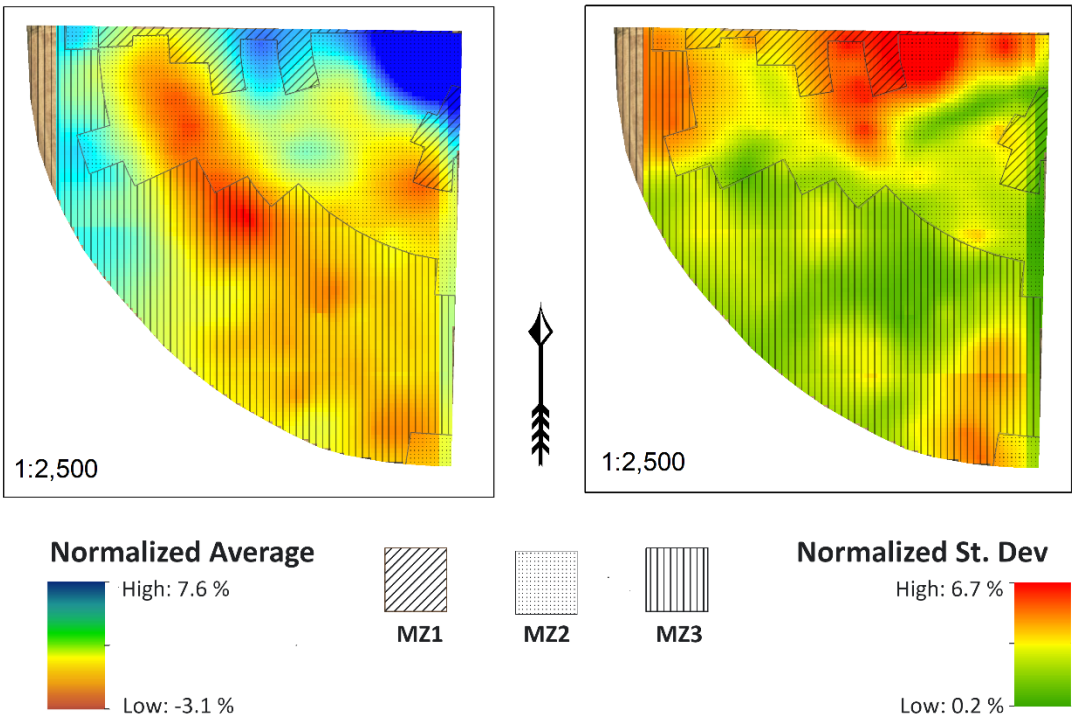

Figure 27: The normalized average and normalized standard deviation of co-kriged VWC maps with an overlay of three management zones. VWC data was collected at 15 cm depth during July - September 2019.

The highest normalized VWC were confined mostly to the north section of the study area with a dry band extending from the northeast to the field midpoint and the southern parts of the field typically drier than average. The standard deviation ranged from 0.2 to 6.7% with low values occurring in the drier southern parts of the study area and the highest values where the normalized VWC was consistently high.

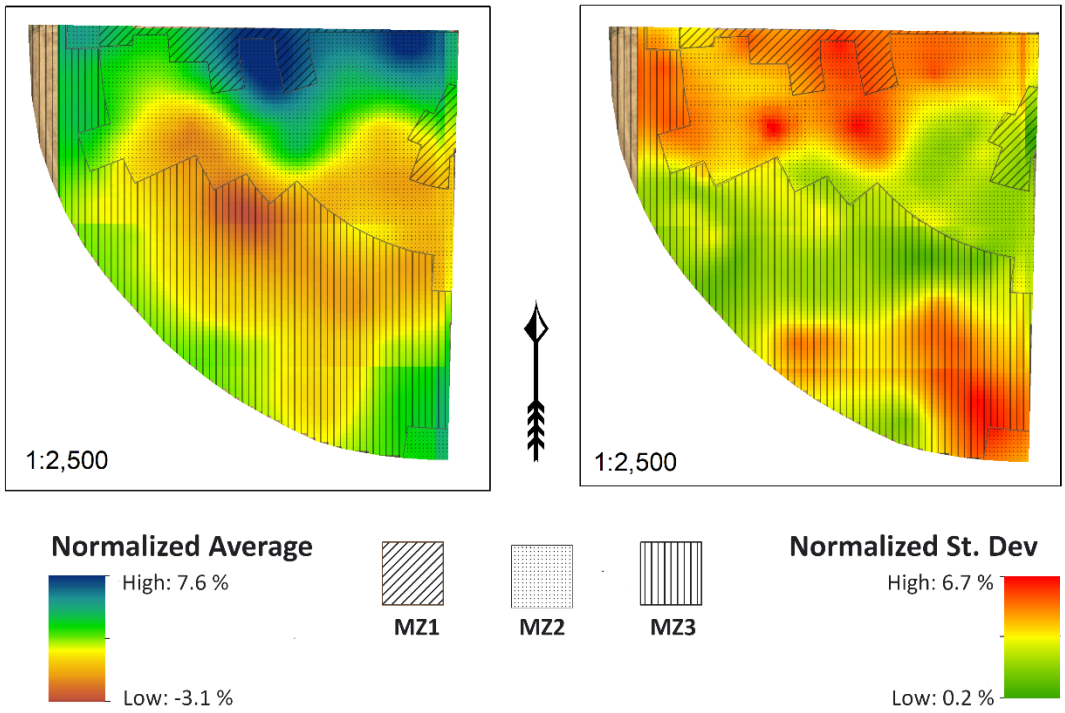

Figure 28: The normalized average and normalized standard deviation of co-kriged VWC maps with an overlay of three management zones. VWC data was collected at 30 cm depth during July - September 2019.

The normalized average and standard deviation VWC maps in 2019 using 30 cm soil moisture survey data display normalized VWC (Figure 28) which ranges from 5.6% above average to 4.6% below average, a total difference of 10.2% or 15 mm in the calculated top layer (22.5 – 37.5 cm). The highest normalized VWC were confined mostly to the north and south sections of the study area with a dry area in the middle. The standard deviation ranged from 0.1 to 7.7% and were similarly distributed as the normalized 15 cm values, with low values occurring in the drier areas of the study area and the high values occurring in the wetter areas.

Table 21: Normalized average soil water content from three management zones in 2019. Normalized soil water content derived from predicted. The mean, standard deviation, skewness, kurtosis, and number of prediction points in each zone used is summarized.

	MZ1	MZ2	MZ3	MZ1	MZ2	MZ3
DEPTH	15 cm			30 cm		
MEAN	1.14	0.28	-0.73	1.95	0.28	-1.08
ST.DEV	1.74	2.21	1.09	2.17	2.22	1.33
KURT	0.76	1.68	-0.02	-0.94	-0.89	-0.19
SKEW	0.68	1.43	0.74	-0.45	0.39	0.19
N	548	2750	3859	548	2750	3859

Table 22: Standard deviation of normalized soil water content from three management zones in 2019. Normalized soil water content derived from predicted. The mean, standard deviation, skewness, kurtosis, and number of prediction points used is summarized.

	MZ1	MZ2	MZ3	MZ1	MZ2	MZ3
DEPTH	15 cm			30 cm		
MEAN	3.05	2.59	1.92	2.89	2.78	2.30
ST.DEV	1.29	1.12	0.78	1.05	0.87	0.93
KURT	-0.24	0.66	0.72	-0.88	-0.20	0.42
SKEW	-0.35	0.94	-0.10	-0.48	-1.11	-0.85
N	548	2750	3859	548	2750	3859

The normalized average VWC (Table 21, Table 22) calculated with all 2019 datasets from each management zone determined that management zone 1 had the highest overall average VWC from the three zones at both depths in 2019 and management zone 3 had the lowest, This was a reversal of the findings from 2018. The overall averages in the normalized 30 cm VWC had a larger distribution of predicted values than the overall averages found in the 15 cm normalized VWC. The VWC differences between management zone 1 and 3 were small in comparison to the total differences in both 15 cm and 30 cm normalized average VWC maps. The standard deviation for the normalized

average at 15 and 30 cm depths (Table 22) was highest in management zone 1, followed by management zone 2 and 3, respectively.

CHAPTER 5. DISCUSSION

5.1 ARE THE THREE MANAGEMENT ZONES DELINEATED IN THE STUDY AREA HYDROLOGICALLY DIFFERENT?

Due to a lack of overlapping soil moisture datasets, the hydrology of the management zones under uniform irrigation conditions in 2018 could not be evaluated. The data collected during the 2019 field season may confirm that the management zones have different hydrology. Consistent differences in total soil moisture in the profile, individual sensor data and precipitation responses were observed under UIM conditions. Total soil moisture calculations showed three different soil moisture profiles in the management zones, particularly in the beginning and the end of the monitoring period (Figure 19). This indicates that there is a variable response to uniform irrigation within the study area in 2019 in each of the delineated zones. Individual soil profiles further elucidate consistent differences in the management zones. The soil profile in UIM1 indicated an accumulation of soil moisture in the 20-35 cm which can be observed in the sensor data and in the 48-hr response to precipitation (Figure 18A). This accumulation was more pronounced in the sensor data in UIM2, but the corresponding response to precipitation was not observed (Figure 18B). UIM2 35-60 cm layer is drier than the soil moisture of this layer in either UIM1 or UIM3 throughout the monitoring period. This may indicate an increase in drainage to deeper soil layers over the other monitored areas or a change in bulk density which confines moisture above this depth. However, a change in bulk density is not supported by the precipitation responses, which were relatively consistent throughout the profile. UIM3 displays a soil moisture profile which reflects a soil moisture profile

without confining layers (Richards, Gardner, & Ogata, 1956) (Figure 18C). Soil moisture in 35-60 cm layer in all management zones remained stable or showed an increased throughout the monitoring period despite plant development which suggests that the water was inaccessible to the effective rootzone or that the soil moisture was replenished with irrigation at the same rate as plant uptake. Pachepsky, Guber and Jacques (2005) found consistent similarities in temporal trends of VWC at different depths taken in the same 6 m study area. Therefore, consistent differences found between the monitoring stations supports the conclusion that the three management zones have different hydrology. However, all conclusions on soil moisture under UIM conditions are drawn from a single VWC monitoring station in each management zone. Additional monitoring stations would provide the ability to confirm that each management zone has a more homogenous response to precipitation when compared to responses in other management zones. Using a single monitoring station makes it difficult to determine whether the VWC observations in the management zones are indicative of the hydrology for the entire management zone.

There is also evidence which supports hydrological differences within the field can be managed using SSIM. This was provided inadvertently in 2019 due to difficulty in uploading site-specific irrigation schedules. Until July 20, the SSIM plots received the same irrigation schedule as the UIM study areas, resulting in a split monitoring season where both UIM and SSIM soil water responses were observed in the same plot. This provides a more direct comparison of the difference between SSIM and UIM precipitation responses in all three management zones. After SSIM treatments were

applied to the plots on July 20, there was a noticeable decline in total soil water variability which was not observed in the UIM observation data. This indicates that soil water variability can be managed by SSIM and suggests that the hydrological response to uniform irrigation applications is different between the management zones.

Alternatively, irrigation may play an outsized role in the distribution of soil moisture rather than landscape or local dynamics. Hydrology of fields under irrigated conditions are driven by relationships between landscape and local controls. Landscape controls are defined as the lateral movement of water along surface and subsurface pathways while local controls are defined as the influence of soil properties and areas of high convergence (Grayson et al., 1997). These relationships are assumed to be relatively stable at the field scale (Wallender & Grismer, 2002), but this has been studied under uniform irrigation. The study area used a site-specific irrigation system which is employed to reduce water applications in areas under saturated conditions. These areas were specifically targeted, and observations rather than management zones are used to determine where and when irrigation reductions should occur. From July 24 to Aug 10, 2018, less water was applied to the some of northern and eastern parts of the study area which were saturated. This irrigation strategy may have influenced these areas in management zone 1 and subsequently decreased the average normalized soil water content, leading to management zone 1 appearing drier than management zones 2 or 3. This strategy was not employed in 2019 in the study area. Additionally, soil moisture surveys were conducted in the shallow layer of disturbed soil which is more influenced by evaporation and would dry out quicker than the lower depths. A study conducted in

Saskatchewan, Canada determined that VWC does follow topographic controls if the total soil profile is used, but if only the top 30 cm of the soil profile are included in the analysis, the relationship between topography and VWC would not have been evident (Peterson, Helgason, & Ireson, 2019).

5.2 Is the heterogeneity of ECa and elevation the driving factor for soil moisture under uniform irrigation?

The normalized soil moisture maps can provide insight into the spatial dependence of soil moisture in both study areas. The study areas in 2018 and 2019 exhibited a reversal in correlational relationships between soil water content and elevation within the monitoring period (Figure 22) which demonstrates that the relationship between ECa and elevation is not static temporally. A reversal of correlational relationships between soil water content and other measured field properties had been observed by Grayson (1997). Grayson (1997) found that elevation was strongly associated with soil water content at the beginning of the season when moisture is being stored and becomes weaker throughout the season. This is reflected in this study, where a moderate, negative correlation between soil water and elevation was calculated for the soil moisture surveys in 2019. Irrigation was used to recharge the soil water in the study area with low pressure sprinklers that applied water with an intensity focused for maximum infiltration into the soil, which would allow for continued water storage throughout the season, indicated by the relatively unchanging correlations between elevation and soil water until the Sept 17 survey. This survey was conducted during harvest preparation where irrigation was stopped on Sept 5 to allow the soil to dry and had not experienced a precipitation event

after Sept 10. It has been previously established that soil water may have different controls under wet and dry conditions (Peterson et al., 2019) and this survey also had the highest positive correlation between ECa and soil water content at 15 and 30 cm depths. This may indicate that soil water content is more spatially dependent on a local control which is detected by the ECa survey. This provides evidence that the relationships between topographic and local controls and how they influence soil water content is not sufficiently uniform throughout the field to delineate management zones using elevation and ECa observations from the entire field.

Alternatively, delineating the management zones for three quarters of the field as a continuous surface assumes that the relationship between elevation and ECa remains relatively stable in the field. However, ECa may have a higher correlation to soil water content than to soil texture or salinity, as was found by Kachanoski, Gregorich and Van Wesenbeeck (1988). The correlational relationship between ECa and elevation changed between study areas in magnitude and direction when only values pertaining to each study area were correlated. This reversal was also observed in predicted soil moisture maps between the study areas in 2018 and 2019. Management zone 3 in 2018 was determined to be the wettest area when comparing the average normalized predicted soil moisture from each zone, while management zone 1 was the driest, while the inverse was observed in 2019. Management zone 2, which represents the intermediary elevation and ECa areas in both study areas, remained close to the overall average in both years. This was the only consistent relationship found between the two study periods. This may be a result of the delineation of management zones using an ECa map which spatially

characterizes soil water content at one point in time rather than a relationship which remains static throughout the growing season. However, another possible conclusion may be that the spatial relationship between ECa and elevation between the study areas is not stable at the field scale. Yari (2017) noted that the relationship was stronger in the western sections in the study area. The correlations computed between study areas did change between 2018 and 2019. In 2019, a moderately negative correlation was found between elevation and ECa which corresponds to previous findings (Yari, 2017), while in 2018, a low positive correlation was found. This may indicate that delineating management zones using the entire field characteristics hides important inter-field variability. Additionally, other soil properties may be more important factors in determining management zones. Previous studies have shown that bulk density has more influence on predicting soil water content than ECa or elevation (Contreras & Bonilla, 2018).

5.3 CAN SENSOR-BASED SITE-SPECIFIC WATER MANAGEMENT BE USED TO REDUCE POTATO YIELD VARIABILITY?

Potatoes harvested from SSIM3-2018 and SSIM2-2019 did show an increase in productivity with a decreased amount of irrigation when compared to the UIM counterpart, which indicates that SSIM can improve productivity while also increasing water use efficiency. However, improved yield or decreased yield variability were not attained using SSIM. In Southern Alberta, the average yield for potatoes grown under irrigated conditions in 2018 and 2019 was 5.6 kg/m^2, lower than the yield obtained from SSIM2 and SSIM3 in 2018 and SSIM1 and SSIM2 in 2019 and the weighted average SSIM

and UIM yields for both study areas. This also highlights how well-managed the study areas were under UIM, as all yields obtained from UIM areas were above the Southern Alberta average. This indicates that SSIM using delineations in topography and ECa is unnecessary at this site and that using the adaptable approach which can address local concerns is more suitable. Site-specific water management in this study utilized a management zone map which was created using topographic and soil electrical conductivity differences. Topographic differences within a field have been shown to significantly affect yield variability in corn in Michigan, USA (Muñoz et al., 2014), while topography, ECa, and soil brightness accounted for 70% of cotton yield variability in Texas, USA (Guo, Maas, & Bronson, 2012). A study by Al-Gaadi et al (2018) found a positive spatial correlation between elevation and yield in potatoes. This suggests that yield variation from other water-intensive crops may be managed using management zones derived from these factors. However, a study conducted in Tasmania defined the variation of potato yields, elevation and soil EC and determined that a three-fold intra-field variation in total yield will significantly affect the gross margin variation under uniform irrigation (Whelan & Mulcahy, 2017). In this study, the ratio of intra-field averages between the highest and lowest total yields under uniform conditions were 1.3 and 1.5, respectively. The yield variability in this study area may be insufficient to show significant improvement under SSIM.

Previous studies have addressed how available soil moisture can positively influence both the yield and the quality of Russet Burbank potatoes (Redulla et al., 2002). In this study, a noticeable decline in soil moisture variability was observed in 2019 when SSIM was

enabled (Figure 21), but this decline was not associated with a decline in potato yield variability or an increase in total yield. However, moisture deficits can reduce the grade and total yield when total precipitation is reduced by 30% (Onder et al., 2005; Shock, C. C., Feibert, & Saunders, 1998), while a study conducted in Southern Alberta concluded that moisture stress in the early or mid-season can have significant negative effects on total tuber and marketable tuber numbers (Lynch et al., 1995). The yield results in SSIM1-2018 and SSIM3-2019 confirmed both conclusions, which displayed significantly lower yields as a result from a ~40% and ~30% reduction in total water, respectively, from the UIM scheduling. However, results from SSIM2 in 2018 and 2019 both have ~30% reduction in total water but had the same yield in 2018 and an improved yield in 2019. SSIM3-2019 also displayed a reduction in yield but received more water than SSIM2 and, although the total soil profile shows sufficient moisture throughout the monitoring period, a moisture deficit in the top 30 cm may have occurred. The soil moisture of top 30 cm was drier in the beginning of the observation period until mid-July (Figure 18). Using the 60 cm total soil profile to calculate irrigation requirements early in the season may have allowed deficits in the top 30 cm to go unaddressed. This may have reduced the total productivity of the potatoes as the rootzone of potatoes barely extends into the bottom 30 cm until 21-35 days after emergence (Lesczynski & Tanner, 1976). A significant deficit contained to the top 30 cm and a near-saturated lower 30 cm may leave the effective root zone under water stress while still appearing to contain enough water in the total profile. Shock et al (1992) concluded that irrigation deficits which extend through row closure could result in lower yields.

The reduced yield in SSIM1-2018 was anticipated due to the sensor malfunction. The effects of a single sensor malfunction on yield highlight the need to use additional, independent observation stations or additional methods to confirm soil moisture. Soil moisture variability may also be captured within delineated zones if soil moisture is monitored using two or more observation stations.

CHAPTER 6. CONCLUSIONS

Although the primary goal of this study was to improve potato yields using SSIM, it was concluded that the water use efficiency improvements were the primary benefit of SSIM. Improving yields or yield variability may be a result of SSIM but this should not be the primary goal of SSIM. A 10-30% reduction in total water requirements did not affect yield in some areas, which suggests that using SSIM could expand irrigated land in Southern Alberta. This study also suggests that soil moisture variability may be reduced when using soil moisture sensors to inform SSIM decisions. However, this conclusion was determined from a single monitoring location in each of the management zones and the direct comparison occurred in 2019 due to a malfunction in the irrigation schedule upload. Using additional monitoring stations within each management zone would address this and other concerns. A loss of potato production was experienced in SSIM1 in 2018 due to a malfunctioning sensor and additional monitoring stations in the same management zone may have helped detect the malfunction earlier. Additional stations would also provide a method to examine several soil moisture profiles within a management zone to determine whether different areas within a management zone are responding to SSIM similarly. The spatial distribution of VWC did not appear to adhere to the management zones in the study area. Although differences were calculated from the average VWC in each management zone, the differences were small when compared to the differences between the maximum and minimum values in each normalized average VWC map. It may be prudent to assess yield variability and soil moisture variability to determine whether SSIM may be effective before delineating management zones. If there is

insufficient variability for SSIM informed by management zones, using SSIM based on experience may still provide yield benefits by being able to respond to ponding and other adverse conditions which affect yield. Additionally, the effectiveness of MZ-based SSIM may be increased if irrigation prescriptions were targeted to the effective rootzone rather than the total rootzone, which was how MAD was calculated in this study. This method of calculation may overestimate VWC that is accessible to the plants and result in a loss of production, which may have been experienced by SSIM3-2019.

REFERENCES

Ackerman, E. A. (1941). The Köppen Classification of Climates in North America. *Geographical Review, 31*(1), 105-111. doi:10.2307/210420

Alberta Agriculture and Rural Development. (2014). Alberta's irrigation – a strategy for the future. Irrigation and Farm Water Division, Alberta Agriculture and Rural Development, Lethbridge, Alberta, Canada.

Agriculture and Agri-Food Canada, Research Branch, & Alberta Agriculture, Food and Rural Development, Conservation and Development Branch. (2005). Alberta Soil Information Viewer. Edmonton, AB: AARD.

Agriculture and Agri-Food Canada, & Government of Canada. (2013). Moisture Deficits in the Prairie Region. Retrieved Mar 14, 2018, from http://www.agr.gc.ca/eng/science-and-innovation/agricultural-practices/agriculture-and-climate/future-outlook/climate-change-scenarios/moisture-deficits-in-the-prairie-region/?id=1363104397771

Alberta Agricultural and Rural Development. (2010). South Saskatchewan River Basin in Alberta Water Supply Study Summary Government of Alberta.

Alberta Agriculture and Forestry. (2016). Alberta irrigation information 2015.Government of Alberta.

Alberta Agriculture and Forestry. (2019). Current and Historical Alberta Weather Station Data Viewer. Retrieved Dec 19, 2019, from https://agriculture.alberta.ca/acis/alberta-weather-data-viewer.jsp

Alberta Environment. (2007). Current and Future Water use in Alberta. Government of Alberta.

Alberta Environment and Parks. (2006). Water Allocation Policy for Closed River Basins in the South Saskatchewan River Basin Directive. Retrieved Feb 2, 2018, from http://aep.alberta.ca/forms-maps-services/directives/documents/WaterAllocationSouthSaskatchewan-Sep2016.pdf

Alberta Environment and Sustainable Resource Development. (2013). Evaporation and evapotranspiration in Alberta. Government of Alberta.

Al-Gaadi, K., Hassaballa, A. A., Tola, E., Kayad, A. G., Madugundu, R., Assiri, F., Alblewi, B. (2018). Characterization of the Spatial Variability of Surface Topography and Moisture Content and its Influence on Potato Crop Yield. *International Journal of Remote Sensing, 39*(23), 8572-8590. doi:10.1080/01431161.2018.1488290

Al-Gaadi, K., Patil, V., Marey, S., Al-Omran, A., & Al-Dosari, A. (2015). Variable Rate Application Technology for Optimizing Alfalfa Production in Arid Climate. *International Journal of Agriculture and Biology, 17*(1), 71-79

Allen, R. G., Pereira, L. S., Raes, D., & Smith, M. (1998). Crop Evapotranspiration-Guidelines for Computing Crop Water Requirements-FAO Irrigation and Drainage Paper 56. *FAO, Rome, 300*(9), D05109.

Assefa, Y., Roozeboom, K., Staggenborg, S., & Du, J. (2012). Dryland and Irrigated Corn Yield with Climate, Management, and Hybrid Changes from 1939 through 2009. *Agronomy Journal, 104*(2), 473-482. doi:10.2134/agronj2011.0242

Barrow, E., & Yu, G. (2005). Climate Scenarios for Alberta. A Report Prepared for the Prairie Adaptation research Collaborative (PARC) in co-operation with Alberta Environment. PARC, University of Regina, Regina, SK.

Bivand, R. S., Pebesma, E. J., Gómez-Rubio, V., & Pebesma, E. J. (2008). Applied spatial data analysis with R. New York: Springer.

Bivand, R., Keitt, T., et al. (2019). Rgdal: Bindings for the 'Geospatial' Data Abstraction Library. R package version 0.8-16. Retrieved from http://CRAN. R-project. org/package= rgdal.

Bivand, R., & Rundel, C. (2019). Rgeos: Interface to Geometry Engine - Open Source ('GEOS'). R package version 0.3-14. Retrieved from http://CRAN. R-project. org/package= rgeos

Boluwade, A., Madramootoo, C., & Yari, A. (2016). Application of Unsupervised Clustering Techniques for Management Zone Delineation: Case Study of Variable Rate Irrigation

in Southern Alberta, Canada. *Journal of Irrigation and Drainage Engineering, 142*(1), 05015007. doi:10.1061/(ASCE)IR.1943-4774.0000936

Boydell, B., & McBratney, A. (2002). Identifying Potential within-Field Management Zones from Cotton-Yield Estimates. *Precision Agriculture, 3*(1), 9-23. doi:1013318002609

Brady, N. C. (2008). In Weil R. R. (Ed.), The Nature and Properties of Soils (Revised fourteenth edition.). Upper Saddle River, N.J.; Columbus, Ohio; Upper Saddle River, N.J.: Upper Saddle River, N.J.; Columbus, Ohio: Pearson Prentice Hall.

Cambardella, C. A., Moorman, T. B., Novak, J. M., Parkin, T. B., Karlen, D. L., Turco, R. F., et al. (1994). Field-scale Variability of Soil Properties in Central Iowa Soils. *Soil Science Society of America Journal, 58*(5), 1501-1511.

Contreras, C. P., & Bonilla, C. A. (2018). A Comprehensive Evaluation of Pedotransfer Functions for Predicting Soil Water Content in Environmental Modeling and Ecosystem Management. *Science of the Total Environment, 644*, 1580-1590. doi:10.1016/j.scitotenv.2018.07.063

Cox, C., Jin, L., Ganjegunte, G., Borrok, D., Lougheed, V., & Ma, L. (2018). Soil Quality Changes due to Flood Irrigation in Agricultural Fields Along the Rio Grande in Western Texas. *Applied Geochemistry, 90*, 87-100. doi:10.1016/j.apgeochem.2017.12.019

Daugherty, R. B., & Eaton, W. C. (1975). *U.S. Patent No. 3,902,668*. Washington, DC: U.S. Patent and Trademark Office.

de Lara, A., Khosla, R., & Longchamps, L. (2017). Characterizing Spatial Variability in Soil Water Content for Precision Irrigation Management.*8*(2), 418-422. doi:10.1017/S2040470017000279

Downing, D. J., & Pettapiece, W. W. (2006). Natural Regions and Subregions of Alberta. *Canadian Research Index,* Retrieved from Canadian Research Index database.

Evans, R., LaRue, J., Stone, K., & King, B. (2013). Adoption of Site-Specific Variable Rate Sprinkler Irrigation Systems. *Irrigation Science, 31*(4), 871-887. doi:10.1007/s00271-012-0365-x

Fridgen, J. J., Fraisse, C. W., Kitchen, N. R., & Sudduth, K. A. (2000). Delineation and analysis of site-specific management zones. Paper presented at the *Proceedings of the 2nd International Conference on Geospatial Information in Agriculture and Forestry.* pp. 402-411.

Fridgen, J. J., Kitchen, N. R., Sudduth, K. A., Drummond, S. T., Wiebold, W. J., & Fraisse, C. W. (2004). Management Zone Analyst (MZA). *Agronomy Journal, 96*(1), 100-108.

Gleick, P. H., Ajami, N, Christian-Smith, J., Cooley, H., Donnelly, K., Fulton, J., Ha, M., Heberger, M., Moore, E., Morrison, J., Orr, S., Schulte, P., Srinivasan, V. (2014). The

world's water volume 8: The biennial report on freshwater resources. (Vol. 8). Island press.

Government of Canada. (2019). Canadian Climate Normals 1981-2010 Lethbridge Station Data. Retrieved Dec 12, 2019, from https://climate.weather.gc.ca/climate_normals/results_1981_2010_e.html?searchType=stnName&txtStationName=Lethbridge&searchMethod=contains&txtCentralLatMin=0&txtCentralLatSec=0&txtCentralLongMin=0&txtCentralLongSec=0&stnID=2263&dispBack=0

Gräler, B., Pebesma, E., & Heuvelink, G. (2016). Spatio-Temporal Interpolation using Gstat. *The R Journal, 8*(1), 204-218. Retrieved from https://journal.r-project.org/archive/2016/RJ-2016-014/index.html

Grayson, R., Western, A., Chiew, F., & Bloeschl, G. (1997). Preferred States in Spatial Soil Moisture Patterns: Local and Nonlocal Controls. *Water Resources Research, 33*(12), 2897-2908.

Guo, W., Maas, S., & Bronson, K. (2012). Relationship between Cotton Yield and Soil Electrical Conductivity, Topography, and Landsat Imagery. *Precision Agriculture, 13*(6), 678-692. doi:10.1007/s11119-012-9277-2

Haghverdi, A., Leib, B. G., Washington-Allen, R. A., Ayers, P. D., & Bushermohle, M. J. (2015). Perspectives on Delineating Management Zones for Variable Rate Irrigation.

Computers and Electronics in Agriculture, 117, 154-167. doi:10.1016/j.compag.2015.06.019

Haghverdi, A., Leib, B. G., Washington-Allen, R., Buschermohle, M. J., & Ayers, P. D. (2016). Studying Uniform and Variable Rate Center Pivot Irrigation Strategies with the Aid of Site-Specific Water Production Functions. *Computers and Electronics in Agriculture, 123*, 327-340. doi:10.1016/j.compag.2016.03.010

Heil, K., & Schmidhalter, U. (2012). Characterisation of Soil Texture Variability using the Apparent Soil Electrical Conductivity at a Highly Variable Site. *Computers and Geosciences, 39*, 98-110. doi:10.1016/j.cageo.2011.06.017

Hijmans, R. (2019). Raster: Geographic Data Analysis and Modeling. R package version 2.9-5. https://CRAN.R-project.rog/package=raster

Hill, R. W. (2000). Wheelmove Sprinkler Irrigation Operation and Management. *Utah University Extension.* Retrieved from https://digitalcommons.usu.edu/cgi/viewcontent.cgi?article=1152&context=extension_histall

Hokcell, T. (2000). Drops of life in the history of irrigation. *Irrigational Journal, 29*(1), 8-15.

Howell, T. A. (2003). Irrigation Efficiency. *Encyclopedia of Water Science. Marcel Dekker, New York.* pp 467-472.

Kachanoski, R. G., Gregorich, E. G., & Van Wesenbeeck, I. J. (1988). Estimating Spatial Variations of Soil Water Content using Noncontacting Electromagnetic Inductive Methods. *Canadian Journal of Soil Science, 68*(4), 715-722. doi:10.4141/cjss88-069

King, B. A., Wall, R. W., Kincaid, D. C., & Westermann, D. T. (2005). Field Testing of a Variable Rate Sprinkler and Control System for Site-Specific Water and Nutrient Application. *Applied Engineering in Agriculture, 21*(5), 847-853. doi:10.13031/2013.19712

Kulshreshtha, S., Paterson, B., Hart, D., & Nicol, L. (2016). Irrigation's Impact on Economic Growth in Alberta, Canada. *Irrigation Drainage System Engineering, 5*(156), 2.

Lesczynski, D., & Tanner, C. (1976). Seasonal Variation of Root Distribution of Irrigated, Field-Grown Russet Burbank Potato. *American Potato Journal, 53*(2), 69-78. doi:10.1007/BF02852656

Lozoya, C., Mendoza, C., Aguilar, A., Roman, A., & Castello, R. (2016). Sensor-Based Model Driven Control Strategy for Precision Irrigation. *Journal of Sensors, 2016*(2016) doi:10.1155/2016/9784071

Lynch, D. R., Foroud, N., Kozub, G. C., & Fames, B. C. (1995). The Effect of Moisture Stress at Three Growth Stages on the Yield, Components of Yield and Processing Quality of Eight Potato Varieties. *American Potato Journal, 72*(6), 375-385.

Malone, B. (2016). Ithir: Functions and Algorithms Specific to Pedometrics. R package version 1.0/r126. Retrieved from https://R-Forge.R-project.org/projects/ithir

McCutcheon, M. C., Farahani, H. J., Stednick, J. D., Buchleiter, G. W., & Green, T. R. (2006). Effect of Soil Water on Apparent Soil Electrical Conductivity and Texture Relationships in a Dryland Field. *Biosystems Engineering, 94*(1), 19-32. doi:10.1016/j.biosystemseng.2006.01.002

McMaster, G. S., & Wilhelm, W. (1997). Growing Degree-Days: One Equation, Two Interpretations. *Agricultural and Forest Meteorology, 87*(1997), 291-300.

Millard, S. P. (2013). EnvStats: An R Package for Environmental Statistics. New York: Springer. ISBN: 978-1-4614-8455-4

Muñoz, J. D., Steibel, J. P., Snapp, S., & Kravchenko, A. N. (2014). Cover Crop Effect on Corn Growth and Yield as Influenced by Topography. *Agriculture, Ecosystems and Environment, 189*, 229-239. doi:10.1016/j.agee.2014.03.045

Onder, S., Caliskan, M. E., Onder, D., & Caliskan, S. (2005). Different Irrigation Methods and Water Stress Effects on Potato Yield and Yield Components. *Agricultural Water Management, 73*(1), 73-86. doi:10.1016/j.agwat.2004.09.023

Pachepsky, Y. A., Guber, A. K., & Jacques, D. (2005). Temporal Persistence in Vertical Distribution of Soil Moisture Contents. *Soil Science Society of America Journal, 69*(2), 347-352. doi:10.2136/sssaj2005.0347

Payero, J., & Khalilian, A. (2017). Comparison of Irrigated and Dryland Crop Production in SC. *Clemson University Extension Publications.* Retrieved August 30, 2020.

Peterson, A. M., Helgason, W. H., & Ireson, A. M. (2019). How Spatial Patterns of Soil Moisture Dynamics can Explain Field-Scale Soil Moisture Variability: Observations from a Sodic Landscape. *Water Resources Research, 55*(5), 4410-4426. doi:10.1029/2018WR023329

Redulla, C., Davenport, J., Evans, R., Hattendorf, M., Alva, A., & Boydston, R. (2002). Relating Potato Yield and Quality to Field Scale Variability in Soil Characteristics. *American Journal of Potato Research, 79*(5), 317-323. doi:10.1007/BF02870168

Richards, L. A., Gardner, W. R., & Ogata, G. (1956). Physical Processes Determining Water Loss from Soil. *Soil Science Society of America Journal, 20*(3), 310-314.

Rowshon, M., & Amin, M. (2010). GIS-Based Irrigation Water Management for Precision Farming of Rice. *International Journal of Agricultural and Biological Engineering, 3*(3), 27-35. doi:10.3965/j.issn.1934-6344.2010.01.027-035

Sadler, E. J., Evans, R. G., Stone, K. C., & Camp, C. R. (2005). Opportunities for Conservation with Precision Irrigation. *Journal of Soil and Water Conservation, 60*(6), 371-379.

Seidel, S. J., Schutze, N., Fahle, M., Mailhol, J. C., & Ruelle, P. (2015). Optimal Irrigation Scheduling, Irrigation Control and Drip Line Layout to Increase Water Productivity

and Profit in Subsurface Drip-Irrigated Agriculture. *Irrigation and Drainage, 64*(4), 501-518. doi:10.1002/ird.1926

Shock, C. C., Feibert, E. B. G., & Saunders, L. D. (1998). Potato Yield and Quality Response to Deficit Irrigation. *HortScience: A Publication of the American Society for Horticultural Science,* (4), 655-659.

Shock, C., Zalewski, J., Stieber, T., & Burnett, D. (1992). Impact of Early-Season Water Deficits on Russet Burbank Plant Development, Tuber Yield and Quality. *American Potato Journal, 69*(12), 793-803. doi:10.1007/BF02854186

Sojka, R. E., Bjorneberg, D. L., & Entry, J. A. (2002). Irrigation: An historical perspective. *Encyclopedia of soil science (1st edition).* (pp. 745-749). New York: Marcel Dekker, Inc.

Splinter, W. E. (1976). Center-Pivot Irrigation. *Scientific American, 234*(6), 90. doi:10.1038/scientificamerican0676-90

Stalham, M. A., & Allen, E. J. (2004). Water Uptake in the Potato (Solanum Tuberosum) Crop. *Journal of Agricultural Science, 142*, 373-393.

Statistics Canada. (2010). Agricultural Water use in Canada: Analysis. Retrieved March 23, 2018, from http://www.statcan.gc.ca/pub/16-402-x/2011001/part-partie1-eng.htm

Statistics Canada. (2016). Snapshot of Canadian Agriculture: Chapter 1. Retrieved Apr 30, 2018, from http://www.statcan.gc.ca/pub/95-640-x/2011001/p1/p1-01-eng.htm

Taylor, R. (2014). When Wells Run Dry. *Nature, 516*(7530), 179-180.

Venables, W. N., & Ripley, B. D. (2002). Modern Applied Statistics with S (4th ed.). New York: Springer.

Villalobos, F. J., & Fereres, E. (2016). Principles of Agronomy for Sustainable Agriculture. Switzerland: Springer International Publishing.

Vukobratovic, D., Minic, V., Alonso Fernandez, M., Alvarez Osuna, J., Crnojevic, V., & Culibrk, D. (2014). Sensing Technologies for Precision Irrigation. New York, NY: Springer.

Wallender, W., & Grismer, M. E. (2002). Irrigation Hydrology: Crossing Scales. *Journal of Irrigation and Drainage Engineering, 128*(4), 203-211. doi:10.1061/(ASCE)0733-9437(2002)128:4(203)

Wang, J., Klein, K. K., Bjornlund, H., Zhang, L., & Zhang, W. (2015). Changing to More Efficient Irrigation Technologies in Southern Alberta (Canada): An Empirical Analysis. *Water International, 40*(7), 1040-1058. doi:10.1080/02508060.2015.1086257

Whelan, B. M., & Mulcahy, F. (2017). A Strategy to Instigate SSCM in Australian Potato Production. *Advances in Animal Biosciences, 8*(2), 743-748. doi:http://dx.doi.org.ezproxy.library.dal.ca/10.1017/S2040470017000401

Wickham, H. (2011). The Split-Apply-Combine Strategy for Data Analysis. *Journal of Statistical Software, 40*(1), 1-29. Retrieved from http://www.jstatsoft.org/v40/i01/

Wickham, François, R., et al. (2019). Dplyr: A Grammar of Data Manipulation

Yari, A. (2017). Application of variable-rate irrigation technology to conserve water and improve crop productivity. (Doctoral dissertation, McGill University). McGill University Libraries.

Yari, A., Madramootoo, C. A., Woods, S. A., Adamchuk, V. I., & Huang, H. (2017). Assessment of Field Spatial and Temporal Variabilities to Delineate Site-Specific Management Zones for Variable-Rate Irrigation. *Journal of Irrigation and Drainage Engineering, 143*(9), . doi:10.1061/(ASCE)IR.1943-4774.0001222

APPENDIX 1: COMPARISON OF VERTICAL AND HORIZONTAL SOIL MOISTURE SENSOR INSTALLATION

Procedure

Soil was collected from AITC from the top 50 cm in study areas used in 2018 and 2019. The soil was air-dried and used emulate two soil profiles in 20 L containers using a bulk density (BD) of approximately 1.35 g/cm^3 and a soil profile height of 35 cm. Two 10HS sensors were installed vertically or horizontally in one container (Figure 1) to record observations of VWC in 15-minute increments. Water was added to each container in four events over 12 days in 10% ΔGWC increments which simulated irrigation. A 24-hr break between water events to allow the sensors to reach equilibrium. The calibrated moisture content at each depth was used to calculate total moisture content in mm. The total moisture content in mm was then used to calculate the change in total water content detected and compared to the total amount of water added to the soil profile. The change in total water was calculated in three ways to determine if sensor placement improved accuracy. The first calculation used the peaks of each individual event to determine the change in water content in mm and summed the change at the end of the experiment. The second calculation used the minimum and the maximum values throughout the data series to calculate the change in water content in mm. The third used the first observation and subtracted it from the last observation. After VWC data collection was concluded, soil samples were collected from each container in 5 cm intervals to determine gravimetric water content (GWC) at the end point of the

experiment. The GWC was converted to VWC and used to confirm the VWC sensor observations at the end of the study.

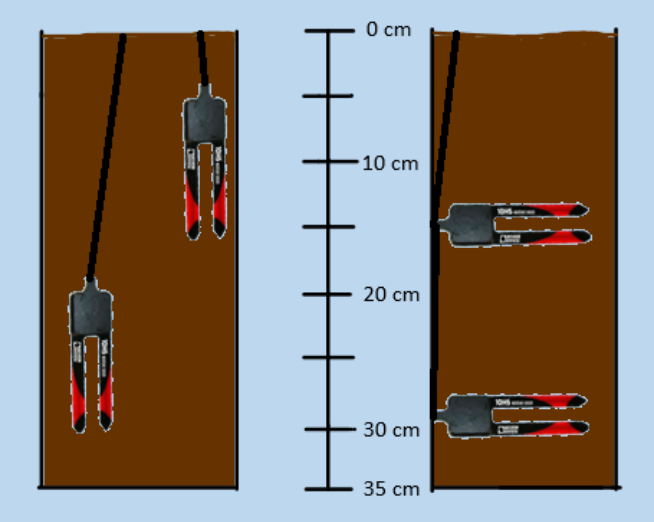

Figure 29: Sensor placement for vertical (left) and horizontal (right) installations.

Results and Discussion

Table 23: Summary of bulk density (BD) and water added in containers using vertical and horizontal installation containers.

Installation	BD (g/cm^3)	Water added (mL)	Water added (mm)
Vertical	1.30	5200	89.6
Horizontal	1.37	5350	92.2

The vertical installation container (VIC) had a calculated bulk density of 1.30 g/cm^3, and the horizontal installation container (HIC) had a calculated BD of 1.37 g/cm^3, which was 96% and 101% of the targeted bulk density of 1.35 g/cm^3, respectively. Water was added on May 21, 22, 23, and 27, 2019 with the VIC receiving a total of 5200 mL or 89.6 mm and HIC receiving a total 5350 mL or 92.2 mm.

Table 24: Comparison of the change in water content (mm) using vertical and horizontal soil water sensors to water added to the soil profile. Sensor-detected total change in water content used three calculations: summing the ΔVWC during and after simulated irrigation (SUM), subtracting the minimum from the maximum (MAX – MIN), and subtracting the first observation from the last observation (1st OBS – LAST OBS).

INSTALLATION	WATER ADDED	SUM		MAX – MIN		1ST OBS – LAST OBS	
	mm	mm	%	mm	%	mm	%
VERTICAL	89.6	99.6	111	96.1	107	80.5	90
HORIZONTAL	92.2	89.1	97	77.4	84	74.0	80

Both the min/max calculation and first/last observation do not account for water lost in the soil profile from evaporation and there are few ways to determine evaporation without specialized equipment, these equations rely on the assumption that water is not lost throughout the experiment. The sum calculation used peaks to indicate separate events and summed each interval which minimized evaporation losses in the calculation. However, using min/max values calculated a similar change in water content. When comparing the actual amount of water added to VIC, the change in soil water was overestimated when using the sum calculation and min-max calculation and underestimated when using the first/last observation calculation. The average change in water content in VIC was 87.0±8.9 mm and in HIC was 80.2±7.9 mm. The average percentage of water change observed to water added in VIC was 103±11% and was 92±10%. HIC consistently underestimated the change in soil water in all calculations and in two calculations, failed to capture more than 15% of the soil moisture change.

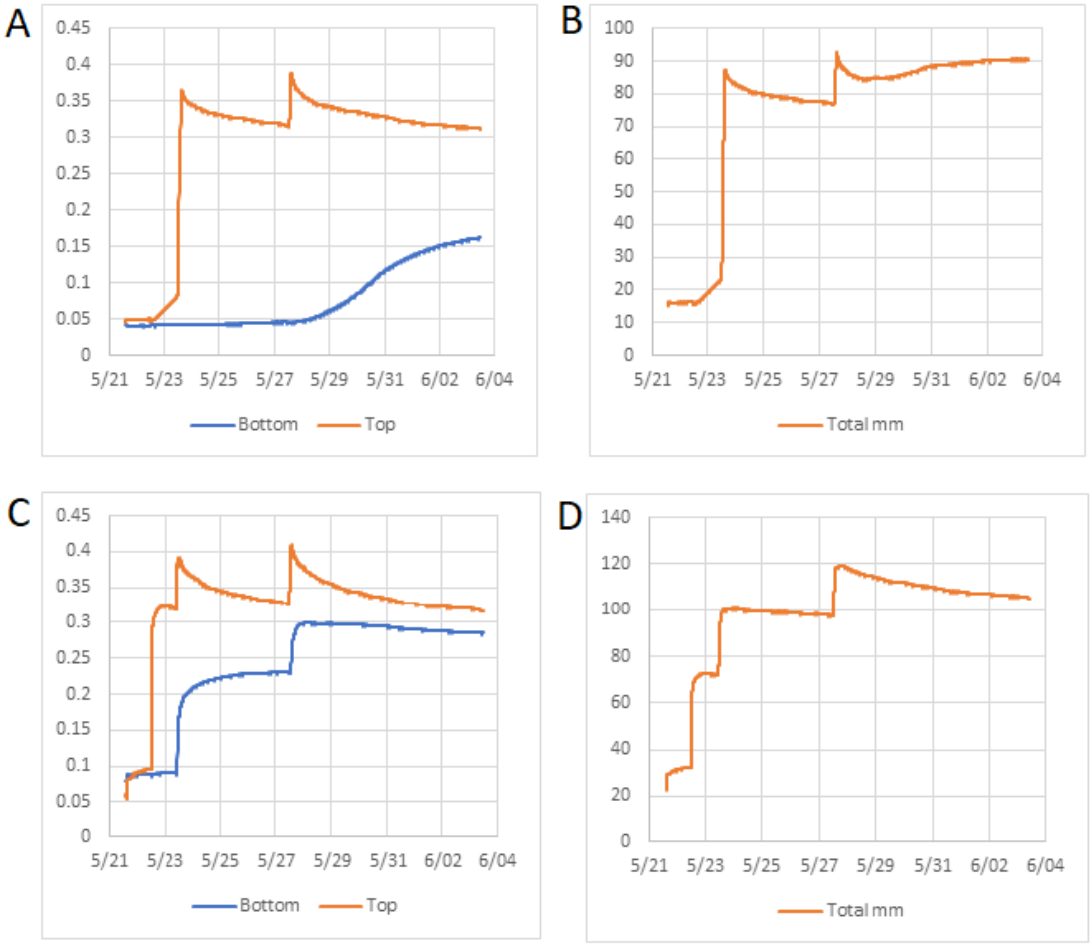

Figure 30: Observations of soil moisture in the horizontal and vertical installation containers. Individual sensor data and the calculated total soil moisture in mm from the horizontal installation (A, B) and the vertical installation (C, D) are displayed.

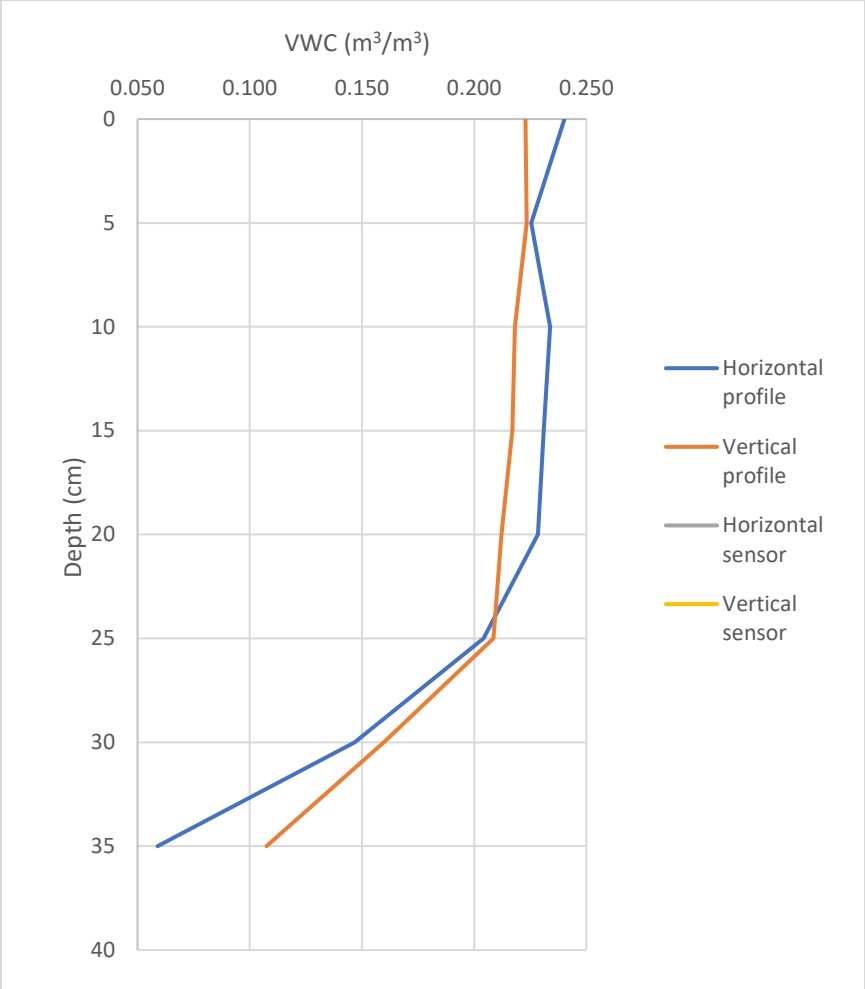

Figure 31: Comparison of the VIC and HIC final volumetric water content observations from the 15 and 30 cm sensors to soil samples obtained at 5 cm intervals at the end of the experiment.

The top VIC sensor responded to each simulated irrigation event but displayed a lower-than-expected response to the first two events. The bottom sensor did not respond during the first two simulated events and had a well-defined response during the last two events. By the third event, the moisture content peaks and drains in the top sensor at the beginning quickly and tapering off at 35% VWC, with the bottom sensor having a slight lag and a steady increase (Figure 30A). The responses to each event are also discernible in the calculated total soil moisture (Figure 30B). The top sensor installed horizontally

displayed a well-defined response in the last two simulated events with no discernible response in the first two events. The bottom sensor had no response that corresponded to any of the four events but did display an increase in VWC 24 hrs after the final event (Figure 30C). This increase is also observed in the calculated total soil moisture (Figure 30D). The vertical installation strategy allows for the change in moisture content to be observed when the soil is dry (~10% VWC) and is relatively accurate when comparing the actual moisture content to the calculated moisture content. The vertical sensor placement has a more consistent margin of error between the top and bottom sensors, which was approximately 8%, while the horizontal sensor placement overestimates the moisture content by less than 2% in the bottom sensor and more than 10% in the top sensor (Figure 31).

Conclusion

The vertical installation plan is an improvement when compared to the horizontal installation plan. It reflects the water added to the container and the moisture conditions at the end of the experiment. It also shows a response to a change in water content under dry conditions.

Soil Moisture Sensor Specifications

Soil moisture sensor specifications were used to determine sensor spacing and accuracy.

- 10HS sensor: range 0 – 0.57 m^3/m^3, accuracy ±0.033 without soil specific calibration ±0.020 with soil specific calibration, probe dimensions 160 x 32 x 2 mm

- EC5 sensor: range 0 – 0.550 m^3/m^3, accuracy ±0.031 without soil specific calibration ±0.020 with soil specific calibration, probe dimensions 89 x 15 x 1.5 mm
- TDR-315: range 0-1 m^3/m^3 accuracy ±0.001, permittivity 1 – 80 accuracy ±0.1, Bulk EC 0-5000 µs/cm, soil temp -40 - +60˚C accuracy ±0.1˚C, pore water EC 0 - 55000 µs/cm, probe dimensions 150 x 3.5 mm

APPENDIX 2: VARIOGRAM MODEL PARAMETERS USED FOR COMPARING UNIVERSAL AND ORDINARY KRIGING AND CO-KRIGING METHODS

A comparison of ordinary and universal kriging and co-kriging methods was done to determine which kriging method would predict soil moisture most accurately in the 2018 and 2019 study areas. Ordinary and universal kriging and co-kriging methods were used to create a prediction map from the soil water content observations obtained during the soil moisture survey on July 22, 2019. Four semivariogram models were used to fit the data for each method: spherical, exponential, Gaussian, and circular

Table 25: Model parameters for semivariograms used for the ordinary kriging method. Spherical (Sph), exponential (Exp), Gaussian (Gau) and circular (Cir) were used as models. Soil water content point data was obtained using a Stevens HydroGo portable moisture probe on July 22, 2019.

ORDINARY KRIGING SEMIVARIOGRAM MODELS

Model	Sill	Nugget	Nugget-to-sill ratio	Range
Sph	24.1	0.0	24.1	120.3
Exp	30.9	0.0	30.9	83.8
Gau	23.6	0.0	23.6	49.6
Cir	23.7	0.0	23.7	101.5

The spherical, Gaussian, and circular models had similar sills of 24.1% VWC, 23.6% VWC and 23.7% VWC, respectively. The ranges were more variable with values of 120.3 m, 49.6 m, and 101.5 m for the spherical, Gaussian, and circular models. The exponential model had a higher sill than the other models at 30.9, and a range of 83.8 m.

Table 26: Model parameters for semivariograms used for the universal kriging method. Spherical (Sph), exponential (Exp), Gaussian (Gau) and circular (Cir) were used as models.

Soil water content point data was obtained using a Stevens HydroGo portable moisture probe on July 22, 2019.

UNIVERSAL KRIGING SEMIVARIOGRAM MODELS

Model	Sill	Nugget	Nugget-to-sill ratio	Range
Sph	17.3	0.0	17.3	81.6
Exp	19.4	0.0	19.4	44.2
Gau	14.1	2.7	5.2	44.2
Cir	17.2	0.0	17.2	71.0

The spherical and circular models had nearly the same sill with values of 17.3% VWC and 17.2% VWC and the two highest ranges at 81.6 m and 71.0 m. The exponential model had a higher sill than the other models at 19.4% VWC, and a range of 44.2 m. The Gaussian model had the lowest sill and the highest nugget, at 14.1% VWC and 2.7% VWC with a range equivalent to the exponential model, at 44.2 m.

Co-kriging methods uses variogram and cross-variogram models which share a range to fit to georeferenced data to determine spatial autocorrelation between a primary variable that is to be predicted and secondary collocated variables that have a correlational relationship with the primary variable. The co-kriging method requires the construction of three variograms and three cross-variograms to predict soil water content using ECa and elevation as collocated variables (Table 27, Table 29) and two variograms and one cross-variogram when using elevation alone

Table 27: Model parameters for semivariograms used in co-kriging. Soil water content (VWC) is the primary variable to be predicted and soil apparent electrical conductivity (ECa) and elevation are used as secondary variables. Soil water content point data was obtained using a Stevens HydroGo portable moisture probe on July 22, 2019.

CO-KRIGING SEMIVARIOGRAM MODELS – TWO SECONDARY VARIABLES

Model	Variable	Sill	Nugget	Nugget-to-sill ratio	Range
Sph	VWC	21.9	1.1	0.05	81.9
	ECa	0.37	0.21	0.57	81.9
	Elevation	2.33	1.02	0.44	81.9
Exp	VWC	30.5	1.4	0.05	81.9
	ECa	0.51	0.35	0.67	81.9
	Elevation	3.47	0.90	0.26	81.9
Gau	VWC	20.3	7.1	0.35	81.9
	ECa	0.33	0.23	0.70	81.9
	Elevation	3.79	0.10	0.03	81.9
Cir	VWC	20.8	1.3	0.06	81.9
	ECa	0.40	0.17	0.43	81.9
	Elevation	2.18	1.18	0.54	81.9

The variograms and cross-variograms constructed using both elevation and ECa shared a range of 81.9 m and showed good to moderate spatial autocorrelation in soil water content variograms given the consistently low nugget-to-sill ratios (Table 27, Table 29). The Gaussian model showed the least autocorrelation in the soil moisture content variogram with a nugget-to-sill ratio of 0.35 and both exponential and circular models showed the most with a nugget-to-sill ratio of 0.05 (Table 27).

Table 28: Model parameters for semivariograms used in co-kriging. Soil water content (VWC) was the primary variable to be predicted and elevation was used as the secondary variable. Soil water content point data obtained using a Stevens HydroGo portable moisture probe on July 22, 2019.

CO-KRIGING SEMIVARIOGRAM MODELS – ELEVATION ONLY

Model	Variable	Sill	Nugget	Nugget-to-sill ratio	Range
Sph	VWC	21.7	1.1	0.05	81.9
	Elevation	2.32	1.08	0.47	81.9
Exp	VWC	31.1	1.0	0.03	81.9
	Elevation	3.45	1.00	0.29	81.9
Gau	VWC	23.1	5.34	0.23	81.9
	Elevation	3.79	0.06	0.02	81.9
Cir	VWC	20.6	1.2	0.06	81.9
	Elevation	2.16	1.22	0.56	81.9

The variograms and cross-variogram constructed using only elevation also shared a range of 81.9 m (Table 28, Table 30). The soil water content variogram constructed using the spherical, exponential, and circular models have similarly low nugget-to-sill ratios, indicating a good spatial autocorrelation using these models with the exponential model showing the lowest nugget-to-sill ratio of 0.03 (Table 28). Both Gaussian models constructed from soil water content had the highest nugget-to-sill ratio, indicating that this model displayed the least spatial correlation, but does show the best spatial autocorrelation in the elevation variogram.

Table 29: Model parameters for cross-variograms used in co-kriging. Soil water content (VWC) was the primary variable to be predicted and soil apparent electrical conductivity (ECa) and elevation were used as secondary variables. Soil water content point data was obtained using a Stevens HydroGo portable moisture probe on July 22, 2019.

CO-KRIGING CROSS VARIOGRAM MODELS WITH TWO SECONDARY VARIABLES

Model	Variable	Sill	Nugget	Nugget-to-sill ratio	Range
Sph	VWC*Elevation	5.19	1.04	0.20	81.9
	VWC*ECa	0.61	0.27	0.44	81.9
	Elevation*ECa	0.40	0.20	0.50	81.9
Exp	VWC*Elevation	7.18	1.06	0.15	81.9
	VWC*ECa	1.39	0.44	0.32	81.9
	Elevation*ECa	0.73	0.23	0.32	81.9
Gau	VWC*Elevation	5.00	0.46	0.09	81.9
	VWC*ECa	1.00	0.64	0.64	81.9
	ECa*Elevation	0.53	0.06	0.11	81.9
Cir	VWC*Elevation	5.30	1.20	0.56	81.9
	VWC*ECa	0.58	0.26	0.38	81.9
	ECa*Elevation	0.38	0.21	0.16	81.9

Table 30: Model parameters for cross-variograms used in co-kriging. Soil water content (VWC) was the primary variable to be predicted and elevation was used as the secondary variable. Soil water content point data obtained using a Stevens HydroGo portable moisture probe on July 22, 2019.

CO-KRIGING CROSS-VARIOGRAM MODELS WITH ELEVATION ONLY

Model	Sill	Nugget	Nugget-to-sill ratio	Range
Sph	5.26	1.07	0.20	81.9
Exp	7.29	0.99	0.14	81.9
Gau	5.16	0.54	0.10	81.9
Cir	5.33	1.21	0.23	81.9

Table 31: Leave-one-out cross-validation results of circular (CIR), exponential (EXP), Gaussian (GAU) and spherical (SPH) semivariogram models using ordinary kriging. The co-efficient of determination (R^2), concordance, mean square error (MSE), root mean square error (RMSE) and bias were used as assessment parameters.

	R^2	CONCORDANCE	MSE	RMSE	BIAS
CIR	0.29	0.52	15.42	3.93	0.14
EXP	0.38	0.58	12.76	3.57	0.10
GAU	0.37	0.60	16.31	4.04	0.10
SPH	0.29	0.49	14.79	3.85	0.39

The exponential theoretical semivariogram model was chosen as the best predictor of soil water content using the ordinary kriging method. The LOOCV results for the ordinary kriging method using four theoretical semivariogram models (Table 31) showed that the exponential theoretical semivariogram model had the highest co-efficient of determination with a moderate correlation between predicted and observed values with predictions being estimated at an average of 3.57% VWC from the true value. The concordance was slightly lower than the results obtained from the Gaussian model and both showed the same amount of overestimation as evidenced by the bias in the models (

Table 31). However, the Gaussian semivariogram model had the highest RMSE indicating a higher prediction error than with the other semivariogram models. The exponential

model was used predict the soil moisture content for the quarter section to compare with other kriging methods.

Table 32: Leave-one-out cross-validation results of circular (CIR), exponential (EXP), Gaussian (GAU) and spherical (SPH) theoretical semivariogram models using universal kriging. The co-efficient of determination (R^2), concordance, mean square error (MSE), root mean square error (RMSE) and bias were used as assessment parameters.

	R^2	CONCORDANCE	MSE	RMSE	BIAS
CIR	0.27	0.51	16.57	4.07	0.35
EXP	0.32	0.54	14.63	3.82	-0.10
GAU	0.22	0.44	16.90	4.11	-0.23
SPH	0.26	0.49	16.27	4.03	-0.23

The exponential theoretical semivariogram model was chosen as the best predictor of soil water content using the universal kriging method. The LOOCV results for the universal kriging method using four theoretical semivariogram models (Table 32) showed that the exponential theoretical semivariogram model had the highest R^2 and concordance between predicted and observed values and predictions being estimated at an average of 3.82% VWC from the true value. The exponential model underestimated the predicted value when compared to the observations but showed the least amount of bias from other models (Table 32). The exponential model was used predict the soil moisture content for the quarter section to compare with other kriging methods.

Table 33: Leave-one-out cross-validation results for co-kriging methods using circular (CIR), exponential (EXP), Gaussian (GAU) and spherical (SPH) theoretical semivariogram models. Semivariogram models were constructed using soil moisture as the primary variable and soil electrical conductivity and elevation as secondary variables. The co-efficient of determination (R^2), concordance, mean square error (MSE), root mean square error (RMSE) and bias were used as assessment parameters.

	R^2	CONCORDANCE	MSE	RMSE	BIAS
CIR	0.27	0.51	15.78	3.97	0.01
EXP	0.38	0.59	12.77	3.57	0.01
GAU	0.04	0.24	48.27	6.95	-0.32
SPH	0.36	0.56	13.13	3.62	0.05

The exponential theoretical semivariogram model was chosen as the best predictor of soil water content using the co-kriging method and elevation as the secondary variable. The LOOCV results for the co-kriging method using four theoretical semivariogram models (Table 33) showed that the exponential theoretical semivariogram model had the highest R^2 and concordance between predicted and observed values and predictions being estimated at an average of 3.57% VWC from the true value. The exponential and circular model showed a minimal amount of bias and the least amount of bias when compared to models (Table 33).

Table 34: Leave-one-out cross-validation results for co-kriging methods using circular (CIR), exponential (EXP), Gaussian (GAU) and spherical (SPH) theoretical semivariogram models. Semivariogram models were constructed using soil moisture as the primary variable and elevation as the secondary variable. The co-efficient of determination (R^2), concordance, mean square error (MSE), root mean square error (RMSE) and bias were used as assessment parameters.

	R^2	CONCORDANCE	MSE	RMSE	BIAS
CIR	0.26	0.49	16.29	4.04	0.02
EXP	0.38	0.58	12.93	3.60	0.03
GAU	0.02	0.17	78.86	8.88	0.02
SPH	0.35	0.55	13.42	366	0.06

The exponential theoretical semivariogram model was chosen as the best predictor of soil water content using the co-kriging method and elevation and ECa as the secondary variables. The leave-one-out cross-validation results for the co-kriging method using four theoretical semivariogram models (Table 34) showed that the exponential theoretical semivariogram model had the highest R^2 and concordance between predicted and observed values and predictions being estimated at an average of 3.60% VWC from the true value. The circular and Gaussian models have the least amount of bias which was calculated at 0.02 for both models (Table 34). The exponential model had a slightly higher bias of 0.03 and the spherical model had the highest bias of 0.06.

The co-kriging method using elevation as the secondary variable was compared to the co-kriging method using ECa and elevation. The circular, exponential, and spherical models with both secondary variables showed a slight improvement in the coefficient of determination, concordance, mean square error, and root mean square error (Table 33, Table 34). The Gaussian model using elevation alone had higher MSE and RMSE, and a lower R^2, concordance, and bias. The exponential model constructed with both secondary variables was used predict the soil moisture content for the quarter section to compare with other kriging methods.

APPENDIX 3: ADDITIONAL SEMIVARIOGRAM MODEL PARAMETERS

Table 35: Model parameters for semivariograms fitted to ECa (ds/m) data and used in co-kriging to predict volumetric water content. ECa was used as a secondary variable. The theoretical model used, partial sill (C), nugget (C_0), total sill ($C+C_0$), nugget-to-sill ratio and range are summarized.

ECa SEMIVARIOGRAM MODELS							
Date	Depth	Model	C	C_0	$C + C_0$	Nugget-to-sill ratio	Range (m)
7/19/18	15 cm	Exp	1.09	0.08	1.17	0.068	81.3
	30 cm	Exp	1.05	0.07	1.12	0.060	74.5
8/02/18	15 cm	Sph	0.82	0.10	0.92	0.113	81.3
	30 cm	Exp	1.26	0.06	1.31	0.045	82.5
8/16/18	15 cm	Exp	0.53	0.23	0.75	0.302	81.7
	30 cm	Exp	0.42	0.11	0.53	0.208	81.7
8/23/18	15 cm	Sph	0.87	0.26	1.13	0.227	81.5
	30 cm	Cir	0.81	0.05	0.86	0.059	72.5
7/10/19	15 cm	Exp	0.42	0.09	0.50	0.171	82.2
	30 cm	Sph	0.27	0.06	0.33	0.176	82.2
7/22/19	15 cm	Sph	0.42	0.24	0.66	0.360	78.1
	30 cm	Exp	0.51	0.35	0.86	0.409	81.9
8/09/19	15 cm	Exp	0.53	0.23	0.75	0.302	81.7
	30 cm	Exp	0.42	0.11	0.53	0.208	81.7
8/28/19	15 cm	Exp	0.32	0.23	0.55	0.413	78.4
	30 cm	Exp	0.38	0.17	0.56	0.313	81.4
9/02/19	15 cm	Sph	0.21	0.09	0.30	0.297	73.9
	30 cm	Sph	0.21	0.01	0.22	0.048	73.9
9/17/19	15 cm	Exp	0.41	0.12	0.52	0.221	62.9
	30cm	Exp	0.47	0.14	0.61	0.233	81.2

Table 36: Model parameters for semivariograms fitted to elevation (m) data and used in co-kriging to predict volumetric water content. Elevation was used as a secondary variable. The theoretical model used, partial sill (C), nugget (C_0), total sill ($C+C_0$), nugget-to-sill ratio and range are summarized.

ELEVATION SEMIVARIOGRAM MODELS							
Date	Depth	Model	C	C_0	$C + C_0$	Nugget-to-sill ratio	Range (m)
7/19/18	15 cm	Exp	0.63	0.13	0.76	0.204	81.3
	30 cm	Exp	0.64	0.14	0.78	0.213	74.5
8/02/18	15 cm	Sph	0.65	0.09	0.74	0.133	81.3
	30 cm	Exp	0.93	0.08	1.01	0.084	82.5
8/16/18	15 cm	Exp	3.30	0.43	3.73	0.130	81.7
	30 cm	Exp	3.23	0.17	3.40	0.054	81.7
8/23/18	15 cm	Sph	0.49	0.23	0.72	0.460	81.5
	30 cm	Cir	0.50	0.17	0.68	0.343	72.5
7/10/19	15 cm	Exp	3.50	0.51	4.01	0.145	82.2
	30 cm	Sph	2.41	0.74	3.16	0.308	82.2
7/22/19	15 cm	Sph	2.14	0.43	2.57	0.203	78.1
	30 cm	Exp	3.47	0.90	4.37	0.260	81.9
8/09/19	15 cm	Exp	3.30	0.43	3.73	0.130	81.7
	30 cm	Exp	3.23	0.17	3.40	0.054	81.7
8/28/19	15 cm	Exp	3.69	0.19	3.88	0.052	78.4
	30 cm	Exp	3.77	0.25	4.01	0.066	81.4
9/02/19	15 cm	Sph	2.03	0.29	2.32	0.141	73.9
	30 cm	Sph	2.17	1.30	3.48	0.601	73.9
9/17/19	15 cm	Exp	2.67	0.80	3.46	0.299	62.9
	30 cm	Exp	3.44	0.59	4.04	0.172	81.2

Table 37: Model parameters for cross-variograms fitted to VWC data collected in 2018 and 2019 and ECa (ds/m) data. The theoretical model used, partial sill (C), nugget (C_0), total sill ($C+C_0$), nugget-to-sill ratio and range are summarized.

MOISTURE AND ECA SEMIVARIOGRAM MODELS							
Date	Depth	Model	C	C_0	$C + C_0$	Nugget-to-sill ratio	Range (m)
7/19/18	15 cm	Exp	-3.31	0.52	3.84	0.136	81.3
	30 cm	Exp	-3.17	0.46	3.63	0.128	74.5
8/02/18	15 cm	Sph	0.71	-0.24	0.95	0.250	81.3
	30 cm	Exp	-0.95	-0.39	1.34	0.292	82.5
8/16/18	15 cm	Exp	0.46	-0.34	0.80	0.424	81.7
	30 cm	Exp	0.59	0.02	0.60	0.026	81.7
8/23/18	15 cm	Sph	-2.60	0.72	3.32	0.218	81.5
	30 cm	Cir	-1.25	0.58	1.83	0.318	72.5
7/10/19	15 cm	Exp	0.71	0.02	0.73	0.023	82.2
	30 cm	Sph	0.86	-0.13	0.99	0.135	82.2
7/22/19	15 cm	Sph	0.87	-0.40	1.27	0.317	78.1
	30 cm	Exp	1.38	-0.44	1.82	0.240	81.9
8/09/19	15 cm	Exp	0.46	-0.34	0.80	0.424	81.7
	30 cm	Exp	0.59	0.02	0.60	0.026	81.7
8/28/19	15 cm	Exp	-0.51	0.34	0.84	0.398	78.4
	30 cm	Exp	0.76	-0.31	1.07	0.287	81.4
9/02/19	15 cm	Sph	-0.76	0.21	0.97	0.217	73.9
	30 cm	Sph	-0.70	0.09	0.79	0.109	73.9
9/17/19	15 cm	Exp	-1.16	0.06	1.23	0.052	62.9
	30 cm	Exp	-0.90	0.27	1.17	0.230	81.2

Table 38: Model parameters for cross-variograms fitted to VWC (%) data collected in 2018 and 2019 and elevation (m) data. The theoretical model used, partial sill (C), nugget (C_0), total sill ($C+C_0$), nugget-to-sill ratio and range are summarized.

MOISTURE AND ELEVATION VARIOGRAM MODELS							
Date	Depth	Model	C	C_0	$C + C_0$	Nugget-to-sill ratio	Range (m)
7/19/18	15 cm	Exp	-0.96	0.63	1.59	0.395	81.3
	30 cm	Exp	-0.36	0.83	1.20	0.697	74.5
8/02/18	15 cm	Sph	1.07	0.10	1.17	0.084	81.3
	30 cm	Exp	-0.08	0.35	0.44	0.807	82.5
8/16/18	15 cm	Exp	-7.04	1.63	8.67	0.188	81.7
	30 cm	Exp	-5.10	1.26	6.36	0.198	81.7
8/23/18	15 cm	Sph	-0.56	0.48	1.04	0.460	81.5
	30 cm	Cir	-0.81	1.08	1.89	0.572	72.5
7/10/19	15 cm	Exp	-4.80	0.90	5.69	0.158	82.2
	30 cm	Sph	-5.68	2.52	8.20	0.307	82.2
7/22/19	15 cm	Sph	-3.69	0.70	4.38	0.159	78.1
	30 cm	Exp	-7.18	1.06	8.24	0.129	81.9
8/09/19	15 cm	Exp	-7.04	1.63	8.67	0.188	81.7
	30 cm	Exp	-5.10	1.26	6.36	0.198	81.7
8/28/19	15 cm	Exp	-1.46	0.35	1.82	0.195	78.4
	30 cm	Exp	-6.94	1.27	8.21	0.154	81.4
9/02/19	15 cm	Sph	-1.33	0.53	1.85	0.285	73.9
	30 cm	Sph	-8.23	2.87	11.10	0.258	73.9
9/17/19	15 cm	Exp	5.15	-1.00	6.15	0.162	62.9
	30 cm	Exp	6.09	-2.08	8.17	0.254	81.2

Table 39: Model parameters for cross-variograms fitted to elevation (m) and ECa (ds/m) data. The theoretical model used, partial sill (C), nugget (C_0), total sill ($C+C_0$), nugget-to-sill ratio and range are summarized.

ELEVATION AND ECA VARIOGRAM MODELS							
Date	Depth	Model	C	C_0	$C + C_0$	Nugget-to-sill ratio	Range (m)
7/19/18	15 cm	Exp	0.39	0.02	0.41	0.046	81.3
	30 cm	Exp	0.38	0.02	0.40	0.053	74.5
8/02/18	15 cm	Sph	0.29	-0.09	0.38	0.236	81.3
	30 cm	Exp	0.33	-0.07	0.40	0.166	82.5
8/16/18	15 cm	Exp	-1.03	0.09	1.12	0.080	81.7
	30 cm	Exp	-0.77	0.08	0.85	0.099	81.7
8/23/18	15 cm	Sph	0.18	0.05	0.24	0.231	81.5
	30 cm	Cir	0.01	0.09	0.11	0.875	72.5
7/10/19	15 cm	Exp	-0.76	0.04	0.80	0.055	82.2
	30 cm	Sph	-0.38	-0.02	0.40	0.058	82.2
7/22/19	15 cm	Sph	-0.35	-0.13	0.48	0.266	78.1
	30 cm	Exp	-0.73	-0.23	0.96	0.239	81.9
8/09/19	15 cm	Exp	-1.03	0.09	1.12	0.080	81.7
	30 cm	Exp	-0.77	0.08	0.85	0.099	81.7
8/28/19	15 cm	Exp	-0.93	0.21	1.14	0.181	78.4
	30 cm	Exp	-0.77	0.09	0.85	0.100	81.4
9/02/19	15 cm	Sph	0.17	0.08	0.25	0.321	73.9
	30 cm	Sph	0.18	0.04	0.21	0.177	73.9
9/17/19	15 cm	Exp	-0.65	-0.01	0.66	0.011	62.9
	30 cm	Exp	-0.76	-0.01	0.76	0.009	81.2